Chapter 2
The Symmetry Groups in Three-Dimensional Space

The theoretical modeling of inorganic nanostructures described in this book is based on the consideration of 3D-2D-1D three-dimensional objects (three-periodic bulk crystals, diperiodic nanolayers, monoperiodic nanotubes and nanorods).

First, the structure and properties of a bulk crystal with 3D periodicity are computed. The prototype bulk crystal structure is one of the main factors that influence the properties of nano-sized systems. This allows one to compare the results calculated with the existing experimental data and thereby check the validity of the calculation method used.

Second, the nanolayer structure and properties are calculated, as the structure and properties of the rolled up nanotubes depend on the slab, used in rolling up procedure.

Finally, the structure and properties of nanotubes and nanorods are calculated applying the same computational method as was applied for the bulk crystals and nanolayers.

The symmetry properties of the system are used in 3D-2D-1D calculations allowing one to make a classification of the electron and phonon states and drastically reduce the computational time.

In this chapter we discuss the following symmetry groups in the three-dimensional space: (1) space groups $G = G_3^3$—230 types of three dimensional groups with three-dimensional translations (triperiodic 3D), (2) layer groups $DG = G_2^3$—80 types of three dimensional groups with two-dimensional translations (diperiodic 2D) and (3) line groups $LG = G_1^3$—three dimensional groups with one-dimensional translations (monoperiodic 1D). 75 rod groups (RG) constitute a subset of the infinite number of line groups.

The description the bulk crystal requires the knowledge of the full symmetry group of the crystal (space group G) and its irreducible representations. The group G includes both translations, operations from the point groups of symmetry and combined operations. The application of symmetry transformations means splitting all space into systems of equivalent points known also as Wyckoff positions in crystals, irrespective of whether there are atoms in these points or not. The crystal-structure type is specified when one decides which sets of the Wyckoff positions for the corresponding space group are occupied by atoms. To distinguish between different

R.A. Evarestov, *Theoretical Modeling of Inorganic Nanostructures*,
NanoScience and Technology, DOI 10.1007/978-3-662-44581-5_2

structures of the same type one needs the numerical values of lattice parameters and additional data if there exist occupied Wyckoff positions with free parameters in the coordinates.

We briefly discuss the 20 bulk crystal structures (cubic, tetragonal, orthorhombic and hexagonal) which form the basis of nanostructure modeling. Among them are structures with both symmorphic and nonsymmorphic space groups, structures with the same Bravais lattice and crystal class but different space groups, structures described by only lattice parameters or by both the lattice parameters and free parameters of the Wyckoff positions occupied by atoms.

The site symmetry approach extension to the layer and line groups is considered.

The symmetry of crystalline orbitals in bulk crystals and nanostructures is defined by the their symmetry group irreducible representations, which are also considered in this chapter.

2.1 Classification of the Symmetry Groups

Let G_m^n mean the symmetry group of the system in the n-dimensional space (n-dimensional group) with m-dimensional translation subgroup ($m \leq n$) [1].

In this chapter we discuss the symmetry groups in the three-dimensional space ($n = 3$): (1) space groups $G = G_3^3$—230 types of three dimensional groups with the three-dimensional translations (triperiodic 3D, $m = 3$), (2) layer groups $DG = G_2^3$—80 types of three dimensional groups with two-dimensional translations (diperiodic 2D, $m = 2$) and (3) line groups—$LG = G_1^3$ three dimensional groups with one-dimensional translations (monoperiodic 1D, $m = 1$). 75 rod groups (RG) constitute a subset of the infinite number of line groups.

17 plane groups $G = G_2^2$ and 7 frieze groups $G = G_1^2$ are the symmetry groups in the two-dimensional space ($n = 2$) being the subsets of the three-dimensional layer and rod groups, respectively.

2 groups in the one-dimensional space $LG = G_1^1$ are called by line groups in [2]. However, we use this term for all monoperiodic three dimensional groups with one-dimensional periodicity. These groups are called in [3] by commensurate line groups.

Independent study of polymers, or, in more rigorous terms, general 1-periodic three-dimensional objects, stimulated the analysis of 1-periodic symmetry groups which could include rotation axes of arbitrary order. Such groups received a collective name ‘line groups’. There are infinitely many line groups and their classification may be performed in a number of ways [3, 4]. Rod groups constitute a subset of the set of line groups but due to their origin enumeration, notations, and geometric realizations rod groups possess certain specificity as compared with the line groups. In this section we establish the explicit correspondence between rod groups and relevant geometric realizations of the corresponding line groups to lay a bridge between crystallography and symmetry description of stereoregular polymers. It seems to be of increasing importance due to the very fast developments in the field

of nanotubes, nanoribbons, and nanowires. These 1-periodic objects originate from crystalline solids but nanotube symmetry elements may include rotation axes of arbitrary order.

The three-dimensional triperiodic groups with the three lattice basic translation vectors $\mathbf{a}_1, \mathbf{a}_2, \mathbf{a}_3$ are called here space groups. The basic translation vectors define the primitive unit cell i.e. the minimal volume unit cell used to reproduce the whole lattice by the tree dimensional basic translations. The so called crystallographic (conventional) unit cell with the crystallographic translation vectors **a**, **b**, and **c** is defined as the minimal volume unit cell in the form of a parallelepiped constructed on vectors of translations and possessing the point symmetry of the lattice.

The layer groups and rod groups are known as subperiodic groups [5]. The three-dimensional rod and layer groups are considered in the context of a three-dimensional space along with their concomitant relationships with space groups. These relationships are the basis for the symbols and classification of the subperiodic groups which are used in [5]. Subperiodic groups are described, as are the space groups, see [2], by means of a crystallographic coordinate system, consisting of a crystallographic basis and a crystallographic origin. For subperiodic groups, not all vectors of the crystallographic basis are lattice vectors. For the three-dimensional layer groups and rod groups, the basis vectors are labeled **a**, **b**, and **c**. The basis vectors **a** and **b** are chosen as lattice vectors in the case of layer groups, and **c** is chosen as a lattice vector in the case of rod groups.

The three-dimensional crystallographic point groups $G = G_0^3$ form 32 crystal classes of space groups. Excluding 5 cubic point groups one obtains 27 classes of layer and rod groups. The 10 point symmetry groups $G = G_0^2$ in two-dimensional space and 2 point symmetry groups $G = G_0^1$ in one-dimensional space are subsets of the three-dimensional point groups $G = G_0^3$ [1].

The triperiodic (3D) space groups $G = G_3^3$ describe the symmetry of bulk crystals. The classification of the crystalline electron and phonon states requires the knowledge of the full symmetry group of a bulk crystal (triperiodic space group G) and its irreducible representations. The group G includes both the three-dimensional translations, operations from the 32 three-dimensional point symmetry groups $G = G_0^3$ and combined operations.

The diperiodic (layer) groups $DG = G_2^3$ are the symmetry groups of the thin films. These groups are used to describe the electronic structure of surface states of crystals in the slab model. In the *single-slab* model a crystal with a surface is approximated by a slab of finite thickness. The symmetry group of this model (diperiodic or layer group) allows the existence of the point symmetry operations that move the atoms out of the plane of the layer but bring them into positions occupied by other atoms of the slab. The diperiodic (layer) group DG includes both the two-dimensional translations, operations from the 27 three-dimensional point symmetry groups $G = G_0^3$ and combined operations.

The layer groups are subperiodic subgroups of the triperiodic groups.The knowledge of the space 3D groups allows one to generate the layer groups corresponding to the different surface orientations in the bulk crystal. The layer groups in turn are used as basic ones in the monoperiodic nanotubes modeling.

The commensurate line groups $LG = G_1^3$ (also called monoperiodic groups) are symmetry groups of three-dimensional objects translationally periodic along a line—stereoregular polymers, nanotubes and nanowires. The symmetry groups of nanoribbons and nanowires (75 rod groups RG) form a finite subset of an infinite number of line groups. Rod group includes both the one-dimensional translations, operations from the 27 three-dimensional point symmetry groups $G = G_0^3$ and combined operations.

2.2 Space (Triperiodic) Symmetry Groups of Bulk Crystals

2.2.1 Translation and Point Symmetry of Bulk Crystals

The classification of the molecular or the crystalline electron and phonon states requires the knowledge of the system symmetry group and its irreducible representations. In both molecules and bulk crystals the symmetry group is the set of transformations in three dimensional space that transforms any point of the space into an equivalent point. The systems of equivalent points are called orbits of points. In equivalent points the properties of a molecule or a crystal (electrostatic potential, electronic density, etc.) are all identical.

The symmetry of molecules in the three dimensional space is described by the three dimensional point groups $F = G_0^3$ without the periodicity. The group F consists of the orthogonal symmetry operations (rotations through symmetry axes, reflections in symmetry planes and their combinations) that transform the equilibrium configuration of the nuclei of a molecule into itself. They form a group F of molecular symmetry. There are no restrictions on the rotation axes order so that the number of point groups is formally infinite.

The space group is the triperiodic group $G = G_3^3$ in the three-dimensional space and includes both the three-dimensional translations, operations from the point groups of symmetry (the crystal classes) and combined operations. The condition of the compatibility of the point and translation symmetry operations restricts the rotation axes by order 1, 2, 3, 4, 6 and therefore the total number of the crystallographic point groups is 32.

As well as molecules, crystals possess point symmetry, i.e. equivalent points of space are connected by the point-symmetry transformations. But in a crystal the number of the point-symmetry elements (the rotation axis or reflection planes) is formally infinite. Therefore, it is impossible to find such a point of space where all the point-symmetry elements intersect. It is connected by the fact that, unlike molecules, in crystals among operations of symmetry there are translations of a group of rather small number of atoms to space. The presence of translation symmetry means the periodicity of the perfect crystals structure: translations of the primitive unit cell reproduce the whole crystal.

In real crystals of macroscopic sizes translation symmetry, strictly speaking, is absent because of the presence of borders. If, however, we consider the so-called bulk properties of a crystal (for example, distribution of electronic density in the volume of the crystal, determining the nature of a chemical bond) the influence of borders can not be taken into account (number of atoms near to the border is small, in comparison with the total number of atoms in a crystal) and we consider a crystal as a boundless system [6].

In the theory of electronic structure two symmetric models of a boundless crystal are used: or it is supposed that the crystal fills all the space (model of an infinite crystal), or the fragment of a crystal of finite size (for example, in the form of a parallelepiped) with the identified opposite sides is considered. In the second case we say, that the crystal is modeled by a cyclic cluster which translations as a whole are equivalent to zero translation (Born–von Karman Periodic Boundary Conditions–PBC). Between these two models of a boundless crystal there exists a connection: the infinite crystal can be considered as a limit of the sequence of cyclic clusters with increasing volume. In a molecule, the number of electrons is fixed as the number of atoms is fixed. In the cyclic model of a crystal the number of atoms (and thus the number of electrons) depends on the cyclic-cluster size and becomes infinite in the model of an infinite crystal. It makes changes, in comparison with molecules, to a one-electron density matrix of a crystal that now depends on the sizes of the cyclic cluster chosen. As a consequence, in calculations of the electronic structure of crystals it is necessary to investigate convergence of results with an increase of the cyclic cluster that models the crystal. For this purpose, the features of the symmetry of the crystal, connected with the presence of translations also are used.

Translation symmetry of a perfect crystal can be defined with the aid of three noncoplanar vectors: $\mathbf{a}_1, \mathbf{a}_2, \mathbf{a}_3$ basic translation vectors. Translation $t_{\boldsymbol{a}}$ through the lattice vector

$$\mathbf{a} = n_1\mathbf{a}_1 + n_2\mathbf{a}_2 + n_3\mathbf{a}_3 \tag{2.1}$$

where n_1, n_2, n_3 are integers, relates the equivalent points $\boldsymbol{r}$ and $\boldsymbol{r}'$ of the crystal:

$$\boldsymbol{r}' = \boldsymbol{r} + \boldsymbol{a} \tag{2.2}$$

Translations $t_{\boldsymbol{a}}$ are elements of the translation group T. If we draw all the vectors $\boldsymbol{a}$ from a given point (the origin), then their endpoints will form the Bravais lattice, or "empty" lattice, corresponding to the given crystal. The endpoints of the vectors in this construction are the lattice points (lattice nodes). Three of the basic translation vectors define the elementary parallelepiped called the primitive unit cell (PUC). The PUC contains lattice points only at the eight corners of the parallelepiped. Each corner belongs to eight PUC, so that by fixing the PUC by one lattice point at the corner we refer the remaining of the corners to the nearest seven PUC's. We note that the basic translation vectors cannot be chosen uniquely. However, whatever the choice of these vectors, the volume of the PUC is always the same. The PUC defines the smallest volume whose translations form the whole Bravais lattice (direct lattice). Usually, the basic vectors are chosen to be the shortest of all those possible.

Atoms of a crystal are not necessarily located in the direct lattice points. In the simplest case when all the crystal is obtained by translations of one atom (such crystals are termed monoatomic, many metals belong to this type) all atoms can be placed in direct lattice points.

As a set of points, the direct lattice possesses not only translation but also point symmetry, i.e. lattice points are interchanged when rotations around one of the axes of symmetry, reflections in planes of symmetry and their combinations are applied. All the point-symmetry operations of the Bravais lattice are defined when the origin of the coordinate system is chosen in one of the lattice points. The corresponding PUC can be defined as the reference unit cell (it is obtained by a zeroth translation ($n_1 = n_2 = n_3 = 0$ in (2.5)). Among point-symmetry operations of a direct lattice it is obligatory to include inversion I in the origin of coordinates since, together with translation on a vector $\boldsymbol{a}$ the group of translations T also includes translation on a vector $-\boldsymbol{a}$. The identity element of group T is t_0—a zeroth translation. Elements R of point group F^0 transform each lattice vector into a lattice vector: $R\boldsymbol{a} = \boldsymbol{a}'$. The point group F^0 of symmetry of the direct lattice determines the crystal system (or syngony). There are seven systems (syngonies) of direct lattices. It turns out that not all point groups can be lattice symmetry groups F^0. The requirement that both $\boldsymbol{a}$ and $R\boldsymbol{a}$ can simultaneously be lattice vectors restricts the number of possible point groups. Let us now establish these limitations [7].

To establish the rotations of the group F^0, let us take the basic lattice vectors $\boldsymbol{a}_1, \boldsymbol{a}_2, \boldsymbol{a}_3$ as the basis unit vectors in the space of the lattice vectors $\boldsymbol{a}$, and write down the matrix $D(R)$ of the transformation R in the new basis, in which all the lattice vectors have integer components. If the matrix of the orthogonal transformation R in this basis is denoted by $D'(R)$, then $D'(R) = U^{-1}D(R)U$, where U is a matrix of the transformation from the initial orthonormal basis to the basis $\boldsymbol{a}_1, \boldsymbol{a}_2, \boldsymbol{a}_3$. If R is a rotation (or mirror rotation) through an angle φ the traces of the matrices $D(R)$ and $D'(R)$ are equal:

$$\mathrm{Sp}D'(R) = \mathrm{Sp}D(R) = \pm 1 + 2\cos(\varphi) \tag{2.3}$$

Since, however, R should transform the lattice vector $\boldsymbol{a}$ into the lattice vector $\boldsymbol{a}' = R\boldsymbol{a}$ it follows that all the elements of $D'(R)$ and hence its trace, must be integers. It follows that $\cos(\varphi) = \cos(2\pi\frac{m}{n}) = \pm 1, \pm 2, 0$. Consequently, the group F^0 can contain only two-, three-, four- and sixfold axes. Finally, it can be shown that if the group F^0 contains the subgroup $C_n,\ n > 2$, it will also contain the subgroup C_{nv}. The above three limitations ensure that the point group of the lattice can only be one of the seven point groups: $S_2, C_{2h}, D_{2h}, D_{3h}, D_{4h}, D_{6h}, O_h$. This is why there are only seven syngonies: namely, triclinic, monoclinic, orthorhombic, rhombohedral, tetragonal, hexagonal and cubic. It is seen that, unlike molecules, in point groups of symmetry of crystals there is no axis of symmetry of the fifth order (rotations around such axes are incompatible with the presence of translations).

Two Bravais lattices with the same group of point symmetry F^0 fall into one type if they can be transferred to each other by the continuous deformation that is not decreasing the point symmetry of a lattice. In three-dimensional space there are

Table 2.1 Distribution of crystal classes F and Bravais lattices on singonies F^0

Syngony F^0 crystal classes F	Direct lattice types	Basic translation vectors	Bravais lattice param.
Triclinic S_2: $C_1, S_2(C_i)$	P	Any noncoplanar	$a, b, c,$ α, β, γ
Monoclinic C_{2h}: C_s, C_2, C_{2h}	P A, B, C	$(0, -b, 0), (a \sin\gamma, -a\cos\gamma, 0), (0, 0, c)$ $(0, -b, 0), (1/2)(a \sin\gamma, -a\cos\gamma, -c),$ $(1/2)(a \sin\gamma, -a\cos\gamma, c)$	a, b, c, γ
Orthorhombic D_{2h}: C_{2v}, D_2, D_{2h}	P A, B, C F I	$(0, -b, 0), (a, 0, 0), (0, 0, c)$ $(1/2)(a, -b, 0), (1/2)(a, b, 0), (0, 0, c)$ $(1/2)(a, 0, c), (1/2)(0, -b, c), (1/2)(a, -b, 0)$ $(1/2)(a, b, c), (1/2)(-a, -b, c), (1/2)(a, -b, -c)$	a, b, c
Tetragonal D_{4h}: $S_4, D_{2d}, C_4, C_{4v},$ C_{4h}, D_4, D_{4h}	P I	$(a, 0, 0), (0, a, 0), (0, 0, c)$ $(1/2)(-a, a, c), (1/2)(a, -a, c), (1/2)(a, a, -c)$	a, c
Hexagonal D_{6h}: $C_3, S_6, C_{3v}, C_{3h}, D_3,$ $D_{3d}, D_{3h}, C_6, C_{6h},$ C_{6v}, D_6, D_{6h}	H	$(a/2, -a/2, 0), (0, a, 0), (0, 0, c)$	a, c
Rhombohedral D_{3d}: $C_3, S_6, C_{3v}, D_3, D_{3d}$	R	$(a, 0, c), (-a/2, a/2, c), (-a/2, -a/2, c)$	a, c
Cubic O_h: T, T_d, T_h, O, O_h	P F I	$(a, 0, 0), (0, a, 0), (0, 0, a)$ $(1/2)(0, a, a), (1/2)(a, 0, a), (1/2)(a, a, 0)$ $(1/2)(-a, a, a), (1/2)(a, -a, a)(1/2)(a, a, -a)$	a

14 types of direct lattices whose distribution on syngonies is shown in Table 2.1. In addition to the translational subgroup T, the space group contains other transformations whose form depends on the symmetry of the Bravais lattice and the symmetry of the components of the crystal, i.e. on the symmetry of the PUC as the periodically repeating set of particles forming the crystal. This last fact frequently ensures that not all the transformations in the point group F^0 are included in the symmetry group of the crystal. Not all transformations that map the sites on each other need result in a corresponding mapping of the crystal components. It is therefore possible that the point group of a crystal F (crystal class) will only be a subgroup of a point group of an empty lattice. So the real crystal structure point-symmetry group F may coincide with the lattice point symmetry group F^0 or be its subgroup. The distribution of crystal classes F and Bravais lattices on syngonies is given in Table 2.1.

The lattice types are labeled by P (simple or primitive), F (face-centered), I (body-centered) and $A(B, C)$ (base-centered). Cartesian coordinates of basic translation vectors written in units of Bravais lattice parameters are given in the third column of Table 2.1. It is seen that the lattice parameters (column 4 in Table 2.1) are

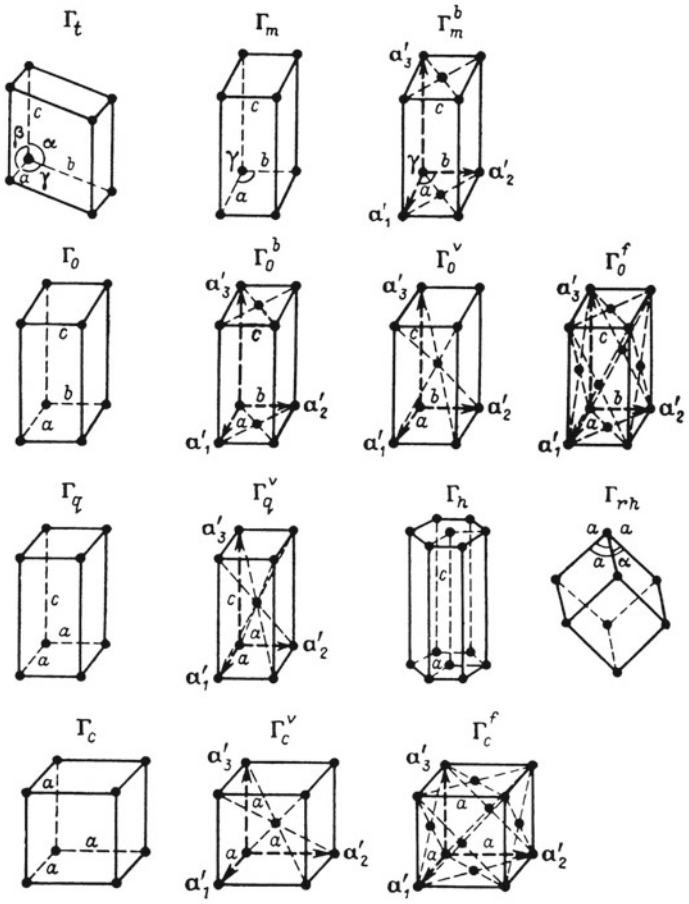

Fig. 2.1 Three-dimensional Bravais lattices

defined only by syngony, i.e. are the same for all types of Bravais lattices with the point symmetry F^0 and all the crystal classes F of a given syngony.

The point symmetry group of a *triclinic* lattice Γ_t (Fig. 2.1) consists of only inversion in the coordinates origin.

Therefore this lattice is defined by 6 parameters—lengths a, b, c of basic translation vectors and angles α, β, γ between their pairs $\boldsymbol{a}_2 - \boldsymbol{a}_3$, $\boldsymbol{a}_1 - \boldsymbol{a}_3$ and $\boldsymbol{a}_1 - \boldsymbol{a}_2$, respectively.

In simple Γ_m and base-centered Γ_m^b *monoclinic* lattices one of the vectors (with length c, for example) is orthogonal to the plane defined by two vectors with length a and b (γ is the angle between these vectors not equal to 90 or 120°). In lattice Γ_m^b the centered face can be formed by a pair of nonorthogonal lattice vectors. For example, in a C centered monoclinic lattice the lattice point appears on the face formed by $\boldsymbol{a}_1$ and $\boldsymbol{a}_2$ basic translation vectors. In the base-centered lattice one can consider so-called

conventional unit cell—the parallelepiped, reflecting the monoclinic symmetry of the lattice. For a simple monoclinic lattice Γ_m the conventional and primitive unit cells coincide, for a base-centered monoclinic lattice Γ_m^b the conventional unit cell contains 2 primitive unit cells (see Fig. 2.1).

All the three translation vectors of a simple *orthorhombic* lattice Γ_o are orthogonal to each other, so that the conventional cell coincides with the primitive cell and is defined by three parameters—lengths of the basic translation vectors. For base-centered Γ_o^b, face-centered Γ_o^f and body-centered Γ_o^v lattices the conventional unit cell contains two, four and two primitive cells, respectively (see Fig. 2.1).

The *tetragonal* lattices Γ_q (simple) and Γ_q^v (body-centered) are defined by two parameters, as two of the three orthogonal translation vectors of a conventional unit cell have the same length a.

The *hexagonal* lattice is defined by two parameters: a—length of two equal basic translation vectors (with the angle 120° between them) and c—length of the third basic translation vector orthogonal two the plane of first two vectors.

In a *rhombohedral(triclinic)* lattice all three translation vectors have the same length a, all three angles α between them are equal (but differ from 90°), so this lattice is defined by two parameters. There are two possibilities to define the rhombohedral lattice parameters. In the first case the parameters a and γ are given directly. In the second case the lengths a and c of the hexagonal unit-cell translation vectors are given: this cell consists of three primitive rhombohedral cells (so-called hexagonal setting for rhombohedral Bravais lattice).

Three *cubic* lattices (simple Γ_c, face-centered Γ_c^f and body-centered Γ_c^v) are defined by one lattice parameter a—the length of conventional cubic cell edge (see Table 2.1 and Fig. 2.1).

The unit cell of a crystal is defined as that volume of space that its translations allow all the space without intervals and superpositions to be covered. The PUC is the minimal volume $V_{\boldsymbol{a}} = \boldsymbol{a}_1[\boldsymbol{a}_2 \times \boldsymbol{a}_3]$ unit cell connected with one Bravais lattice point. Conventional unit cells are defined by two, four and two lattice points, for the base-, face- and body-centered lattices, respectively.

The 32 point groups, enumerated in Table 2.2, are known as crystallographic point groups and are given in Schönflies (Sch) notation. The Sch notation is used for molecules. In describing crystal symmetry the international notation (or Hermann–Mauguin notation) is also of use. In the latter, the point-group notation is determined from the principal symmetry elements: an n fold axis is denoted by the symbol n, a reflection mirror plane by symbol m. The symbols n/m and nm are used for the combinations of an n fold axis with the reflection plane perpendicular to the axis or containing the axis, respectively. Instead of mirror rotation axes, the international system uses inversion axes $\overline{n}$ when a rotation through an angle $2\pi/n$ is followed by the inversion operation. The full international notation of a point group consists of the symbols of group generators. Abbreviated international notations are also used. The Sch and international full and abbreviated notations of crystallographic point groups are given in Table 2.2.

Table 2.2 Crystallographic point groups: schoenflies and international notations

International			International		
Schoenflies	Full	Abbreviated	Schoenflies	Full	Abbreviated
C_n	n	n	D_2	32	32
$C_s(C_{1h})$	m	m	D_4	422	422
$C_i(S_2)$	I	T	D_6	622	622
S_4	$\overline{4}$	$\overline{4}$	D_{2h}	$2/m\ 2/m\ 2/m$	mmm
S_6	$\overline{3}$	$\overline{3}$	D_{3h}	$6m2$	$6m2$
C_{2h}	$2/m$	$2/m$	D_{4h}	$4/m\ 2/m\ 2/m$	$4/mmm$
C_{3h}	$\overline{6}$	$\overline{6}$	D_{6h}	$6/m\ 2/m\ 2/m$	$6/mmm$
C_{4h}	$4/m$	$4/m$	D_{2d}	$42m$	$42m$
C_{6h}	$6/m$	$6/m$	D_{3d}	$32/m$	$3m$
C_{2v}	$2mm$	$2mm$	T	23	23
C_{3v}	$3m$	$3m$	T_h	$2/m3$	$m3$
C_{4v}	$4mm$	$4mm$	T_d	$43m$	$43m$
C_{6v}	$6mm$	$6mm$	O	432	432
D_2	222	222	O_h	$4/m\ 3\ 2/m$	$m3m$

Let us make a linear transformation of PUC translation vectors:

$$\boldsymbol{A}_j = \sum_{i=1}^{3} l_{ji}\boldsymbol{a}_i, \quad |\det \boldsymbol{l}| = L \tag{2.4}$$

where the integer coefficients l_{ji} form the matrix l. Vectors $\boldsymbol{A}_j$ and their integer linear combinations

$$\boldsymbol{A_n} = \sum_{j=1}^{3} n_j \boldsymbol{A}_j \tag{2.5}$$

define for $L > 1$ new, "rare" Bravais lattice for which it is possible to consider various unit cells also. The primitive cell of a new lattice with volume $V_{\boldsymbol{A}} = L \times V_{\boldsymbol{a}}$ will be the so-called large unit cell (supercell), in relation to an initial primitive unit cell. At $L = 1$ transformation (2.4) means transferring to other vectors of the basic translations, to another under the form, but not on the volume primitive cell (see Fig. 2.2).

The so called crystallographic(conventional) unit cell with the translation vectors **a**, **b**, and **c** is defined as the minimal volume unit cell in the form of a parallelepiped constructed on vectors of translations and possessing the point symmetry of the lattice. The conventional unit cell coincides with the primitive unit cell for the simple lattices. The conventional unit cell for the centered lattices consists of integer number of the primitive unit cells forming the supercell of the Bravais lattice.

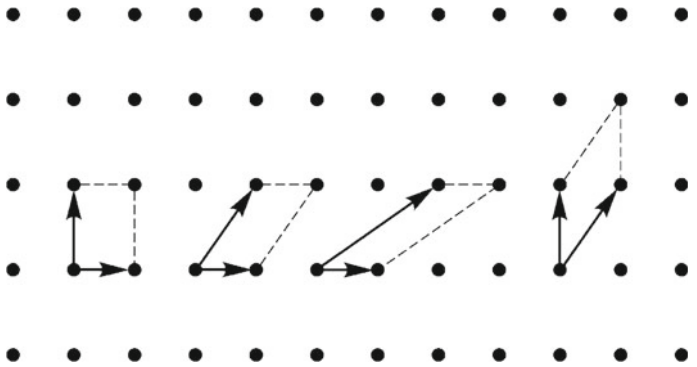

Fig. 2.2 Different primitive unit cell choices

Indeed, for simple lattices P of all syngonies, except for hexagonal (H), the defining primitive unit cell vectors of the basic translations $\boldsymbol{a}_1, \boldsymbol{a}_2, \boldsymbol{a}_3$ can be chosen in such a manner that the primitive cell constructed on them is crystallographic. For the centered lattices the crystallographic unit cells consist of 2, 4 and 2 primitive cells for base-, face- and body-centered lattices, respectively (Fig. 2.1). In the description of symmetry of a trigonal crystal both rhombohedral and hexagonal cells are used. The latter is defined by transformation (2.4) with a matrix

$$l = \begin{pmatrix} 2 & 1 & 0 \\ -1 & 1 & 0 \\ 1 & 1 & 1 \end{pmatrix} \tag{2.6}$$

and $L = 3$. As $L = 3$ for this matrix the hexagonal unit cell contains 3 rhombohedral unit cells.

2.2.2 Symmorphic and Nonsymmorphic Space Groups

As considered in the previous section Bravais lattices define the group T of lattice translations. The general symmetry transformation of a Bravais lattice ("empty" lattice) can be written in the form $t_{\boldsymbol{a}} R$. Operations R transform any translation vector $\boldsymbol{a}$ to another translation vector $R\boldsymbol{a}$ and form point group F^0 (holohedric point group). The combined operation $t_{\boldsymbol{a}} R$ transforms the point of space with radius-vector $\boldsymbol{r}$ to an equivalent point $\boldsymbol{r}' = R\boldsymbol{r} + \boldsymbol{a}$. The identity element of the Bravais lattice symmetry group is $t_{\boldsymbol{0}} E$. The multiplication law for operations $t_{\boldsymbol{a}} R$ is:

$$t_{\boldsymbol{a}_1} R_1 t_{\boldsymbol{a}_2} R_2 \boldsymbol{r} = R_1 R_2 \boldsymbol{r} + \boldsymbol{a}_1 + R_1 \boldsymbol{a}_2 = t_{\boldsymbol{a}_1 + R_1 \boldsymbol{a}_2} R_1 R_2 \boldsymbol{r} \tag{2.7}$$

so that

$$(t_{\boldsymbol{a}} R)^{-1} \boldsymbol{r} = R^{-1} \boldsymbol{r} - R^{-1} \boldsymbol{a} = t_{-R^{-1}\boldsymbol{a}} R^{-1} \boldsymbol{r} \tag{2.8}$$

The operations $t_{\boldsymbol{a}}$ and R do not commute. Indeed

$$t_{\boldsymbol{a}} R\boldsymbol{r} = R\boldsymbol{r} + \boldsymbol{a}; \quad \boldsymbol{a}\boldsymbol{r} = R(\boldsymbol{r} + \boldsymbol{a}) = R\boldsymbol{r} + t_{R\boldsymbol{a}} = t_{R\boldsymbol{a}} R\boldsymbol{r} \tag{2.9}$$

so that

$$t_{\boldsymbol{a}} R = R t_{R^{-1}\boldsymbol{a}} \tag{2.10}$$

Operations $t_{\boldsymbol{a}} R$ form the space group G^0 of an "empty" Bravais lattice. As lattice translations (also called proper translations) $t_{\boldsymbol{a}}$ and point-symmetry operations R do not commute the space groups $G^0 = T \wedge F^0$ are a semidirect product of the translation and point groups of lattice symmetry. The point symmetry operations R form subgroup F^0 of space group G^0 (such space groups are termed symmorphic space groups). The group T of pure translations forms an invariant subgroup of G^0. As $\boldsymbol{t}_{\boldsymbol{a}}^{-1} = \boldsymbol{t}_{-\boldsymbol{a}}$ we have $(\boldsymbol{t}_{\boldsymbol{a}} R)^{-1} \boldsymbol{t}_{\boldsymbol{a}'} \boldsymbol{t}_{\boldsymbol{a}} R = (\boldsymbol{t}_{\boldsymbol{a}} R)^{-1} \boldsymbol{t}_{\boldsymbol{a}+\boldsymbol{a}'} R = \boldsymbol{t}_{R\boldsymbol{a}'}$.

The group of translations T is a subgroup of the full group symmetry G (space group) that also contains operations of point group F and their combinations with translations.

Any symmetry operation g of a crystal with space group G can be written in the form of $g_i = t_{\boldsymbol{v}_i + \boldsymbol{a}} R_i$ where $\boldsymbol{v}_i$ is the so-called improper (fractional) translation, depending on element R_i of a point group of a crystal and satisfying the requirements described below. The operation g_i transforms the point of space with radius-vector $\boldsymbol{r}$ to an equivalent point $\boldsymbol{r}' = g_i \boldsymbol{r} = R_i \boldsymbol{r} + \boldsymbol{v}_i$. The operations $t_{\boldsymbol{a}}$ are elements of the group of translations T – translations on the corresponding vector of the Bravais lattice.

In crystals, unlike molecules, together with rotations through axes of symmetry and reflections in planes there exist rotations through screw axes (rotation followed by translation along a rotation axis on a part of a vector of translation) and reflections in planes with partial translation in a plane (such planes are termed glide planes). Translation along a screw axis of symmetry cannot be arbitrary and depends on the order of this axis. Let the order of an axis be equal to n (n rotations through axis are equivalent to an identity operation). Thus, n translations along an axis should give a vector of translation of a lattice, i.e. an element of group T that forms a subgroup of a space group of a crystal. Otherwise, rotation through a screw axis will not be an operation of symmetry. For example, rotation through an axis of the fourth order can be accompanied by translation along this axis on a quarter or half of the vector of translation. A similar requirement is imposed on the operation of sliding reflection: two sequential reflections in a glide plane should be equivalent to translation on a vector of a lattice. By definition, any symmetry operation g of a space group transforms any atom of a crystal to equivalent atom. The equivalent atoms are always the atoms of the same chemical identity but the latter can be nonequivalent.

Therefore, fractional (improper) translations can appear only in those crystals that contain several equivalent atoms in the primitive unit cell. The presence of identical atoms in a primitive cell—a condition necessary, but insufficient for the occurrence of fractional translations in the space-group elements. As an example, we consider in Sect. 2.3 the perovskite $CaTiO_3$ structure with three equivalent oxygen atoms in a primitive unit cell and symmorphic space group O_h^1.

The set of fractional translations $\boldsymbol{v}$ in the space-group elements $g = t_{\boldsymbol{v}} R$ depends on the choice of origin (with respect to which the space-group elements are written) and on the labeling of axes (choice of setting) [2].

By definition, the symmorphic space groups contain, together with each element $t_{\boldsymbol{a}} R$, the elements R and $t_{\boldsymbol{a}}$ of the point group F and translation group T, respectively. This means that for a symmorphic space group the origin of the coordinate system may be chosen in such a way that the local (site) symmetry group of origin coincides with the point group of the crystal F. This means that all fractional translations $\boldsymbol{v}$ are zero. Such a choice of origin is accepted for symmorphic space groups in the International tables [2]. For nonsymmorphic space groups some fractional translations will be nonzero for any choice of origin.

The full information on space groups is given in the International Tables for Crystallography [2] and presented on a site [8]. The knowledge of general principles of the space-group designations is necessary to use the crystal-structure databases correctly.

There are three systems of designations of space groups. First, all groups are numbered from 1 upto 230 in order of increasing point symmetry of the corresponding Bravais lattice (syngonies from triclinic to cubic). For fixed syngony the ordering is made over Bravais lattice types and for the fixed Bravais lattice type—over crystal classes (point group F) beginning from the symmorphic space group. In this list, the space groups of "empty" lattices appear as the first ones for fixed type of the lattice. Secondly, the more informative Schönflis symbol is used for space groups. This contains the Schönflis symbol of point group F of a crystal class and the upper numerical index distinguishing space groups within the limits of one crystal class.

Thirdly, the most detailed information on a space group is contained in so-called international (Hermann–Mauguin) designations. In these is there both a symbol of the Bravais lattice type, and a symbol of a crystal class with the indication of the elements of symmetry (axes and planes).

For a designation of types of Bravais lattices the following symbols are used: P simple (or primitive); A, B, C—one face (base-) centered; F—face-centered; I—body-centered. For hexagonal and trigonal (rhombohedral) lattices symbols H and R are accepted.

The centering type symbol is followed by a set of characters indicating the symmetry elements. These sets are organized in the following way.

The two dimensional (plane) lattice symmetry directions are chosen along the conventional unit cell translation vectors **a** and **b**. The one or two entries refer to one or two kinds of the plane lattice symmetry directions.

The one, two or three entries after the centring letter refer to the one, two or three kinds of symmetry directions of the three-dimensional lattice belonging to the

space group. The three-dimensional lattice symmetry directions are chosen along the conventional unit cell translation vectors **a**, **b**, and **c** and occur either as singular directions (as in the monoclinic and orthorhombic crystal systems) or as sets of symmetrically equivalent symmetry directions (as in the higher-symmetrical crystal systems).

The (sets of) lattice symmetry directions and their sequence for the different lattices are summarized in Table 2.3 given in [2] for two-dimensional (plane) and three-dimensional lattices.Only one representative of each set is required. According to their position in this sequence, the symmetry directions are referred to as primary, secondary and tertiary directions.This sequence of lattice symmetry directions is transferred to the sequence of positions in the corresponding Hermann-Mauguin space-group symbols. Each position contains one or two characters designating symmetry elements (axes and planes) of the space group that occur for the corresponding lattice symmetry direction. Symmetry planes are represented by their normals; if a symmetry axis and a normal to a symmetry plane are parallel, the two characters (symmetry symbols) are separated by a slash. The plane lattices have only two lattice symmetry directions as the primary symmetry direction is the rotation point in plane. The plane lattices are discussed in the next section, where the layer groups are considered.

The list of 230 three-periodic space groups is given in Appendix A.

The seven holohedric point groups F^0 and all their subgroups form 32 crystallographic point groups (32 crystalline classes). By combining these 32 point groups with the translation groups of 14 Bravais lattices, 73 symmorphic space groups are obtained, including 14 space groups of the symmetry of empty Bravais lattices (see Table A.1). The remaining 157 space groups include point-symmetry operations with improper (partial) translations, i.e. rotations through screw axes and reflections in glide planes.

There exist only two triclinic space groups (1, 2) with symbols $P1$ (no point-symmetry operations) and $P\overline{1}$ (the inversion operation appears, this is the symmetry group of triclinic Bravais lattice). For monoclinic space groups (3–15) one symbol is needed that gives the nature of the twofold axis (rotation axis 2 or screw axis 2_1) or reflection plane (mirror plane m or glide plane c). Two settings are used for monoclinic space groups: y-axis unique, or, used in Table A.1, z-axis unique. Primitive and base-centered (z-axis unique) monoclinic Bravais lattices symmetry groups are $P2/m$ (10) and $C2/m$ (11), respectively.

The symbols of orthorhombic space groups (16–74) contain the three sets. For symmorphic groups as a symbol of a crystal class the international designation of point groups corresponding to it serves. In Table A.1 conformity of Schönflies's symbols (applied for molecules) and international symbols for point groups of symmetry of crystals is given. For example, $N225$, O_h^5 and $Fm\overline{3}m$—three symbols of the same space group of symmetry of a crystal with NaCl structure.

For nonsymmorphic groups in a symbol of the point group it is underlined also, which axes are screw and which planes are planes of the sliding reflections.

Table 2.3 Lattice symmetry directions for two and three dimensions

	Symmetry direction (position in Hermann-Mauguin symbol)		
	Primary	Secondary	Tertiary
Two dimensions			
Oblique	Rotation point in plane		
Rectangular		[10]	[01]
Square		{[10], [01]}	{$[1\bar{1}]$, [11]}
Hexagonal		{[10], [01], $[\bar{1}\bar{1}]$}	{$[1\bar{1}]$, [12], $[\bar{2}\bar{1}]$}
Three dimensions			
Triclinic	None		
Monoclinic	[010] ('unique axis *b*') [001] ('unique axis *c*')		
Orthorhombic	[100]	[010]	[001]
Tetragonal	[001]	{[100], [010]}	{$[1\bar{1}0]$, [110]}
Hexagonal	[001]	{[100], [010], $[\bar{1}\bar{1}0]$}	{$[1\bar{1}0]$, [120], $[\bar{2}\bar{1}0]$}
Rombohedral (hexagonal axes)	[001]	{[100], [010], $[\bar{1}\bar{1}0]$}	
Rombohedral (rhombohedral axes)	[111]	{$[1\bar{1}0]$, $[01\bar{1}]$, $[\bar{1}01]$}	
Cubic	{[100], [010], [001]}	{[111], $[1\bar{1}\bar{1}]$, $[\bar{1}1\bar{1}]$, $[\bar{1}\bar{1}1]$}	{$[1\bar{1}0]$[110], $[01\bar{1}]$[011], $[\bar{1}01]$[101]}

Directions that belong to the same set of equivalent symmetry directions are collected between braces. The first entry in each set is taken as the representative of that set

For example, for the group of symmetry of rutile structure it is possible to use designations $N136$, D_{4h}^{14} or $P4_2/mnm$, where the symbol 4_2 means that an axis of the fourth order is a screw axis, with translation on half a period along this axis on rotation by angle $\pi/2$, and a symbol n means that two of the four vertical planes are planes of sliding reflection. A more detailed explanation of the principles of international designations can be found in [2].

2.2.3 Orbits of Triperiodic Groups. Wyckoff Positions

To characterize a space group G an analytical description may be employed, which states for a space group the coordinates of all points that are equivalent to a chosen point $\boldsymbol{q}$ with coordinates (xyz). An analytical description of all 230 space groups is given in the International Tables for Crystallography [2] and is based on the fact that for a given space group G all points of a three-dimensional space are subdivided into sets of symmetrically equivalent points called crystallographic orbits (G-orbits).

All the points of a given crystallographic orbit may be obtained from one (arbitrary) G-orbit point $\boldsymbol{q}$ (generating point) by applying to the latter all the operations of space group G. Due to the infinite number of translations (in the model of an infinite crystal) there is an infinite number of points in each space group crystallographic orbit. Any one of the crystallographic orbit points may represent the whole crystallographic orbit, i.e. may be a generating point $\boldsymbol{q}$ of the crystallographic orbit.

All the space group G symmetry operations $t_{\boldsymbol{v}_i+\boldsymbol{a}}R_i = (R_i|\boldsymbol{v}_i + \boldsymbol{a}), i = 1, 2, \ldots, n_{\boldsymbol{q}}$ that satisfy the condition $t_{\boldsymbol{v}+\boldsymbol{a}}R\boldsymbol{q} = \boldsymbol{q}$ (i.e. map a point $\boldsymbol{q}$ onto itself) form a finite site-symmetry group $\mathrm{G}_{\boldsymbol{q}}$ of $\boldsymbol{q}$ with respect to G. This finite size group is called by stabilizer of the G-orbit. The site-symmetry group $\mathrm{G}_{\boldsymbol{q}}$ is isomorphic to one of the 32 crystallographic point groups. If the origin of the space group is at the position $\boldsymbol{q}$, the elements of the site-symmetry group $\mathrm{G}_{\boldsymbol{q}}$ will be of the form $t_{\boldsymbol{0}}R$.

The site-symmetry groups G_j of different points $\boldsymbol{q}_j$ of the same G-orbit are conjugate groups of $\mathrm{G}_1 = \mathrm{G}_{\boldsymbol{q}}$, i.e. the site-symmetry groups G_1 and G_j of points $\boldsymbol{q}_1 = \boldsymbol{q}$ and $\boldsymbol{q}_j$ of the same orbit are related by $g_j\mathrm{G}_1g_j^{-1} = G_j (g_j \in G, g_j \notin G_j, g_j\boldsymbol{q}_1 = \boldsymbol{q}_j)$. For a point $\boldsymbol{q}$ at a general position the site-symmetry group $\mathrm{G}_{\boldsymbol{q}}$ consists of only the identity operation $t_{\boldsymbol{0}}E = (E|\boldsymbol{0})$; the site-symmetry group of a point at a special position includes at least one other symmetry operation in addition to the identity operation.

An infinite number of crystallographic orbits for a given space group G can be subdivided into sets of so-called Wyckoff positions of G. All the crystallographic orbits that have the same set of stabilizers (not only isomorphic but the same!) belong to the same Wyckoff position and can be called by equivalent G-orbits. If the coordinates of the generating point of a crystallographic orbit do not contain free parameters, the corresponding Wyckoff position consists of only one crystallographic orbit; in other cases an infinite number of crystallographic orbits belongs to the same Wyckoff position with variable parameters.

The different Wyckoff positions are the sets of the non-equivalent G-orbits and are labeled by small Roman letters. The maximum number of different Wyckoff positions of a space group is 27 (in the orthorhombic space group D_{2h}^1—$Pmmm$). The various possible sets of Wyckoff positions for all the space groups are given in the International Tables for Crystallography [2] and reproduced on an Internet site [8]. The oriented site-symmetry symbols are employed to show how the symmetry elements at a site are related to the symmetry elements of the crystal lattice. The site-symmetry symbols display the same sequence of lattice symmetry directions as the space-group symbol (see Table 2.3). Sets of equivalent symmetry directions that do

not contribute any element to the site symmetry group are represented by a dot. In this way, the orientation of the symmetry elements at the site is emphasized as illustrated by the several examples in [2]. We consider here one of these examples—the cubic space group $G = Pn\bar{3}n$ (the space group number 222). G-orbit b consists of six points and has 42.2 as its oriented site-symmetry symbol. This cubic site-symmetry symbol displays a tetragonal site symmetry. The position of the dot indicates that there is no symmetry along the four secondary cubic directions. The fourfold axis is connected with one of the three primary cubic symmetry directions and two equivalent twofold axes occur along the remaining two primary directions. Moreover, the group contains two mutually perpendicular (equivalent) twofold axes along those two of the six tertiary cubic directions [110] that are normal to the fourfold axis. Each pair of equivalent twofold axes is given by just one symbol 2. (Note that at the six sites of position 6b the fourfold axes are twice oriented along the simple cubic lattice vector **a**, twice along **b** and twice along **c**.)

As a second example, Table 2.4 lists the oriented site-symmetry symbols for the space group $D_{4h}^{14}(P4_2/m2_1/n2/m)$, the symmetry group of a rutile structure (see Sect. 2.3.3).

For this group there are 11 different Wyckoff positions (11 types of non-equivalent orbits) denoted by letters from a to k. The number of crystallographic orbit points in the primitive unit cell (multiplicity) equals $n_F/n_{\boldsymbol{q}}$ where $n_F = 16$ is the order of the point group D_{4h} and $n_{\boldsymbol{q}}$ is the order of the site symmetry group $G_{\boldsymbol{q}}$. The number of points in a Wyckoff position and their coordinates are given in the International Tables with respect to the conventional unit cell of the lattice (for the space group D_{4h}^{14} with a simple Bravais lattice, the conventional unit cell coincides with the primitive unit cell). Use of the Wyckoff general position $k(xyz)$ points allows one to determine the appropriate Seitz space-group symbols for the coset representatives in the decomposition

$$G = \sum_{i=1}^{n_F} (R_i|\boldsymbol{v}_i)T = \sum_{i=1}^{n_F} t_{\boldsymbol{v}_i} R_i T \tag{2.11}$$

of space group G with respect to the translation group T. In Table 2.4 these symbols are written under the coordinates of the points obtained from the point $\boldsymbol{r}(x, y, z)$ by performing the space-group operation $t_{\boldsymbol{v}}R$. The orientation of the symmetry elements with respect to the tetragonal lattice translation vectors $\boldsymbol{a}_1(a, 0, 0)$, $\boldsymbol{a}_2(0, a, 0)$ and $\boldsymbol{a}_3(0, 0, c)$ is shown in Fig. 2.3. In the point group D_{4h} there are four rotations around twofold axes ($U_x, U_y, U_{xy}, U_{\bar{x}y}$) and four rotations (including the identity operation) around the main fourfold z-axis ($E, C_{4z}, C_{4z}^2 = C_{2z}, C_{4z}^3 = C_{4z}^{-1}$).

The remaining 8 symmetry operations are all products of inversion I with rotations: I, reflections $\sigma_x, \sigma_y, \sigma_{xy}, \sigma_{\bar{x}y}, \sigma_z$ in the planes perpendicular to the corresponding twofold axes and z-axis; mirror rotations S_{4z}^{-1}, S_{4z}. It is seen from Table 2.4 that the elements of the point group $D_{2h}(E, C_{2z}, U_{xy}, U_{\bar{x}y}, I, \sigma_z, \sigma_{xy}, \sigma_{\bar{x}y})$ appear in the cosets decomposition (2.11) without fractional translations. These elements form the site symmetry group of the coordinate system origin placed at the point

Table 2.4 Wyckoff positions of space group 136 ($P4_2/mnm$)

Multipl.	Wyck. letter	Site symm.	Coordinates
16	k	1	$(x, y, z)(-x, -y, z)(-y + 1/2, x + 1/2, z + 1/2)$ $(y + 1/2, -x + 1/2, z + 1/2)(-x + 1/2, y + 1/2, -z + 1/2)$ $(x + 1/2, -y + 1/2, -z + 1/2)(y, x, -z)(-y, -x, -z)$ $(-x, -y, -z)(x, y, -z)(y + 1/2, -x + 1/2, -z + 1/2)$ $(-y + 1/2, x + 1/2, -z + 1/2)(x + 1/2, -y + 1/2, z + 1/2)$ $(-x + 1/2, y + 1/2, z + 1/2)(-y, -x, z)(y, x, z)$
8	j	..m	$(x, x, z)(-x, -x, z)(-x + 1/2, x + 1/2, z + 1/2)$ $(x + 1/2, -x + 1/2, z + 1/2)(-x + 1/2, x + 1/2, -z + 1/2)$ $(x + 1/2, -x + 1/2, -z + 1/2)(x, x, -z)(-x, -x, -z)$
8	i	m..	$(x, y, 0)(-x, -y, 0)(-y + 1/2, x + 1/2, 1/2)$ $(y + 1/2, -x + 1/2, 1/2)(-x + 1/2, y + 1/2, 1/2)$ $(x + 1/2, -y + 1/2, 1/2)(y, x, 0)(-y, -x, 0)$
8	h	2..	$(0, 1/2, z)(0, 1/2, z + 1/2)(1/2, 0, -z + 1/2)$ $(1/2, 0, -z)(0, 1/2, -z)(0, 1/2, -z + 1/2)$ $(1/2, 0, z + 1/2)(1/2, 0, z)$
4	g	m.2 m	$(x, -x, 0)(-x, x, 0)(x + 1/2, x + 1/2, 1/2)$ $(-x + 1/2, -x + 1/2, 1/2)$
4	f	2.m m	$(x, x, 0)(-x, -x, 0)(-x + 1/2, x + 1/2, 1/2)$ $(x + 1/2, -x + 1/2, 1/2)$
4	e	2.m m	$(0, 0, z)(1/2, 1/2, z + 1/2)(1/2, 1/2, -z + 1/2)$ $(0, 0, -z)$
4	d	$\bar{4}$..	$(0, 1/2, 1/4)(0, 1/2, 3/4)(1/2, 0, 1/4)$ $(1/2, 0, 3/4)$
4	c	2/m..	$(0, 1/2, 0)(0, 1/2, 1/2)(1/2, 0, 1/2)(1/2, 0, 0)$
2	b	m.m m	$(0, 0, 1/2)(1/2, 1/2, 0)$
2	a	m.m m	$(0, 0, 0)(1/2, 1/2, 1/2)$

Equivalent sets of Wyckoff positions
(ab)(c)(d)(e)(fg)(h)(i)(j)(k)

of Wyckoff position $a(0, 0, 0)$. The second point of this position (1/2, 1/2, 1/2) is obtained from the first one by application of any symmetry operation from these eight (C_{4z}, C_{4z}^{-1}, S_{4z}, S_{4z}^{-1}, U_x, U_y, σ_x, σ_y) that come into the coset representatives in (2.15) with fractional translation $\boldsymbol{v} = (1/2, 1/2, 1/2)$. We therefore write the space group D_{4h}^{14} (for the case when the Wyckoff position a is taken as the origin) as

$$D_{4h}^{14} = \sum_{R \in D_{2h}} \left[(R|0)\mathrm{T} + (U_x|\frac{1}{2}\frac{1}{2}\frac{1}{2})(R|0)\mathrm{T} \right] \tag{2.12}$$

Considering the full international symbol $P4_2/m2_1/n2/m$ of the space group D_{4h}^{14}, we see that the coset representatives in the decomposition of (2.12) with respect

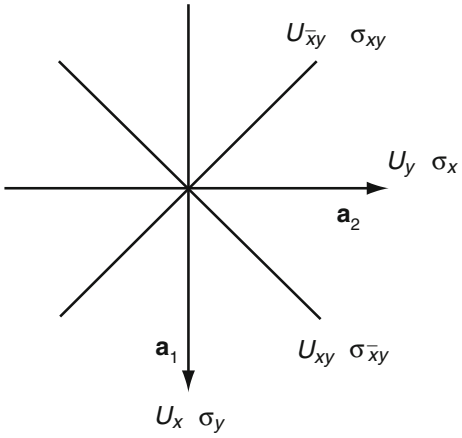

Fig. 2.3 Orientation of the symmetry elements with respect to the tetragonal lattice translations

to the translation group T correspond to this symbol. Indeed, in our example of a tetragonal lattice the three positions in this symbol correspond to the symmetry directions [001]; [100], [010]; and [1$\bar{1}$0], [110], respectively. Rotation through the angle $\pi/2$ about the z-axis is followed by translation along this axis by one-half of the translation vector $\boldsymbol{a}_3$ as is seen from the symbol for the element $(C_{4z}|l/2, 1/2, 1/2)$. The notations 2_1 and 2 for twofold x- and xy-rotation axes agree with the fourfold symbols for $(U_x|\frac{1}{2}\frac{1}{2}\frac{1}{2})$ and $(U_{xy}|000)$. Finally, the notations m, n, m for the reflection planes perpendicular to the corresponding symmetry directions in the international symbol for the space group agree with the Seitz symbols $\sigma_z|000)$, $(\sigma_x|\frac{1}{2}\frac{1}{2}\frac{1}{2})$, and $(\sigma_x y|000)$, respectively. The space group D_{4h}^{14} may also be described by its six generators: three primitive translations $t_{\boldsymbol{a}_i} = (E|\boldsymbol{a}_i)(i = 1, 2, 3)$ of the simple tetragonal lattice and three generating elements $(C_{4z}|1/2, 1/2, 1/2)$, $(U_x|1/2, 1/2, 1/2)$, $(I|0, 0, 0)$.

The coordinates of Wyckoff positions a, b, c, d do not contain free parameters (Table 2.4); those of e, f, g, h positions contain one free parameter; the coordinates of the positions i and j contain two free parameters. This means that an infinite number of Wyckoff sets e–f exists in the crystal but the sets a, b, c, d consist of only one crystallographic orbit. Pairs of Wyckoff positions a–b, f–g, and i–j have isomorphic site symmetry groups (D_{2h}, C_{2v} and C_s, respectively).

As is seen from the Table pairs of Wyckoff positions a–b and f–g have the same point-group symmetry and the same orientation of the symmetry elements with respect to the lattice. The orbits in each pair of these Wyckoff positions form physically equivalent orbits [9]. The physically equivalent orbits have the different sets of the stabilizers and therefore refer to the non-equivalent orbits. It becomes evident if one moves the coordinate system origin from a-point to b-point: the new set of a- and f- orbit stabilizers differs from the former one by the pure translations. At the same time the different origin choice can not change the physical properties of the crystal structure defined by a space group G. For example, the rutile TiO_2 structure with the space group $D_{4h}^{14}(P4_2/m2_1/n2/m)$ and two formula units in the

primitive cell (Z = 2) can be given in two equivalent descriptions: Ti($2a$)O($4f$) or Ti($2b$)O($4g$). The physically equivalent sets of Wyckoff positions for all the space groups can be found on the Internet site [8]. This information will be used in the next section for the description of different crystal lattice structures. This means that if equivalent points are occupied by atoms in the crystal lattice there are possible equivalent descriptions of this structure. For $NbOCl_3$ structure ($Z = 4$) with the same space group two equivalent descriptions can be given: Nb($4f$)O($4g$)Cl($4g$)Cl($8i$) and Nb($4g$)O($4f$)Cl($4f$)Cl($8i$). In this case, the Cl($8i$) position is the same but Cl($4f$) and Cl($4g$) positions interchange.

The difference between oriented site-symmetry groups of different Wyckoff positions is due to different orientations of the elements of the site-symmetry group $G_{\boldsymbol{q}}$ with respect to the lattice. The difference arises when similar symmetry elements (reflections in planes and rotations about twofold axes of symmetry) occur in more than one class of elements of the point group F. Only eleven site groups [$C_2(2)$, $C_s(m)$, $C_{2h}(2/m)$, $C_{2v}(2mm)$, $C_{3v}(3mm)$, $D_2(222)$, $D_3(322)$, $D_{2d}(42m)$, $D_{3d}(32m)$, $D_{2h}(mmm)$, and $D_{3A}(62m)$] can have different orientations with respect to the Bravais lattice. Oriented site-symmetry symbols show how the symmetry elements at a site are related to the symmetry elements of a space group. The site-symmetry symbols display the same sequence of symmetry directions as the space-group international symbol. Sets of equivalent symmetry directions that do not contribute any element to the site-symmetry group $G_{\boldsymbol{q}}$ are represented by a dot. In our example of the space group D_{4h}^{14} the site-symmetry groups G_a, G_b do not contain reflection in the planes σ_x, σ_y (the dot is at the second position) and the site group $G_e = 2.mm$ does not contain reflection in the plane σ_z (a dot is at the first position, Table A.1).

The *Bravais lattice* is an infinite set of points generated by three nonparallel basic translation vectors, such that each point is identical in itself and its surroundings, see Sect. 2.2.1. With each Bravais lattice point may be associated a number of atoms (so-called basis). If atomic coordinates relative to the lattice point are given, together with the lengths and directions of the lattice vectors chosen to define the axes of reference, the complete structure (crystal lattice) is defined. The Internet page [10] currently contains links to about 300 structures in more than 90 of the 230 space groups. A graphical representation as well as useful information about these crystal lattices can be obtained. Other sources of information can be found at various sites linked with [11].

The application of symmetry transformations means splitting all space into systems of equivalent points. The sets of these points for molecules are given in [12]. The sets of equivalent points for crystals are known as Wyckoff positions, irrespective of whether there are atoms in these points or not. The total number of possible splittings of the three-dimensional space of a crystal on systems of equivalent points is finite and for the three-dimensional periodicity case equals 230 (number of space groups of crystals) [2].

The crystal-structure type is specified when one states which sets of Wyckoff positions for the corresponding space group are occupied by atoms. To distinguish different structures of the same type one needs the numerical values of lattice

parameters and additional data if Wyckoff positions with free parameters in the coordinates are occupied. The various ways of filling of equivalent points by atoms generate a huge (hundreds of thousands) number of real crystalline structures.

When describing the crystal-structure type one also gives the value of Z (the number of formula units in the conventional unit cell). This information is, in principle, not necessary as Z is defined by the chemical formula of the compound and the multiplicity of Wyckoff positions in the unit cell occupied by atoms. It is also necessary to take into account that the primitive unit cell of any crystal contains half the number of atoms in a body-centered cell, one-quarter the number in a face-centered, and half the number in an A, B, or C base-centered cell. Trigonal cells contain one-third the number of atoms in the corresponding hexagonal cell. The Wyckoff-site description of a crystal-structure type is also origin dependent (see Sect. 2.2.3). It was shown that equivalent alternatives often arise if two or more sets of sites are physically equivalent (see Sect. 2.2.3). The crystal lattice structure types can be indexed in different ways [10]. In *Strukturbericht* designation symbols A and B are used for monoatomic and diatomic (with equal numbers of atoms of each type) crystal types, symbols C and D—for AB_2 and A_nB_m compounds, respectively. Symbols $E, F, G, \ldots, K$ specify more complex compounds, symbols L, O, and S specify alloys, organic compounds and silicates. *The Pearson symbol* indicates the crystal symmetry and the number of atoms in the conventional unit cell. For example, rocksalt NaCl structure has a face-centered (F) cubic (c) structure with 8 atoms in the cubic (nonprimitive!) unit cell, so it is designated $cF8$. The letters m, o, t, h, c are used in Pearson symbols for monoclinic, orthorhombic, tetragonal, hexagonal, trigonal and cubic Bravais lattice-types, respectively. Pearson symbols do not necessarily specify a unique structure: diamond, NaCl and zincblende $cF8$ structures differ by symbols $A, B1$ and $B3$ (numbers in symbols $B1$ and $B3$ were assigned in roughly the historical order of the study of crystal lattices). *The prototype index* is an index of the various crystal structures by prototype compound (diamond, rocksalt, zincblende structures). Some compounds can be associated with more than one prototype: ZnS compound can be found in zincblende and wurtzite structure. Finally, the *space group index* of a structure can be used. Space groups are listed in the order they appear in the International Tables [2]. As space groups refer to one of seven syngonies the structures are ordered as triclinic (space groups 1 and 2), monoclinic (3–15), orthorhombic (16–74), tetragonal (75–142), trigonal (143–167), hexagonal (168–194) and cubic (195–230). For example, cubic structures correspond to the three Pearson symbols cPn, cFn and cIn.

In the next subsections we give short descriptions of those crystal structures which are basis for the nanotubes and nanowires modeling discussed in Part II Applications. We use space-group and prototype indexes in subsection titles. In the corresponding tables we give for each structure all the mentioned indexes. These tables show that the same compound can be found in different structures (C—diamond, graphite, ZnS—sphalerite, wurtzite, $CaTiO_3$—cubic perovskite, distorted (orthorhombic) perovskite, TiO_2—rutile, anatase). Different structures can have the same Bravais lattice (diamond, NaCl, fluorite, sphalerite) or even the same space group (rocksalt NaCl—fluorite CaF_2). For any structure type we give the prototype, space group (number and

international symbol), number of formula units in the primitive and conventional unit cells, the occupation of Wyckoff positions by atoms and the equivalent Wyckoff-site description.

This possibility of different equivalent descriptions of the crystal-structure types has to be taken into account when the symmetry of electron and phonon states in crystals is analyzed. Furthermore, when preparing the input data for modern computer codes one usually takes crystal-structure data from the database or original papers. These data often contain information about the structure in the form accepted in ICSD (Inorganic Crystal Structure Database), see site [13].

As an example, we take the data for rutile structure given in this database (in brackets some clarifications are given).

COL ICSD Collection Code 82656

DATE Recorded June 26, 1998; updated Nov 30, 1999

NAME Titanium dioxide

MINERAL Rutile—synthetic at 1573 K

REFERENCE Journal of Solid State Chemistry 127 (1996) 240–247

CELL (lattice parameters for simple tetragonal lattice, unit cell volume and number of formula units in conventional cell): $a = 4.594(0)$ $b = 4.594(0)$ $c = 2.959(0)$ $\alpha = 90.0$ $\beta = 90.0$ $\gamma = 90.0$ $V = 62.4$ $Z = 2$

SGR (space group) $P\,4_2/m\,n\,m$ (136)—tetragonal

CLAS (point symmetry group F of crystal) $4/mmm$ (Hermann–Mauguin)—D_{4h} (Schoenflies)

PRS (Pearson symbol) tP6

PARM (Wyckoff positions occupied by atoms and their parameters)

Atom	*No*	*OxStat*	*Wyck*	---*X*---	---*Y*---	---*Z*---
Ti	1	4.000	2*a*	0.	0.	0.
O	1	−2.000	4*f*	0.3047(2)	0.3047(2)	0.

As $Z = 2$ (two formula units in primitive unit cell, the conventional unit cell coincides with the primitive one as the Bravais lattice is simple tetragonal) one needs 2 sets of coordinates for Ti atom (2a) and four sets for O atom (4f). As is seen for each Wyckoff position occupied by an atom there are given coordinates of only one representative. The others can be found on the site [8] for space group 136:

$$2a : (0,0,0)(\tfrac{1}{2},\tfrac{1}{2},\tfrac{1}{2});\ 4f : (x,x,0)(-x,-x,0)(-x+\tfrac{1}{2},x+\tfrac{1}{2},\tfrac{1}{2})(x+\tfrac{1}{2},-x+\tfrac{1}{2},\tfrac{1}{2})$$

In this case, $x = 0.3047$ as follows from the structure data. To the best of our knowledge only computer code CRYSTAL [14] allows one to include the space-group information in input data so that any occupied Wyckoff position can be presented by one representative. In the other computer codes the coordinates of all atoms in the PUC are introduced and the point symmetry of the structure is found by the code itself and used in calculations. From this example it is seen that the necessary information for structures requires the use not only of the database but also IT.

Obviously, atoms of different chemical elements are always nonequivalent in a crystal, i.e. cannot be connected by operations of symmetry. But atoms of one chemical element in a crystal can not to be connected by operations of symmetry. These atoms are not equivalent in a crystal structure even when they occupy the same Wyckoff position with different free parameters (examples of such the structures can be found in the next sections).

In the next section we consider those crystal structures which form the basis of the nanostructures modeling. As will be seen, the different crystal structures can be considered as one or another means of the distribution of the atoms between the Wyckoff positions of the corresponding space group. The crystal structure can also be described by Pearson symbol indicating the crystal lattice type and the number of atoms in the conventional (crystallographic) unit cell. The Bravais lattice type is given at the beginning of Pearson symbol: cP,cI,cF- for cubic lattices, tP,tI- for tetragonal lattices, oP,oS,oF- for orthorhombic lattices, hP and hR for hexagonal and rhombohedral lattices. The number of atoms in the crystallographic unit cell follows the Bravais lattice type.

2.3 Bulk Crystal Structures

2.3.1 Structures with Cubic Lattices

In Table 2.5 we give general information about all the cubic structures under consideration: prototype name, Pearson designation, space group symbol, Wyckoff positions occupations, and possible equivalent description of the structure. All these structures

Table 2.5 Cubic structures

Prototype	Pearsons symbol	Cubic lattice parameter a (Å)	Space group	Wyckoff positions	Equivalent description
Diamond (C)	cF8	3.567	Fd3m(227)	C(8a)	C(8b)
Fluorite (CaF_2)	cF12	5.463	$Fm\bar{3}m$(225)	Ca(4a) F(8c)	Ca(4b) F(8c)
Zincblende (ZnS)	cF8	5.409	$F\bar{4}3m$(216)	Zn(4a) S(4c)	Zn(4b) S(4d)
Perovskite (cubic) ($ATiO_3$)	cP5	3.795	$Pm\bar{3}m$(221)	A(1a) Ti(1b) O(3c)	Ti(1a) A(1b) O(3d)

Equivalent sets of Wyckoff positions for space groups [8]
216 (abcd)(e)(fg)(h)(i)
221 (ab)(cd)(ef)(g)(h)(ij)(kl)(m)(n)
225 (ab)(c)(d)(e)(f)(g)(hi)(j)(k)(l)
227 (ab)(cd)(e)(f)(g)(h)(i)

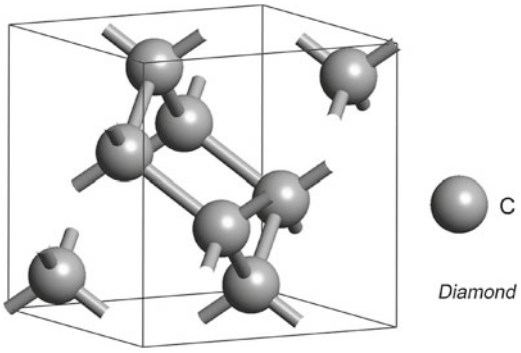

Fig. 2.4 Diamond structure

contain one formula unit in the primitive unit cell ($Z = 1$). For the structures cF with a face-centered cubic lattice the number of atoms is given for the cubic unit cell consisting of four primitive unit cells (this is traditional for crystal-structure databases). In computer calculations only the atoms inside the primitive unit cell have to be included: two atoms for diamond and zincblende, three and five atoms for fluorite and cubic perovskite structures, respectively.

The third column of Table 2.5 contains the numerical values of the cubic lattice parameter a, taken from [13].

Diamond structure (Fig. 2.4) is described by nonsymmorphic space group N227 with the face-centered cubic lattice: the macroscopic cubic symmetry of this crystal appears as the direct product of the first carbon atom site symmetry group T_d and inversion I at the center of C–C bond moving the first carbon to the equivalent second carbon atom in the primitive unit cell.

The coordinates of the carbon atoms can be given in fractions of primitive lattice vectors (these vectors are nonorthogonal for a face-centered cubic lattice) or in Cartesian coordinates. The primitive vectors themselves are usually given in Cartesian coordinates that for cubic lattices are directed along the translation vectors of the conventional (cubic) unit cell (see Fig. 2.1). To describe the diamond structure it is enough to give the numerical value of one parameter—the length of the cubic unit-cell translation vector (cubic lattice parameter a). One can find [10] the following numerical data for diamond structure (for an experimental value of 3.57 Å of the lattice parameter) in the form:

Primitive vectors $\boldsymbol{a}_1 = (0.000, 1.785, 1.785)$ $\boldsymbol{a}_2 = (1.785, 0.000, 1.785)$ $\boldsymbol{a}_3 = (1.785, 1.785, 0.000)$ Volume $= 11.37482325$. These numerical data correspond to the origin choice 2 for the space group N227 in [2] and the diamond structure description C(8a) with the shifted origin.

The space group N225 is the symmetry group of the *fluorite* CaF_2 structure (Ca(4a)F(8c)) (Fig. 2.5).

Some fluorite type compounds form the basis for the nanostructures: TiO_2, ZrO_2.

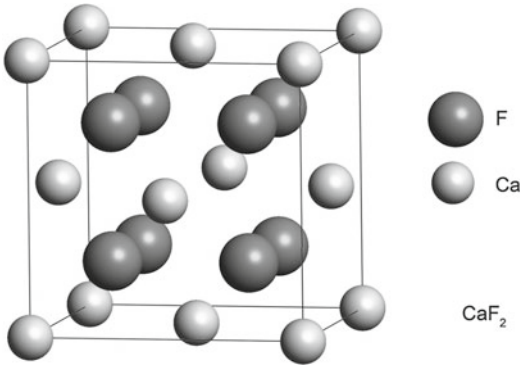

Fig. 2.5 Fluorite structure

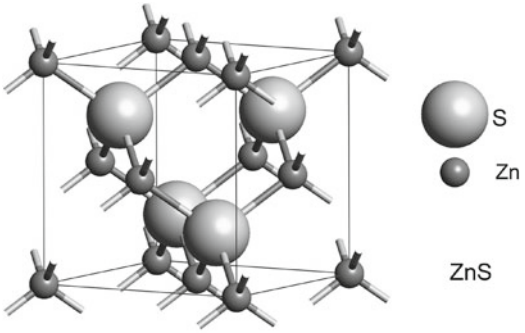

Fig. 2.6 Zincblende structure

The Ca atom in the fluorite structure can be placed also in Wyckoff position b (0.5, 0.5, 0.5). The symmorphic space group N225 is given in [2] for one origin choice (in Wyckoff position a with the site symmetry group O_h).

The point symmetry of the *sphalerite(zincblende)* ZnS (Fig. 2.6) structure is tetrahedral, but the lattice is cubic face-centered.

This structure can be obtained from the diamond structure by exchanging two carbon atoms with Zn and S atoms, so that the operation of interchange of two atoms in the primitive unit cell disappears. The zincblende structure is known for different compounds, which form nanotubes and nanowires (SiC, TiC, GeSi, BN, AlN, GaN). For an equivalent description of the structure the Zn and S atoms can be interchanged.

The *cubic perovskite* $CaTiO_3$ structure (Fig. 2.7) is more complicated and found as the high-temperature modification of different crystals ($SrTiO_3$, $BaTiO_3$, $PbTiO_3$, $SrZrO_3$, $PbZrO_3$). The structure is defined by one simple cubic lattice parameter a. In the cubic perovskite structure the Ti–O distance is equal to one half of the translation vector length. In the equivalent structure description (when Ca and Ti atoms are interchanged) the three oxygen atoms positions need to be taken as (0.5, 0.5, 0), (0.5, 0, 0.5) and (0, 0.5, 0.5).

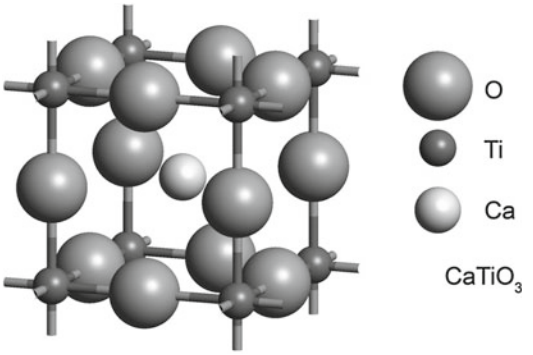

Fig. 2.7 Perovskite structure

The considered different cubic structures are defined by one numerical parameter—the cubic lattice constant. This is due to the fact that in these structures atoms occupy Wyckoff positions that have no free parameters. The definition of the more complicated structures requires the knowledge of both the lattice constants and the numerical values of the free parameters for the free-parameter-dependent Wyckoff positions occupied by atoms.

2.3.2 Structures with Tetragonal and Orthorhombic Lattices

In Table 2.6 we give general information about the tetragonal and orthorhombic crystals, being the basis of the nanostructures formation: two modifications (rutile and anatase) of titanium dioxide, zirconia, ferroelectric phases of the titanates, vanadium pentoxide and lepidocrocite. Tetragonal (a,c) and orthorhombic (a,b,c) lattice parameters are given in Åin the third column of Table 2.6.

Both TiO_2 modifications contain 6 atoms (two formula units) in the primitive cell.

The *rutile structure* (Fig. 2.8) belongs to the $P4_2/mnm$ nonsymmorphic space group.

The unit cell of the primitive tetragonal lattice is defined by the lattice vectors $\boldsymbol{a}_1 = \boldsymbol{a}_2$ (in the xy-plane) and $\boldsymbol{c}$ (along z-axis). The rotations through a fourth-order axis are followed by the improper translations along the z-axis of one half of the $\boldsymbol{c}$-vector length to ensure transformation of any of the oxygen atoms to another one, see Table 2.4. As is seen from Table 2.6 two Ti atoms of the primitive cell occupy Wyckoff position a(000;1/2, 1/2, 1/2), four oxygen atoms occupy Wyckoff position f with one free parameter v: $(\pm(v, v, 0); \pm(v + 1/2, 1/2 - v, 1/2))$. The Wyckoff positions coordinates are given in units of a, a, c. Thus, the rutile structure is defined by three parameters: a, c and v. The numerical data for rutile structure are given in [10].

The *anatase* structure (Fig. 2.9) belongs to the I4/amd nonsymmorphic space group.

Table 2.6 Tetragonal and orthorhombic structures

Prototype	Pearsons symbol	Lattice parameters (a,c) or (a,b,c) in Å	Space group	Wyckoff positions	Equivalent description
Rutile ($Ti(Sn)O_2$, MgF_2)	tP6	4.587.2.959	$P4_2/mnm(136)$	Ti(Mg)(2a)	Ti(Mg)(2b)
				O(F)(4f)	O(F)(4g)
Anatase (TiO_2)	tI12	3.764,9.502	$I4_1/amd(141)$	Ti(2a)	Ti(2b)
				O(4e)	O(4e)
Zirconia (ZrO_2)	tP6	3.598,5.165	$P4_2/nmc(137)$	Zr(2a)	Zr(2b)
				O(4d)	O(4d)
Strontium titanate ($SrTiO_3$)	tI14	5.513,7.807	I4/mcm(140)	Sr(4b)	Sr(4b)
				Ti(4c)	Ti(4c)
				O_1(4a)	O_1(4a)
				$O_2(8h)$	$O_2(8h)$
Barium(Lead) titanate ($Ba(Pb)TiO_3$)	tp5	4.318,4.106	P4mm(99)	Ba(Pb)(1a)	Ba(Pb)(1b)
				Ti(1b)	Ti(1a)
				O_1(1b)	O_1(1a)
				O_2(2c)	O_2(2c)
Barium titanate ($BaTiO_3$)	oS10	4.009,5.621,5.639	Amm2(38)	Ba(2a)	Ba(2b)
				Ti(2b)	Ti(2a)
				$O_1(2a)$	O_1(2b)
				O_2(4e)	O_2(4d)
Vanadium pentoxide (V_2O_5)	oP14	11.544,3.571,4.383	Pmmn(59)	V(4f)	V(4f)
				$O_1(4f)$	$O_1(4f)$
				O_2(4f)	O_2(4f)
				O_3(2b)	O_3(2a)
Lepidocrocite (FeO(OH))	oS16	3.072,12.516,3.873	Cmcm(63)	Fe(4c)	Fe(4c)
				O1(4c)	O1(4c)
				O_2(4c)	O_2(4c)
				H(8f)	H(8f)

Equivalent sets of Wyckoff positions for space groups [8]
136 (ab)(c)(d)(e)(fg)(h)(i)(j)(k)
137 (ab)(c)(d)(e)(f)(g)(h)
140 (a)(b)(c)(d)(e)(f)(g)(h)(i)(j)(k)(l)(m)
141 (ab)(cd)(e)(f)(g)(h)(i)
99 (ab)(c)(d)(f)(e)(g)(h)(ij)(k)(l)(m)(n)(o)
63 (ab)(c)(d)(e)(f)(g)(h)
59 (ab)(cd)(e)(f)(g)
38 (ab)(c)(de)(f)

The tetragonal unit cell of a body-centered tetragonal lattice is defined by the lattice vectors $\boldsymbol{a}_1 = \boldsymbol{a}_2$ (in the xy-plane) and $\boldsymbol{c}$ (along the z-axis) and contains 2 primitive unit cells. To describe the primitive unit cell the translation vectors $\boldsymbol{a}_1(a, 0, 0), \boldsymbol{a}_2(0, a, 0), \boldsymbol{a}_3(1/2a, 1/2a, 1/2c)$ are used. As is seen from Table 2.6. two Ti atoms of the primitive cell occupy Wyckoff position 2a(0, 0, 0; 0, 1/2, 1/4),

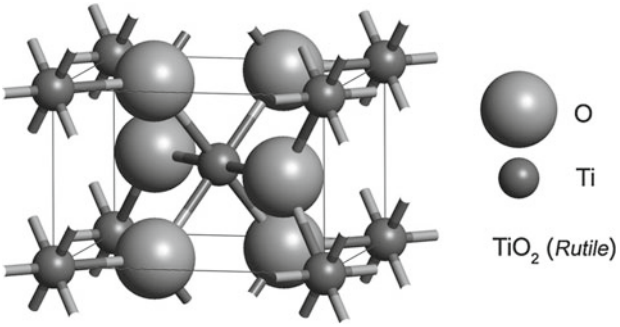

Fig. 2.8 Rutile structure

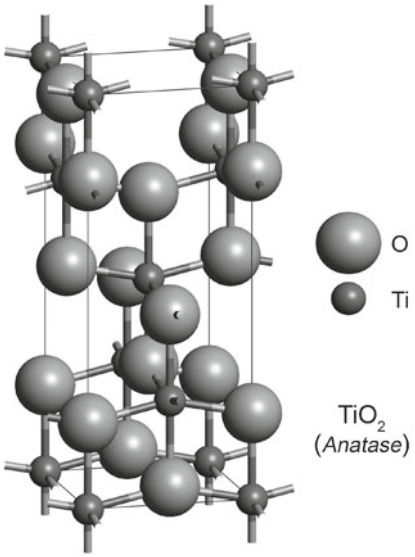

Fig. 2.9 Anatase structure

four oxygen atoms occupy Wyckoff position 4e $(0, 0, v; 1/2, 0, -v+1/2; 0, 1/2, v+1/4; 1/2, 1/2, -v+1/2)$. The anatase structure is defined by three parameters: a, c, v. The numerical data for anatase structure are given in [10]. These data correspond to the coordinate system origin shifted by $(1/8, -1/8, -1/4)$ (in the units of primitive translations), in comparison with the origin choice made in [2].

Zirconia is an oxide which exhibits a large variety of polymorphs. The properties of bulk ZrO_2 are well studied experimentally [15]. It was established that ZrO_2 has three zero-pressure modifications. At high temperatures (t $\geq$2,350 C), zirconia adopts a cubic fluorite structure, see Table 2.5 while at low temperatures (t$\leq$1,150 C), a monoclinic baddeleyite ($P2_1/c$) structure is preferred thus representing a ground state of zirconia. A tetragonal zirconia phase (see Fig. 2.10) belongs to the nonsymmorphic space group $P4_2/nmc$ and exists at intermediate temperatures; it can be

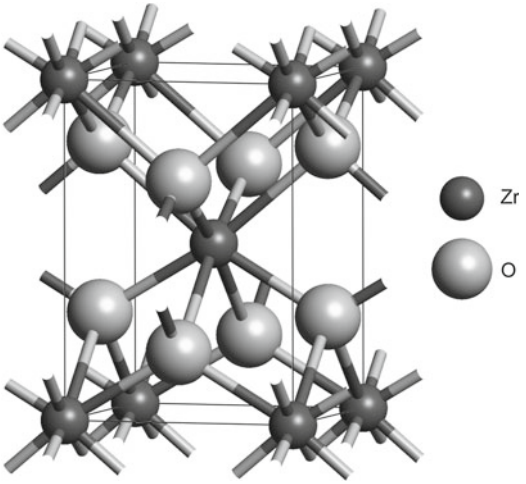

Fig. 2.10 Tetragonal zirconia structure

viewed as a simple perturbation of the cubic fluorite phase, see Fig. 2.5 in which the oxygen atoms are displaced alternately along the 4_2 axis by 0.2 Å. The relative stability of ZrO_2 zero pressure phases can be influenced by the crystallite size. It is well known that small zirconia particles suspended in a host matrix do not transform from tetragonal to monoclinic, even well below the bulk transition temperature unless subjected to an external stress field or heating above 700 K [16]. Moreover, Wang et al. [17] have found that tetragonal zirconia can be obtained in particles with sizes below 40 nm at room temperature. Structure studies [18] of ZrO_2 deposition on the amorphous silica have shown that the thin ZrO_2 film growth starting from the formation of amorphous phase proceeds with preferential growth of crystallites of tetragonal and cubic structures in the direction [001]. The structure analysis of the fabricated zirconia nanotubes (ZNT) also gives evidence that the small particle size may stabilize the virtually unstable phases. This means that ZNT can possess cubic, tetragonal or orthorhombic morphology.

The unit cell of the tetragonal zirconia primitive tetragonal lattice is defined by the lattice vectors $\boldsymbol{a}_1 = \boldsymbol{a}_2$ (in the xy-plane) and $\boldsymbol{c}$ (along z-axis). The rotations through a fourth-order axis are followed by the improper translations along the z-axis of one half of the $\boldsymbol{c}$-vector length to ensure transformation of any of the oxygen atoms to another one. As is seen from Table 2.6 two Zr atoms of the primitive cell occupy Wyckoff position $a(3/4, 3/4, 3/4; 1/4, 3/4, 1/4)$, four oxygen atoms occupy Wyckoff position d with one free parameter v: $(1/4, 1/4, v;\ 1/4, 1/4, v + 1/2;\ 3/4, 3/4, -v;\ 3/4, 3/4, -v + 1/2)$. The Wyckoff positions coordinates are given in units of a, a, c, the origin choice 2 is chosen, see [8]. Thus, the tetragonal zirconia structure is defined by three parameters: a, c and v. The numerical data for tetragonal zirconia structure are given in [13].

The structure of the $SrTiO_3$ low temperature antiferrodistortive (AFD) phase (Fig. 2.11b) belongs to the nonsymmorphic space group I4/mcm with the

body-centered tetragonal lattice and contains two formula units in the primirive unit cell (four formula units in the conventional cell of the body centered tetragonal lattice). The lattice parameters are: a = 5.511 Å, c = 7.796 Å.

The Sr and Ti atoms atom occupy Wyckoff positions 4b(0, 0.5, 0.25) and 4c (000), respectively. The nonequivalent oxygen atoms O_1 and O_2 occupy Wyckoff positions 4a(0, 0, 0.25) and 8h(0.2451, 0.2451.0), respectively. The structure is defined by two tetragonal lattice parameters (lengths of $\boldsymbol{a}_1 = \boldsymbol{a}_2$ primitive translations and of $\boldsymbol{c}$—translation vector of the tetragonal unit cell containing two primitive cells) and v-parameter defining the positions of O_2 atoms. The numerical data for this structure are given [10]. The primitive translation vector $\boldsymbol{a}_3$(1/2,1/2,1/2) is given in units of a, a, c.

$BaTiO_3$ (BTO) crystallizes either in the perovskite crystal structure or in its hexagonal modification. The crystal structure of the perovskite polymorph changes from cubic ($Pm\bar{3}m$) to tetragonal (P4 mm) at 403 K, then to orthorhombic (Amm2) at 278 K, and to rhombohedral (R3 m) at 183 K [19]. The cubic phase is paraelectric and the other phases are ferroelectric. In all four phases, there is one BTO formula unit in the unit cell so that phase transitions to ferroelectric phases are due to the soft mode

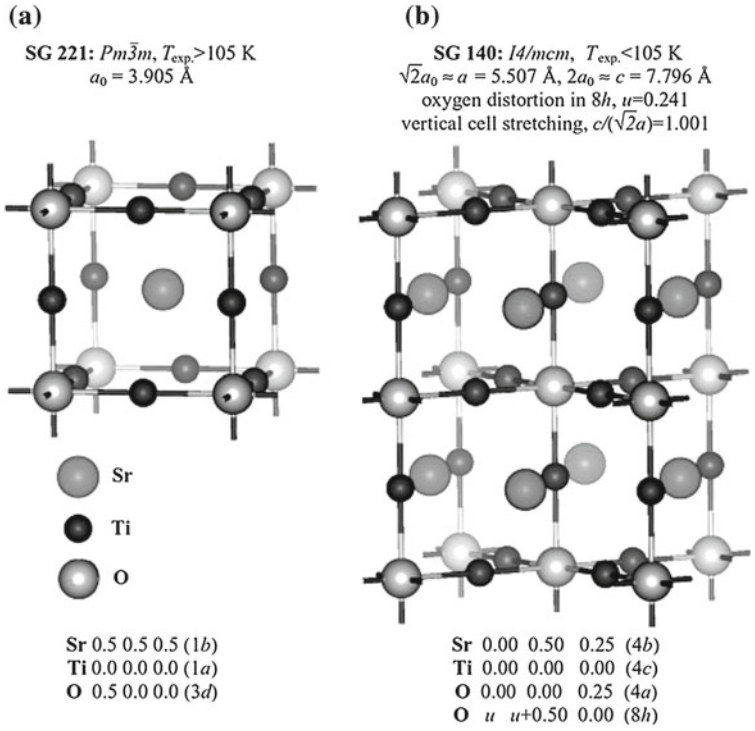

Fig. 2.11 Cubic (**a**) and tetragonal AFD (**b**) $SrTiO_3$ structures. Online (*Green balls*) Sr atoms, (*gray balls*) Ti, and (*red balls*) O atoms

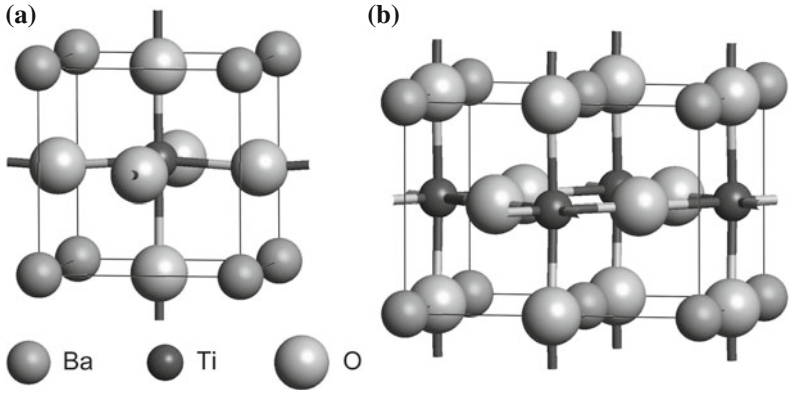

Fig. 2.12 Tetragonal (**a**) and Orthorhombic (**b**) Barium titanate structures

at Γ point of cubic BTO Brillouin zone (BZ). Lead titanate $PbTiO_3$ (PTO) is one of the simplest ferroelectrics with the perovskite structure and undergoes successive phase transitions from tetragonal to monoclinic to rhombohedral under pressure at low temperetures.

The structure of $BaTiO_3$ and $PbTiO_3$ zero-pressure ferroelectric tetragonal phases (Fig. 2.12a) belongs to the symmorphic space group P4mm with the simple tetragonal lattice and contains one formula unit in the primitive unit cell. The structure is defined by two tetragonal lattice parameters (lengths of $\boldsymbol{a}_1 = \boldsymbol{a}_2$ primitive translations and $\boldsymbol{c}$) and three v-parameters defining the positions of the Ti, O_1 and O_2 atoms. The lattice parameters are: a = 3.9988 Å, c = 4.0222 Å and a = 3.9009 Å, c = 4.1526 Å, for BTO and PTO, respectively [13]. The unit cell volumes are 64.32 (BTO) and 63.19 (PTO). The Ba (Pb) and Ti atoms atom occupy Wyckoff positions 1a(0, 0, 0) and 1b(0, 0, u_{Ti}), respectively. The nonequivalent oxygen atoms O_1 and O_2 occupy Wyckoff positions 1b(0, 0, u_1) and 2c(1/2, 0, u_2), (0, 1/2, u_2) respectively. The numerical data for these parameters taken from [13] are the following: $v_{Ti} = 0.5021(0.5340)$ for BTO(PTO); $v_1 = -0.0153(0.1120)$ for BTO(PTO); $v_2 = 0.5130(0.6220)$ for BTO(PTO).

Table 2.6 also gives the information about the orthorhombic structures of $BaTiO_3$, vanadium pentoxide V_2O_5 and lepidocrocite. The vanadium pentoxide contains two formula units V_2O_5 in the primitive cell (Z = 2) and forms nanotubes, which are not considered in this book. The lepidocrocite is used for TiO_2-based nanotube modeling after the change of iron atoms by titanium atoms and removing hydrogen atoms (see Chap. 7).

2.3.3 Structures with Hexagonal Lattices

In this section we consider hexagonal structures (graphite, BN honeycomb, MoS_2, titanium disulfide and diboride, ZnS (wurtzite), see Figs. 2.13, 2.14, 2.15, 2.16, 2.17 and 2.18, respectively).

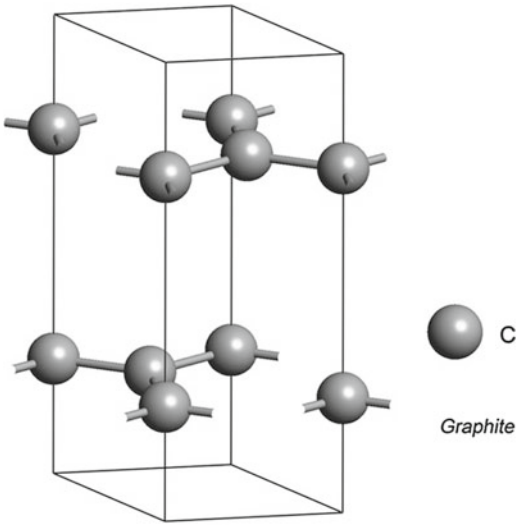

Fig. 2.13 Graphite structure

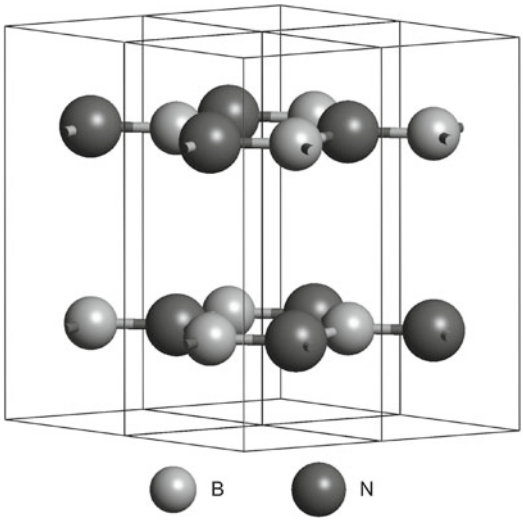

Fig. 2.14 Hexagonal BN structure

Table 2.7 shows that the graphite, hexagonal boron nitride BN and molibdenum disulfide MoS_2 structures, see Figs. 2.13, 2.14 and 2.15, belong to the nonsymmorphic space group $P6_3/mmc$. The symmorphic space groups $P\bar{3}m1(164)$ and $P6/mmm(191)$ describe the symmetry of TiS_2 and TiB_2 crystals, respectively. Wurtzite and α-quartz SiO_2 structures symmetry is given by nonsymmorphic groups $P6_3\,mc(186)$ and $P3_121(152)$, respectively. The rhombohedral structure of α boron

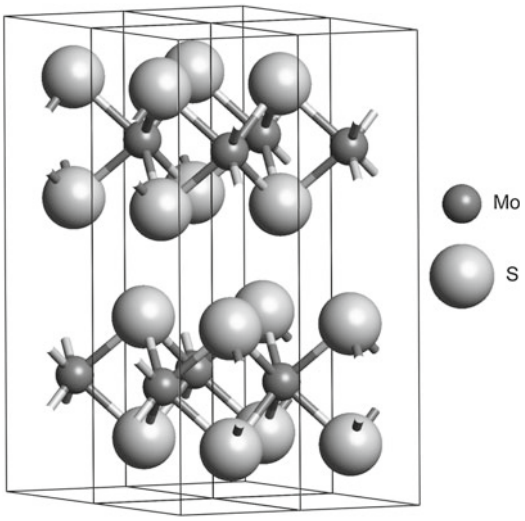

Fig. 2.15 Molybdenite MoS_2 structure

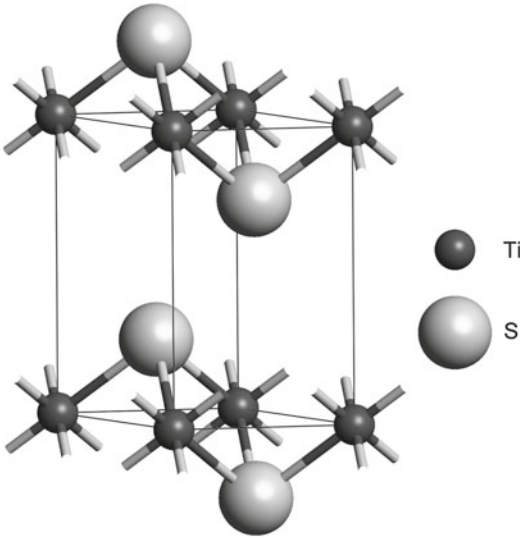

Fig. 2.16 Titanium disulfide TiS_2 structure

(symmorphic space group $R\bar{3}m(166)$) is given in the hexagonal setting (3 primitive unit cells in the hexagonal cell).

The unit cell of the hexagonal lattice is defined by the lattice vectors $\boldsymbol{a}_1 = \boldsymbol{a}_2$ (in the xy-plane) and $\boldsymbol{c}$ (along z-axis). The rotations through a six-order axis are followed by the improper translations along the z-axis of one half of the $\boldsymbol{c}$-vector

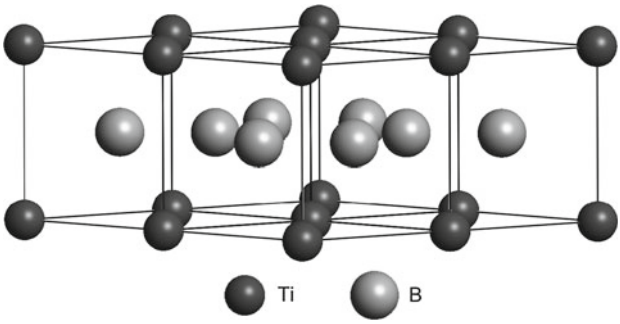

Fig. 2.17 TiB_2 structure

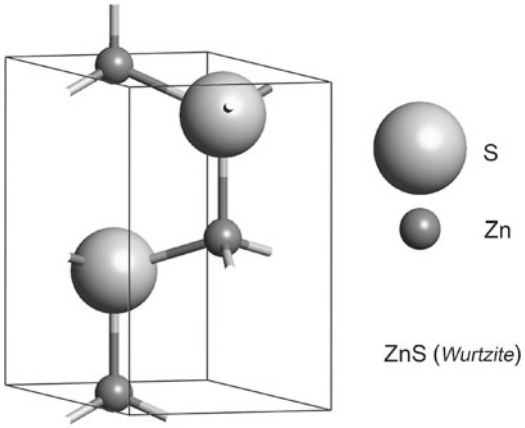

Fig. 2.18 Wurtzite structure

length. Belonging to the same space group, the three structures in consideration differ by the atom distribution over Wyckoff positions in the primitive unit cell of the hexagonal lattice. As it is seen from Table 2.7, the following Wyckoff positions of the space group $P6_3/mmc$ are used to describe the structures in consideration: 2b (0 0 1/4, 0 0 3/4), 2c (1/3 2/3 1/4, 2/3 1/3 3/4), 2d (2/3 1/3 1/4, 1/3 2/3 3/4) and 4f (1/3 2/3 z, 2/3 1/3 z+1/2, 2/3 1/3 −z, 1/3 2/3 −z+1/2). All the coordinates of Wyckoff positions are given in units of the three hexagonal lattice parameters.

In graphite structure four carbon atoms atoms occupy two nonequivalent Wyckoff positions 2b and 2c. The hexagonal lattice parameters are a = 2.4642 Å, c = 6.7114 Å, the unit cell volume is 35.29 [13]. The graphite structure consists of atomic layers separated by a distance larger than the interatomic distance in one layer. Therefore, the one-layer approximation (graphene layer) is used in nanotubes modeling: only two carbon atoms in the primitive cell of the plane hexagonal lattice are included in the graphene structure. In BN_{hex} structure two boron atoms and two nitrogen atoms occupy nonequivalent Wyckoff positions 2c and 2d. The hexagonal lattice

Table 2.7 Hexagonal structures

Prototype	Pearsons symbol	Lattice constants (a,c) in Å	Space group	Wyckoff positions	Equivalent description
Graphite C	hP4	2.464, 6.711	$P6_3/mmc(194)$	C(2b)	–
				C(2c)	
BN honeycomb	hP4	2.489, 6.561	$P6_3/mmc(194)$	B(2c)	B(2d)
				N(2d)	N(2c)
Molybdenite 2H (MoS_2)	hP6	3.169, 12.324	$P6_3/mmc(194)$	Mo(2c)	Mo(2d)
				S(4f)	S(4f)
Titanium Disulfide (TiS_2)	hP3	3.312, 5.449	$P\bar{3}m1(164)$	Ti(1a)	Ti(1b)
				S(2d)	S(2d)
Titanium Diboride (TiB_2)	hP3	3.024, 3.124	$P6/mmm(191)$	Ti(1a)	Ti (1b)
				B(2d)	B(2c)
Wurtzite (ZnS)	hP4	3.777, 6.188	$P6_3mc(186)$	Zn(2b)	–
				S(2b)	
Alpha quartz (SiO_2)	hP9	4.913, 5.405	$P3_121(152)$	Si(3a)	Si(3b)
				O(6c)	O(6c)
Alpha Boron (B)	hR12	4.906, 12.566	$R\bar{3}m(166)$	B_1(18h)	–
				B_2(18h)	

Equivalent sets of Wyckoff positions for space groups [8]
194 (a)(b)(cd)(e)(f)(g)(h)(i)(j)(k)(l)
164 (ab)(c)(d)(ef)(gh)(i)(j)
191 (ab)(cd)(e)(fg)(h)(i)(jk)(lm)(n)o(pq)
186 (a)(b)(c)(d)
152 (ab)(c)
166 (ab)(c)(de)(fg)(h)(i)

parameters are a = 2.4860 Å, c = 6.5160 Å, the unit cell volume is 34.88 [13]. As the graphite BN_{hex} consists of atomic layers separated by a distance larger than the interatomic distance in one layer. Therefore, the one-layer approximation is used in BN nanotubes modeling: only two atoms (boron and nitrogen) in the primitive cell of the plane hexagonal lattice are included in the structure. In molibdenum disulfide MoS_2 structure two molibdenum atoms and four sulfur atoms occupy Wyckoff positions 2c and 4f, respectively. The hexagonal lattice parameters are a = 3.1690 Å, c = 12.324 Å, the unit cell volume is 107.18 [13]. The sulfur atom position is defined by parameter z = 0.621. The layered structure of MoS_2 is used in nanotubes modeling.

The structure of titanium disulfide (TiS_2) belongs to the symmorphic space group $P3m1$ and contains one furmula unit in the primitive unit cell of the hexagonal lattice, see Fig. 2.16. Metal and sulfur atoms occupy parameter-free Wyckoff positions 1a (0 0 0) and 2d (1/3 2/3 1/2, 2/3 1/3 1/2), respectively. The structure of aluminium and titanium diborides (AlB_2,TiB_2) belongs to the symmorphic space group $P6/mmm$ and contains one furmula unit in the primitive unit cell of the hexagonal lattice, see Fig. 2.17. Metal and boron atoms occupy parameter-free Wyckoff

positions 1a (0 0 0) and 2d (1/3 2/3 1/2, 2/3 1/3 1/2), respectively. The structure is defined by the lengths a and c of the hexagonal lattice translation vectors $\boldsymbol{a}_1 = \boldsymbol{a}_2$ (in the xy-plane) and $\boldsymbol{c}$ (along z-axis) for AlB_2 (TiB_2): a = 3.016(3.024) Å, c = 3.268(3.154) Å, V = 25.74(24.98) [13].

The wurtzite structure of ZnS, see Fig. 2.18, is the hexagonal analog of the zincblende (sphalerite) structure of ZnS (see Sect. 2.3.1) and belongs to the nonsymmorphic space group $P6_3mc$ with a hexagonal lattice. The boron, aluminium and gallium nitrides (BN, AlN and GaN) and ZnO bulk crystals have the wurtzite structure. The primitive unit cell contains two formula units, two metal and two nitrogen (oxygen) atoms occupy the same Wyckoff position 2b(1/3, 2/3, z; 2/3, 1/3, z+1/2) with the different values of internal parameter z for metal atom and for sulfur atom. Thus, the wurtzite structure is defined by 4 parameters—two lattice and two internal ones. The numerical values of the structure data from [13] are the following for BN (AlN,GaN): a = 2.538 Å(3.115 Å, 3.221 Å); c = 4.197 Å(4.988 Å, 5.237 Å); V = 23.41(41.91, 47.05). The internal parameter $z_1 = 0$ for all the three structures, the internal parameter z_2 =0.373(0.305,0.378). The wurtzite structure can also be described in hexagonal axes.

The figures showing the α-Boron and α-quartz structures are given in Chap. 4 when the based on these structures nanotubes are considered.

2.4 Diperiodic (Layer) Symmetry Groups of Nanolayers

2.4.1 Two Factorizations of the Layer Groups

The diperiodic groups are the symmetry groups of the three-dimensional systems with translational periodicity in two directions. The diperiodic groups belong to the so-called subperiodic groups. The latter include 7 frieze groups (two-dimensional groups with one-dimensional translations), 75 rod groups (three-dimensional groups with one-dimensional translations), and 80 layer groups (three-dimensional groups with two-dimensional translations). The information presented about the subperiodic groups in [5] is in the same format and consists of the same content as that provided in [2] for space groups G. There are 80 diperiodic groups; 17 of them are plane, i.e. describe the symmetry of the two-dimensional systems with translational periodicity in two directions.

Diperiodic groups are subgroups of the three dimensional triperiodic space groups G. In the *single-slab* model a crystal with a surface is approximated by a slab of finite thickness. The symmetry group of this model allows the existence of symmetry operations that move the atoms out of the plane of the layer but bring them into positions occupied by other atoms of the slab. These are diperiodic groups (DG) in three dimensions. They are also called the layer groups. These groups also describe the symmetry of thin films. In layered crystals the interaction between the nearest layers is usually weaker than that between nearest atoms in the same layer plane.

Therefore, the slab model is a convenient approximation for such crystals. Layer groups describe the symmetry of this model.

Under standard crystallographic approach any diperiodic group (DG) may be presented in the form

$$\mathrm{DG} = \mathrm{T}(\mathbf{a})\mathrm{F} \tag{2.13}$$

where F is a finite system of representatives of DG decomposition in cosets of two-dimensional translation group T(**a**). Choice of representatives in not unique and any specific set F is, in general, not a subgroup of DG. However, since DG is the extension of G by T(a), F can be interpreted as a group with multiplication modulo pure two-dimensional translations. Factorization (2.13) of diperiodic group DG will be referred to as standard and is used in [5].

Any element of the layer group may be written as $(R_i|\boldsymbol{v}_i + \boldsymbol{a}_n)$, where $\boldsymbol{a}_n$ and $\boldsymbol{v}_i$ are lattice and improper translations, $i = 1, 2$.

Let $\boldsymbol{a}_3$ be a vector that does not lie in the layer plane. A set of elements $(E|n_3\boldsymbol{a}_3)$ forms a group T_3 of one-dimensional translations. Consider the elements

$$(R_i|\boldsymbol{v}_i + \boldsymbol{a}_n)(E|n_3\boldsymbol{a}_3), \quad (R_i|\boldsymbol{v}_i + a_n) \in \mathrm{DG}, i = 1, 2, \ (E|n_3\boldsymbol{a}_3) \in T_3 \tag{2.14}$$

The set (2.14) of symmetry operations contains a group of three-dimensional translations $(E|\boldsymbol{a}_n + n_3\boldsymbol{a}_3) \in \mathrm{T}$. The set (2.14) is some space group provided the translational symmetry (the group T) is compatible with the point symmetry $\mathrm{F_{DG}}$ of the layer group DG. This condition is fulfilled if the vector $\boldsymbol{a}_3$ is chosen perpendicular to the layer plane. Indeed, the translations $(E|\boldsymbol{a}_n) \in T^{(2)} \subset \mathrm{T}$ are compatible with $\mathrm{F_{FD}}$ as they are the elements of DG. The compatibility of the translations $(E|n_3\boldsymbol{a}_3) \in T_3$ with point group $\mathrm{F_{FD}}$ follows from the fact that the rotations (proper and improper) from DG transform the layer into itself and, therefore, the vector perpendicular to the layer is transformed into a vector also perpendicular to the layer. Thus, the set of elements (2.14) forms one of the three-periodic space groups G. Moreover, the translational group T_3 is invariant in G: with the translation $(E|\boldsymbol{a}_3)$ it contains also the translation $(E|R_i\boldsymbol{a}_3)$ for any R_i from (2.14). Therefore, the group G may be expressed as a semidirect product

$$\mathrm{G} = T_3 \wedge \mathrm{DG} \tag{2.15}$$

and be decomposed into cosets with respect to T_3

$$\mathrm{G} = \sum_i (R_i|\boldsymbol{v}_i + \boldsymbol{a}_n)T_3, \quad (R_i|\boldsymbol{v}_i + \boldsymbol{a}_n) \in \mathrm{DG}, \ i = 1, 2 \tag{2.16}$$

Thus, subperiodic layer group DG is isomorphic to factor group G/T_3. A relationship between factor groups of space groups and subperiodic groups is studied in [20, 21].

In [5] a relationship is considered between space (triperiodic) and subperiodic groups: given a crystal of a specific space-group symmetry and a plane transecting

the crystal, one can enquire as to what is the layer subgroup of the space group that leaves this plane invariant. The physical motivation for answering this question is clear as this problem arises, for example, in the surface modeling by a single slab. The information about subperiodic groups is followed in [5] by the scanning tables in which the layer symmetries of sectional planes are tabulated for all crystallographic orientations and for all positions (locations) of these planes. These tables also contain explicitly the orbits of these planes (an orbit is defined as a set of planes connected by the symmetry operations) and implicitly, via the so-called "scanning groups", information about the rod symmetries of straight lines that penetrate through the crystal.

Both the short and the full DG Hermann-Mauguin symbols consist of a letter indicating the centring type of the conventional cell (primitive P or centered rectangular C) and a set of characters indicating symmetry elements of the subperiodic group. The one or three entries after the centring letter refer to the one or three kinds of symmetry directions of the conventional crystallographic basis. Symmetry directions occur either as singular directions or as sets of symmetrically equivalent symmetry directions. Only one representative of each set is given. The sets of symmetry directions and their sequence in the Hermann-Mauguin symbol are summarized in Table 2.8.

Each position in the Hermann-Mauguin symbol contains one or two characters designating symmetry elements, axes and planes that occur for the corresponding crystallographic symmetry direction. Symmetry planes are represented by their normals; if a symmetry axis and a normal to a symmetry plane are parallel, the two characters are separated by a slash. Crystallographic symmetry directions that carry no symmetry elements are denoted by the symbol 1, e.g. P3m1 (DG69). If no misinterpretation is possible, entries 1 at the end of the symbol are omitted, as in p4 (DG49) instead of P411. Subperiodic groups that have in addition to translations

Table 2.8 Sets of symmetry directions and their positions in the Hermann-Mauguin symbol

	Symmetry direction (position in Hermann-Mauguin symbol)		
	Primary	Secondary	Tertiary
(*a*) *Layer groups and rod groups*			
Triclinic	None		
Monoclinic Orthorhombic	[100]	[010]	[001]
Tetragonal	[001]	[100]	$[1\bar{1}0]$
		[010]	[110]
Trigonal Hexagonal	[001]	[100]	$[1\bar{1}0]$
		[010]	[120]
		$[\bar{1}\bar{1}0]$	$[\bar{2}\bar{1}0]$
(*b*) *Frieze groups*			
Oblique	Rotation point in plane		
Rectangular		[10]	[01]

In the standard setting, periodic directions and their positions are [100] and [010] for the layer groups, [001] for the rod groups, and [10] for the frieze groups

no symmetry directions or only centres of symmetry have only one entry after the centring letter. These are the layer-group types P1 (DG1) and p$\bar{1}$ (DG2).

Table B.1 given in Appendix B, shows the correspondence DG $\leftrightarrow$ G/T_3 between three-dimensional diperiodic (DG) and three-periodic (G) space groups. This correspondence was at first given by Wood [22] in the setting that differs for rectangular diperiodic groups from that given in Table B.1 (the setting in this Table corresponds to the standard setting of [5]).

The second approach to the diperiodic groups description was suggested in [23] and is based on the non-standard factorization

$$\mathrm{DG} = \mathrm{ZP} \tag{2.17}$$

where Z is a cyclic generalized translation group, and P is a finite point group.

The non-standard DG factorization was used in [23] for the construction of the DG irreducible representations as the non-standard factorization allows the simple construction of irreducible representations, involving neither projective representations, nor the representations of the space supergroups.

Table B.2 is given in Appendix B and presents the non-standard factorization of the diperiodic space groups.The generalized translational group, Z describes the periodical arrangement of the elementary motifs along two independent directions (these two directions are assumed to be in the xy-plane). Therefore, Z can be formed of the generalized one-dimensional (1D) translational groups leaving the xy-plane invariant. There are only four generalized 1D translational groups satisfying this condition: (1) pure translational group T along an axis in the plane, (2) screw axis group 2_1 with the C_2 axis in the plane, (3) glide plane group T_h of the horizontal, xy, glide plane, (4) glide plane group T_v of the vertical glide plane (containing z-axis). All these groups are infinite cyclic groups. The first of them is generated by pure translation; as for the remaining three groups, pure translations are the index-2 subgroup generated by the square of the generator of the glide plane or the screw axis. The generalized 2D translational groups are direct or weak direct products of the listed four 1D generalized translations: (1) The pure 2D translational group T is the direct product of the two 1D translational groups T along independent directions, with, in general, different translational periods and an arbitrary angle between the translational directions. (2) The horizontal 2D glide plane group $T_h = TT_h$; translational periods of T and T_h may be different, and their directions form an arbitrary angle. (3) The 2D screw axis group $2_1 = T2_1$ (horizontal screw axis). (4) The vertical 2D glide plane group $T_v = TT_v$ (vertical glide plane). (5) The product 2_1T_h of the groups 2_1 and T_h generated by $(U_x|1/2, 0)$ and $(\sigma_h|0, 1/2)$ In the last three cases the screw axis (glide plane) can be chosen in the direction orthogonal to the translations of the group T or T_h, while the translational periods of the groups T and T_h are not related to those of 2_1 (respectively T_v).

These five 2D generalized translational groups form the lattices classified according to the four holohedries: the oblique (holohedry C_{2h}; arbitrary angle between the translational directions, with different periods), the rectangular (D_{2h}; orthogonal translational directions with different periods), the square one (D_{4h}; orthogonal

translational directions and equal periods) and the hexagonal one (D_{6h}; the angle $2\pi/3$ between the translational directions with the equal periods) [5]. If together with the primitive rectangular translations **a** and **b**, the lattice contains the vector $(\mathbf{a}+\mathbf{b})/2$ it is called the centred rectangular, to differ from the primitive ones (these generalized translational groups are emphasized by primes in the Table B.1). Depending on the type of the lattice, various orthogonal symmetries can be involved. They combine into the point factors, being the axial point groups, leaving the z-axis invariant. Since the crystallographic conditions on the order of the principal axis of rotation must be imposed (analogously to the space groups, but in the contrast to the line groups, see next section), the possible point factors are: C_n, C_{nv}, C_{nh}, D_n, D_{nh} (for $n = 1, 2, 3, 4, 6$), D_{nd} and S_{2n} (for $n = 1, 2, 3$). These are also the possible isogonal point groups, which are obtained by adding the orthogonal part of the generalized translational generators to the point factor (thus the point factor P is either the isogonal point group, or its index-2 subgroup).

Diperiodic group DG contains a subgroup of two-dimensional translations $T^{(2)}$ with elements $(E|\boldsymbol{a}_n)$, where

$$\boldsymbol{a}_n = n_1\boldsymbol{a}_1 + n_2\boldsymbol{a}_2 \tag{2.18}$$

is an arbitrary translation vector of the plane lattice, and $\boldsymbol{a}_1$, $\boldsymbol{a}_2$ are unit cell (primitive) translation vectors. The ends of all vectors $\boldsymbol{a}_n$ beginning at some origin O form a two-dimensional Bravais lattice. The point-symmetry group F_{DG} of this lattice must satisfy the following requirements: symmetry axes of order n (with $n > 2$) must be perpendicular to the plane of vectors $\boldsymbol{a}_1$, $\boldsymbol{a}_2$ (layer plane), reflection planes must be either perpendicular or parallel to this plane. These requirements restrict the number of possible two-dimensional lattices. The two-dimensional lattice of a layer group is also a two-dimensional lattice of a plane group (two-dimensional groups with two-dimensional translations). There exist five plane lattices, distributed over four crystal systems: oblique, rectangular (2 lattices—primitive and centered), square and hexagonal.

The point symmetry of the oblique, rectangular, square and hexagonal systems is given by C_2, C_{2v}, C_{4v} and C_{6v} point groups, respectively. Note that in a plane lattice the inversion at the origin of the coordinate system is equivalent to the rotation through the second-order axis normal to the plane. Screw axes in layer groups may be only the second-order axes lying in the layer plane. Improper translations in operations of reflection in glide planes (parallel or perpendicular to the layer plane) must be oriented along the layer plane.

One can find the information about subperiodic groups in [5] and on the Bilbao Crystallographic server [8]. These groups are specified by their number as given in [5] or by the international symbols. The international symbol of layer group DG contains, first, the information about the plane Bravais lattice type: P (primitive) or C (centered). Then the information about symmetry elements is given. The screw axes (of second order) have the subscript 1. The reflection planes are denoted as follows: m (mirror planes), n, a, b (glide planes, depending on the direction of the improper translations). The subperiodic groups are described by means of a crystallographic

coordinate system consisting of a crystallographic origin, denoted by O, and a crystallographic basis. The conventional basis vectors for the three-dimensional layer groups are labeled $\boldsymbol{a}$, $\boldsymbol{b}$, and $\boldsymbol{c}$. Unlike triperiodic space groups, not all basis vectors of the crystallographic basis are lattice vectors (for primitive lattices vectors $\boldsymbol{a}$ and $\boldsymbol{b}$ coincide with the primitive translations $\boldsymbol{a}_1$, $\boldsymbol{a}_2$).

Like space groups, the crystallographic coordinate system is used to define the symmetry operations and the Wyckoff positions. The symmetry operations are defined with respect to the directions of both lattice $\boldsymbol{a}$, $\boldsymbol{b}$ and nonlattice $\boldsymbol{c}$ basis vectors. A Wyckoff position, denoted by a coordinate triplet (x, y, z) for the three-dimensional layer groups, is defined in the crystallographic coordinate system by $O + \boldsymbol{r}$, where $\boldsymbol{r} = x\boldsymbol{a} + y\boldsymbol{b} + z\boldsymbol{c}$.

Like space groups, the term setting will refer to the assignment of the labels $\boldsymbol{a}$, $\boldsymbol{b}$, and $\boldsymbol{c}$ (and the corresponding directions [100], [010] and [001], respectively) to the basis vectors of the crystallographic basis. In the standard setting, those basis vectors that are also lattice vectors are labeled for layer groups with their two-dimensional lattice by $\boldsymbol{a}$ and $\boldsymbol{b}$. Note that the setting of the layer groups for rectangular lattices may be chosen different for the same group (symbols $P211$ or $P121$ refer to the same group in two different settings) but at the same time $P112$ and $P211$ denote different layer groups. In the first group the axis of second order (oriented along the z-axis) is perpendicular to the layer plane, in the second it lies in the layer plane xy and is directed along the x-direction. In the first case, the second-order axis is oriented along the plane translation lattice vector, in the second case along the nonlattice vector. Respectively, the Wyckoff positions for both groups are different, see [8].

For some layer groups of oblique and rectangular crystal systems (DG 1, 2, 8–18) the vector $\boldsymbol{a}_3$ may be inclined to the layer plane.

In the cases when a space group G may be represented as a semidirect product (2.15) in two different manners it generates two nonisomorphic layer groups. For example, the layer groups $P112$ and $P211$ are related to one space group $P2(C_2^1)$ with two different settings (the second-order axis is oriented along the z- and x-directions, respectively). The space group $P2/b$ (C_{2h}^4) generates two layer groups $P112/a$ and $P2/b11$. In the first group the rotation axis is perpendicular to the layer and the layer plane itself is a glide plane with an improper translation on a half-period along the x-direction. In the second group the rotation axis is directed along the x-axis; the glide reflection plane is perpendicular to the layer (and to the rotation axis) and reflection in this plane is followed by improper translation on the half-period along the y direction. The latter corresponds to the space group, with a nonconventional setting.

A particular case of layer groups is that of the so-called plane groups mentioned above. Formally, they are the symmetry groups of diperiodic systems in two dimensions. They correspond to the layer groups that do not contain the rotation axes lying in the layer plane and the reflection planes coinciding with the layer plane. Semi-infinite crystals with plane diperiodic surfaces have plane groups as the groups of symmetry.

2.4.2 Orbits of Layer Groups

The Wyckoff positions (the sets of non-equivalent orbits of the diperiodic groups -DG-orbits) for the 80-layer groups can be found in [5, 8]. The Wigner–Seitz (WS) cell for an arbitrary group DG is a right prism with a directrix lying in the layer plane. The projection of the Wigner–Seitz (WS) cell on the layer plane is a polygon constructed from the basis vectors $\boldsymbol{a}_1$ and $\boldsymbol{a}_2$ [6]. The WS cell of the corresponding triperiodic group G is derived by construction of additional planes perpendicular to the vectors $\boldsymbol{a}_3$ (and perhaps to their integer combinations with the vectors $\boldsymbol{a}_1$ and $\boldsymbol{a}_2$) and passing though their midpoints. Thus, the WS of the group G is a part of that for the corresponding group DG.

The site-symmetry groups of Wyckoff positions for the majority of positions belonging to both WS cells (of G and of DG) are identical since they are determined by the same set of symmetry operations. The only exception may be for the points on the sides of the group G cell that are absent in that of the group DG. The existence of translational symmetry in the third dimension in the group G may give rise to additional symmetry operations in site-symmetry groups for these points in the group G with respect to DG. The part of the WS cell of the layer group DG that has no common points with the cell of the corresponding group G contains the points of general position and the points with site symmetry defined by vertical planes and rotation axes. These types of site symmetry are already represented in the common part of the cells for G and DG. Therefore, the set of points with different types of site symmetry in the group G is larger than that in the group DG. Thus, the points of different types of site symmetry (Wyckoff positions) in DG may be specified by the same roman letters as in the corresponding groups G [8]. In layer groups the inversion center and the points of intersection of vertical and horizontal symmetry elements may be situated only in the layer plane. This means that the symmetry points of the Wigner–Seitz cell for a layer group DG may appear only in its intersection with the layer plane. An example illustrating the Wyckoff positions connection in space group C_{2h}^5 and layer DG 18, is given in [6].

Oriented site symmetry symbols for layer groups are used to show how the symmetry elements at a site are related to the conventional crystallographic basis. The site-symmetry symbols display the same sequence of symmetry directions as the subperiodic group symbol. Sets of equivalent symmetry directions that do not contribute any element to the site-symmetry group are represented by a dot. Sets of symmetry directions having more than one equivalent direction may require more than one character if the site-symmetry group belongs to a lower crystal system. For example, for the 2c position of tetragonal layer group P4mm (DG55), the site-symmetry group is the orthorhombic group 2 mm.. The two characters mm represent the secondary set of tetragonal symmetry directions, whereas the dot represents the tertiary tetragonal symmetry direction.

2.4.3 Slab Models of Nanolayers

The thin films and surface modeling is connected with the basic concepts, introduced by Tasker [24] in a discussion of the stability of surfaces of ionic or partly ionic crystals. According to classical electrostatic criteria, the stability of a compound surface depends on the characteristics of the charge distribution in the structural unit that repeats itself in the direction perpendicular to the surface. The surface can be studied by considering the crystal as a stack of atomic planes. Each plane consists of sublattices of nonequivalent atoms, a sum over each sublattice on each plane gives the total electrostatic potential. For perpendicular distances z greater than a few interionic spacings, the contribution from a planar sublattice reduces to the particularly simple form

$$V(z) = \frac{2\pi}{S} qz \tag{2.19}$$

where S is the area of the unit cell in the plane and q is the planar sublattice charge. This expression is identical to the potential due to an infinite charged plane of charge density $\rho = \frac{q}{S}$; the field $E = \frac{2\pi}{S} q$ due to the charged plane is constant. Since $V(z)$ and E do not diminish with increasing distance z the electrostatic sum must be over the whole crystal as stacks of planes unless cancellation of these terms occurs. Although the potential $V(z)$ becomes infinite at infinite distances from the plane, it should be noted that when the crystal is constructed as a neutral block the infinities cancel and the potential becomes constant at large distances. In fact, it becomes zero in all cases except where there is a dipole moment perpendicular to the surface. Similarly the field E cancels to zero outside a neutral crystal block, irrespective of the stacking sequence.

The repeat unit of a stack of planes is introduced when analyzing the distribution of the bulk structure atoms over the atomic planes in the direction z normal to the surface. This distribution depends on the crystal bulk structure and Miller index, defining the surface. The three different possible stacking sequences define three types of surfaces.

As a simplest case of the *type-1 surface* we can mention the (001) surface of MgO crystal with the sodium chloride structure. The neutral bulk unit cell consists of two atoms (Mg and O) and both of them occupy the same atomic plane. Each atomic plane has overall zero charge since it consists of both anions and cations in stoichiometric ratio. The potential $V(z)$ cancels on each plane since the contributions of the sublattices are equal and opposite. Additional planes in the surface of the crystal make no contribution to the energy of ions in the bulk of crystal, and the lattice sums required for the Madelung energy at any ion site need include only a few planes either side of that site.

The diperiodic symmetry groups of the rutile and the anatase and the corresponding 3D space groups are given in Table 2.9.

Table 2.9 Symmetry of slabs

Crystal	Index	Space Group		International Symbol		Layer Group	
		Even	Odd	Even	Odd	Even	Odd
Rutile	001	113	65	$P-42_1m$	Cmmm	58	47
	100	31	10	$Pm2_1n$	$P2/m11$	32	14
	101	14	14	$Pm2_1/b11$	$P2_1/b11$	17	17
	110	51	47	$Pmmb$	$Pmmm$	41	37
Anatase	001	51	115	$Pmmb$	$P-4m2$	41	59
	100	53	51	$Pman$	$Pmam$	42	40
	101	12	–	$C2/m11$	–	18	–
	110	13	21	$P112/b$	C222	7	22

Figure 2.19 shows stacking of densely-packed atomic planes under the (110), (100), (101) and (101) surfaces of rutile.

In the case of (110) and (101) slabs, the thinnest repeating layers consisting of three atomic planes each (with Ti atoms positioned in the middle of layer), i.e., $-O-Ti_2O_2-O-$ (Fig. 2.19a) and $-O_2-Ti_2-O_2-$ (Fig. 2.19c) are repeated along the directions of stacking which are inclined from the normal axes of slabs. Both types of layer units possess the zero dipole moment along the stacking direction although each of three planes inside the layer unit is charged (Fig. 2.19a, c). In two other densely-packed rutile slabs, the stacking directions are perpendicular to the slab surfaces while dipole moments of layer units equal to zero again. Inside the (100) slab (Fig. 2.19b), the repeating layer units consist of six $-O-Ti-O-O-Ti-O-$ atomic planes while inside the (001) slab (Fig. 2.19d), each of two TiO_2 atomic planes per repeating layer unit $-TiO_2-TiO_2-$ is electrically neutral. The layer symmetry groups of the rutile strucure thinnest slabs are the following: (110)-Pmmm; (100)-$Pm2_1n$; (101)-$P2_1/b11$; (001)-$P-42_1m$.

For the type-2 surface each plane contributes a term in the potential $V(z)$, but a sum over the planes in repeat units cancels the potential to zero. Addition of extra neutral repeat units at the type-2 surface of the crystal cannot therefore affect the energy of ions in the bulk, and again the Madelung sums for the potential at any ion site are rapidly convergent. The (110) surface of the TiO_2 rutile structure (Fig. 2.19a) is an example of a type-2 surface. Indeed, the bulk crystal unit Ti_2O_4 atoms are distributed over three planes with the surface unit cells consisting of one oxygen atom (two planes) or Ti_2O_2 units (one plane). The atomic planes in this repeating unit are charged (in the ionic model $q = -2$ for oxygen planes and $q = +4$ for Ti_2O_2 planes). However, the stacking of planes with the repeat unit as O–Ti_2O_2–O allows one to obtain zero as its dipole moment along the z-direction. Two other terminations (O–O–Ti_2O_2 and Ti_2O_2–O–O) give the repeat unit that bears a nonzero dipole moment. This example demonstrates that the surface orientation only is not always sufficient to refer the surface to the one of three types, especially when various terminations may be produced. The atomic TiO_2 planes in the repeat unit of the (001) surface of rutile (Fig. 2.19d) are neutral and the dipole moment of any stack of an integer number of such planes is again zero (type-2 surface). The repeat units for

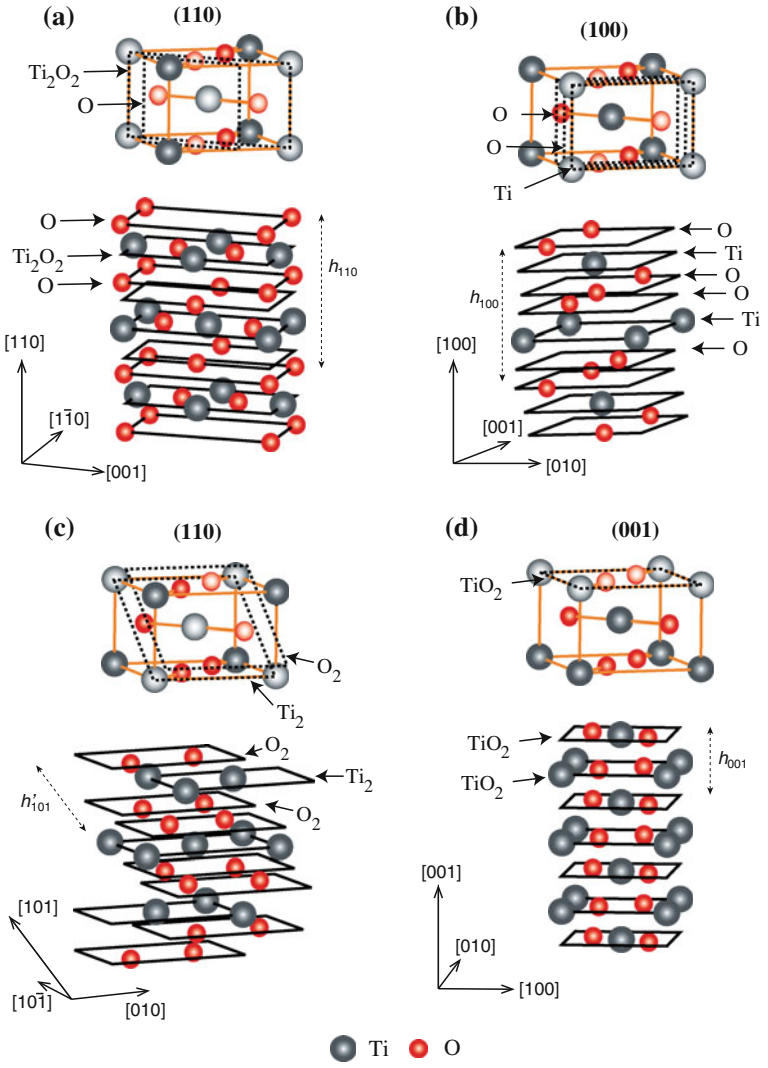

Fig. 2.19 Stacking of atomic planes for densely-packed rutile TiO_2 surfaces cut from bulk unit cells by planes imaged using *dashed lines*. One-two parallel section planes (110) (**a**), (100) (**b**) and (101) (**c**), crossing unit cells and containing oxygen atoms only are shown additionally. For (001) slab (**d**), no additional section plane is necessary. Directions of layer stacking for (110) (a) and (101) (c) slabs are inclined from the axes normal to slab surfaces, however, they are perpendicular to axes [1$\bar{1}$0] and [10$\bar{1}$], respectively. In the cases of (100) (b) and (001) (d) slabs directions of stacking coincide with the normal to slab surfaces

(100) and (101) type-2 surfaces have also zero dipole moment (O- and O_2-terminated repeat units of 6 and 3 atomic planes, respectively, can be chosen).

For the majority of cases of the oxide surfaces the stacking sequence of charged planes has a dipole moment perpendicular to the surface. In particular, the stacks of

alternately charged planes form the repeat unit for (101) surface of TiO_2 (Fig. 2.19c).

Figure 2.20 shows stacking of densely-packed atomic planes under the (001), (101), (110) and (100) surfaces of anatase.

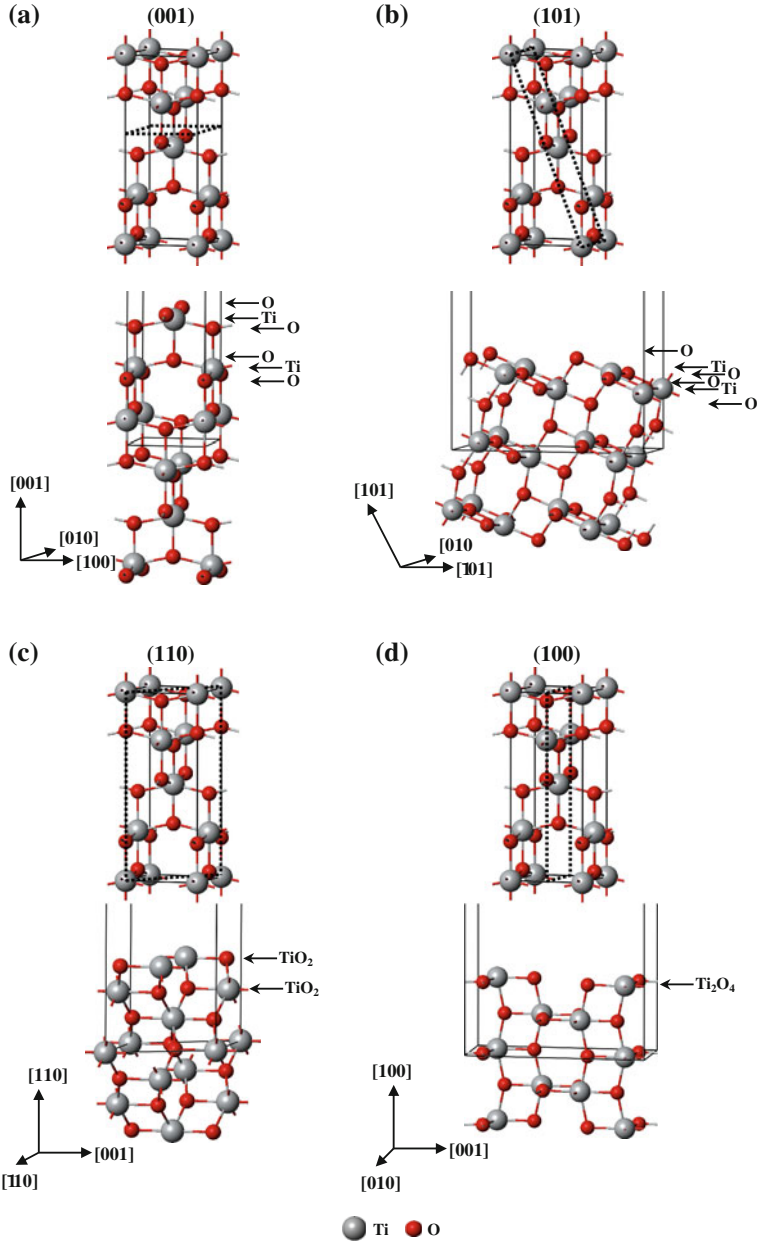

Fig. 2.20 Stacking of atomic planes for anatase TiO_2 surfaces

In the case of (110) and (101) slabs, the thinnest layers are repeated along the directions of stacking which are inclined from the normal axes of slabs. In two other densely-packed slabs, the stacking directions are perpendicular to the slab surfaces. The thinnest (110) layer consists of two $-TiO_2-TiO_2$ atomic planes, see Fig. 2.20c. The thinnest (001) and (101) layers consist of six $-O-Ti-O-O-Ti-O-$ atomic planes each, see Fig. 2.20a, b. At last, the thinnest (110) anatase slab consists of one plane $-Ti_2O_4-$, see Fig. 2.20d. In (100) and (001) densely-packed slabs, the stacking directions are perpendicular to the slab surfaces. All the four anatase layer units possess the zero dipole moment along the stacking direction. Each of six planes inside the (001) and (101) layer units is charged while $-Ti_2O_4-$ and $-TiO_2-TiO_2-$ planes in (100) and (110) layer units are electrically neutral. The thinnest layer symmetry groups of the anatase structure are the following: (110)-P112/b; (100)-Pmam; (101)-C2/m11; (001)-Pmmb.

Figure 2.21 shows the stacking of atomic planes for cubic perovskite ABO_3 surfaces.

All the surfaces in cubic perovskite structure are type-3 surfaces being stacks of alternately charged planes. It is less obvious in the case of the (001) surface in $A^{II}B^{IV}O_3$ as the repeat unit consists of neutral atomic planes (see below). It is also seen that the charge of the atomic plane depends both on the oxidation states of A and B atoms (the sum of oxidation states is in all cases 6) and Miller indexes of the surface.

For the stacking sequence of alternately charged planes (producing a dipole moment perpendicular to the surface) the two-plane repeat unit produces a potential at large distances whose magnitude is given by

$$V = 2\pi|q|\frac{a}{S} \tag{2.20}$$

where a is the interplanar spacing. Addition of an extra neutral repeat unit of two planes on the surface of the crystal will affect the energy of ions an infinite distance below the surface. Consequently, the Madelung sum cannot be truncated and must

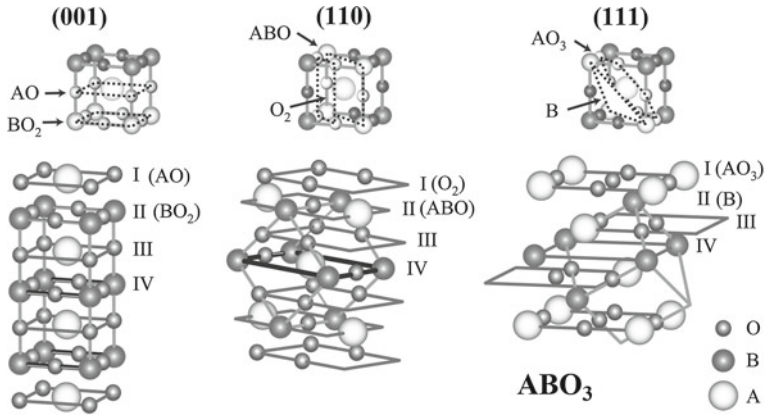

Fig. 2.21 Stacking of atomic planes for cubic perovskite ABO_3 surfaces

include contributions from every plane out to the surface. The potential at any ion site never reaches a constant bulk value, the energy of a neutral pair of ions never reaches the usual cohesion energy and the surface energy is infinite [24]. The stacking of planes for rutile (100), (101) and (111) type-3 surfaces is more complicated as it can not be named as the stacking sequence of alternatively charged planes.

The classification of the surfaces by Tasker is based on the formal ionicities (oxidation states) of metal atoms. As we already noted, the oxidation state and calculated atomic charges are close only in purely ionic compounds (MgO, for example). In fact, the transition-metal atoms charges differ essentially from the oxidation states due to the covalence part of the chemical bonding with oxygen atom.

Type-1 or -2 surfaces have a zero dipole moment in their repeat unit and are thus potentially stable. By contrast, polar type-3 surfaces have a diverging electrostatic surface energy due to the presence of a nonzero dipole moment not only on the outer layers, but on all the repeat units throughout the material [25]. An electrostatic instability of type-3 surfaces results from the presence of that macroscopic dipole. Type-3 surfaces can be stabilized when the macroscopic field is removed by surface reconstruction, absorption of charged specks and so on. The modification of the surface electronic structure due to the reconstruction introduces compensating charges in the outer planes, stabilizing the surface structure. The absorption of charged specks is also a very effective mechanism to achieve the stabilization of polar orientations. Indeed, polar orientations are generally much more reactive than cleavage planes [25].

The classification of surfaces considered above was introduced for ionic or semi-ionic metal oxides. In covalent solids, the creation of a surface requires cutting covalent bonds, which means that dangling bonds would be present at the surface. The saturation of dangling bonds by chemisorption is important, for example, in silicates. When a surface is cut out from the bulk, unstable Si–O radicals at the surface react readily with water to give a fully hydroxylated surface with hydrophilic character.

Tasker's classification of surfaces allows some qualitative conclusions to be made about the surface stability. The quantitative calculations of the surface formation energy in slab models are considered in the next sections.

The crystals with wurtzite structure are layered compounds. Figure 2.22 shows the stacking of the atomic planes in the ZnO wurtzite structure for different slabs. The bulk unit cell consists of two ZnO formula units.

The thinnest (001) layer consists of four $Zn - O - Zn - O$ atomic planes, see Fig. 2.22a. The (001) surface of wurtzite structure is the most stable and used in the nanostructures modeling. In the thinnest (110) all four atoms of the bulk unit cell occupy the same plane forming type-1 surface structure (2.22b). The layers (100) and (101) consist of two and four atomic planes respectively (see Fig. 2.22c, d). In the former each of two atomic planes is neutral (2D unit cell contains ZnO formula unit); in the latter each of four atomic planes O–O–Zn–Zn is monoatomic. The (110) and (100) surfaces refer to the type 1, while (001) and (101)- to the types 3 and 2, respectively. The relative stability of the different wurtzite surface structures depends also on the interlayer distance. In particular the most stable (001) slab in the wurtzite

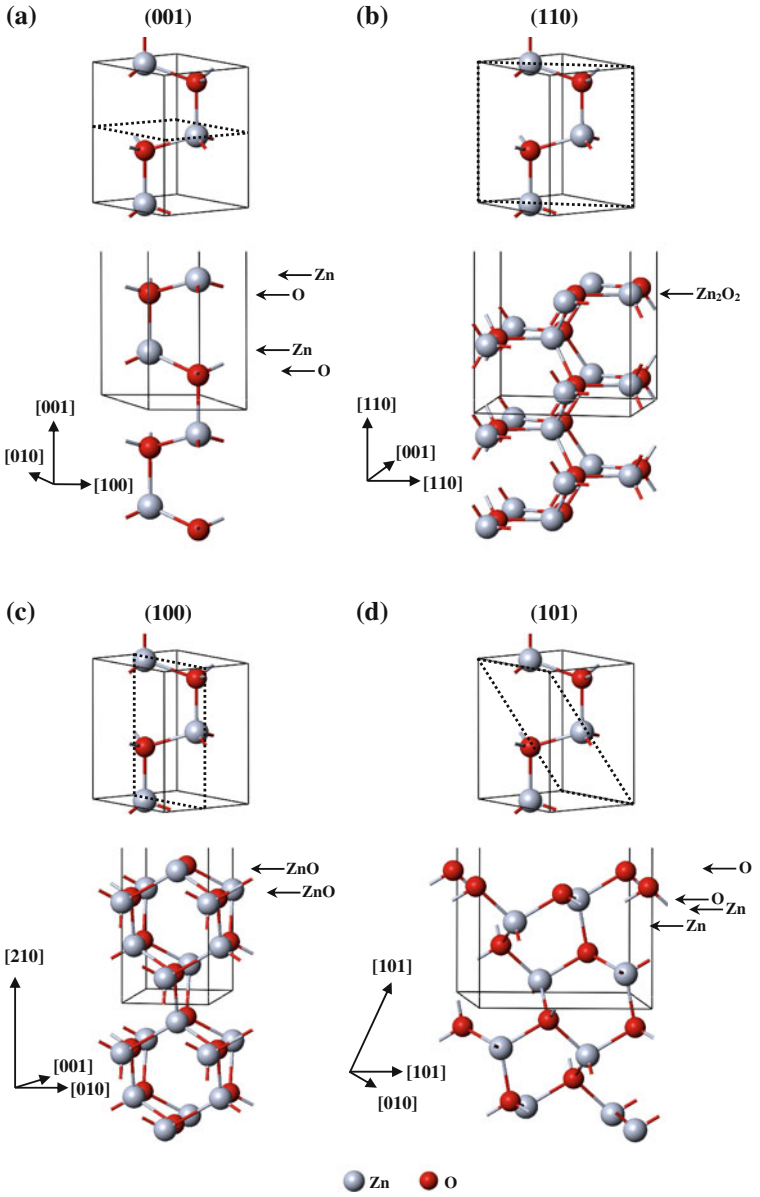

Fig. 2.22 Stacking of atomic planes for wurtzite ZnO surfaces

structure consists of two-plane neutral fragments separated by the relatively large interlayer distance.

Figure 2.23 shows atomic planes for TiS_2 structure (space group $P\tilde{3}m1$, hexagonal 3D lattice. The bulk unit cell consists of two formula units. The minimal size (001) slab consists of three atomic planes: the middle is formed of Ti atoms, while two

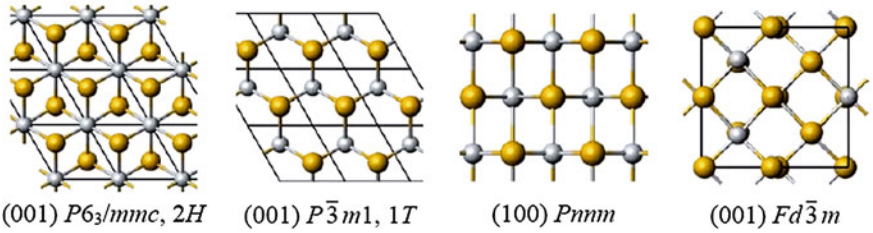

Fig. 2.23 Atomic planes in TiS_2 structures

other sheets are from sulfur atoms, see Fig. 2.23. Just this slab is used in the nanotube rolling for TiS_2 structure, see Sect. 3.5.

2.5 Line and Rod Symmetry Groups of Stereo-Regular Polymers and Monoperiodic Nanostructures

2.5.1 Different Factorization of Line and Rod Groups

Line groups L are divided into two classes: incommensurate and commensurate [3]. Incommensurate line groups contain rotohelical transformations $(C_\varphi|f)$ with rotation angles φ that are not commensurate with π.

By definition, commensurate line groups (also called monoperiodic groups) are discrete symmetry groups of three-dimensional objects translationally periodic along a line: stereo-regular polymers, nanotubes, nanowires, nanoribbons and quasi-one-dimensional subsystems in the bulk (threeperiodic) crystals. In the objects mentioned the basic constituents (monomers) are repeated regularly.

The number of line groups is infinite as the translation axis can be the rotation or screw axis of any integer order q. The relevance of line groups for polymers was discussed by Vainstein [1]. The derivation of commensurate line groups as the symmetry groups of stereo-regular polymer molecules was presented in [4].

Normally the z-axis is chosen as a line group principal axis and with such a convention the elements of pure translation subgroup T(a) are of the form $(E|0, 0, na)$, n-integer. Here a is a translation period defined as a smallest positive real number such that $(E|0, 0, a)$ belongs to the group under consideration. For elements of T(a) the symbol $(E|a)$ instead of $(E|0, 0, a)$ will be used. The symbol T will stand for the discrete group of pure translations along z-axis when $a = 1$.

Under the standard for crystallography approach any commensurate line group may be presented in the form

$$\mathrm{L} = \mathrm{T}(\vec{a})\mathrm{F} \tag{2.21}$$

where F is a finite system of coset representatives of line group decomposition in cosets of $\mathrm{T}(a)$-invariant subgroup of L. The choice of representatives in not unique

and any specific set F is, in general, not a subgroup of L. However, since L is the extension of F by T(a), F can be interpreted as a group with multiplication modulo pure translations (factor group L/T(a)). The group F is isomorphic to the axial point group P_I known as isogonal point group. Factorization (2.21) of line group L will be referred to as standard [26].

The derivation of the commensurate line groups is given in [4]. The line groups are described in the standard factorization (2.21) as an extension of a one-dimensional translation group by an isogonal point group. The isogonal point group is either cyclic or a semi-direct product of cyclic groups.

The method of derivation of the line groups consists of first extending by the cyclic isogonal point groups and then obtaining the rest of the line groups by unification within the Euclidean group. To this purpose, a simple test is given to decide whether two line groups multiply into a third one. The method displays the subgroup structure of the line groups, relevant to the construction of their irreducible representations. All the commensurate line groups are derived and tabulated in [4].

An alternative method considered in [3] exploits elementary group-theoretical means (with quite a bit of Number Theory) but embraces both commensurate and incommensurate line groups. This method is based on the factorization

$$\mathrm{L} = \mathrm{ZP} \tag{2.22}$$

where Z is a cyclic generalized translation group, and P is a finite point group. The requirement that L contains a subgroup of pure translations immediately implies that Z must be of one of the following two forms:

$$\mathrm{Z} = \mathrm{T}_q^r(f) = \langle (C_q^r|f) \rangle \quad \text{or} \quad \mathrm{Z} = \mathrm{T}'(a) = \langle (\sigma_v|\frac{a}{2}) \rangle \tag{2.23}$$

where f is a *fractional* translation, $\mathrm{r} = 0, 1, 2, \ldots, q-1$.

If the factorization (2.22) is used, then the structure of line groups may be studied in several steps.

As the first step it is reasonable to analyze the discrete point groups operating on cylindrical surfaces. Such an analysis (used also in [4]) is not complicated and gives 7 families of the point groups which leave cylinder invariant (the so-called axial point groups P_I):

$$\mathrm{C}_q, \quad \mathrm{S}_{2q}, \quad \mathrm{C}_{qh}, \quad \mathrm{D}_q, \quad \mathrm{C}_{qv}, \quad \mathrm{D}_{qd}, \quad \mathrm{D}_{qh} \tag{2.24}$$

Then step by step it is necessary to consider the products ZP to find out when each concrete product is a group, and to ascertain that it has not occurred at previous steps, probably in a different guise.

The orthogonal transformations of axial point groups P_I leave the z-axis invariant (rotations C_q around the z-axis, reflections σ_v in vertical planes) or reverse the direction of the z-axis (rotations U around the second order axis perpendicular to the z-axis, reflections σ_h in horizontal planes). The former transformations are called

the positive ones, the latter—the negative ones. As the product of negative elements is positive, the set of positive elements is either the whole group (positive group P_I^+) or a halving subgroup, when the group is called negative: $\mathrm{P}_I^- = \mathrm{P}_I^+ + p^- \mathrm{P}_I^+$. It was shown that the isogonal point groups of equivalent line groups are necessarily conjugated by proper rotations which leave the z-axis invariant.

The construction of the physically distinct line groups in both factorizations is based on the fact that all isogonal point groups are either cyclic ($\mathrm{C}_q, \mathrm{S}_{2q}$) or the product of cyclic groups: $\mathrm{C}_{qv} = \mathrm{C}_q \wedge \mathrm{C}_{1v}$; $\mathrm{C}_{qh} = \mathrm{C}_q \times \mathrm{C}_{1h}$; $\mathrm{D}_q = \mathrm{C}_q \wedge \mathrm{D}_1$; $\mathrm{D}_{qd} = (\mathrm{C}_q \wedge \mathrm{C}_{1v}) \wedge \mathrm{D}_1$; $\mathrm{D}_{qh} = (\mathrm{C}_q \wedge \mathrm{C}_{1v}) \wedge \mathrm{C}_{1h}$.

In Table C.1 (given in Appendix C) from [3] the result of such an analysis is presented: all line groups are divided into 13 families, each family includes infinitely many line groups. Among these families there are 5 symmorphic (families 2, 3, 6, 9, 11) for which factorization (2.22) coincides with the standard one. The families 1 and 5 contain both incommensurate and commensurate (symmorphic and nonsymmorphic) line groups.

Table C.1 lists the line groups of 13 families for any order q of the rotation or screw axis written in the form L = ZP, [3]. The line group decomposition:

$$\mathrm{L}^{(\mathrm{F})} = \sum_{i=1}^{N_F} l_i^{(F)} \mathrm{L}^{(1)} \tag{2.25}$$

contains the subgroup $\mathrm{L}^{(1)}$—a set of all roto-helical transformations and in the case of the first family groups $\mathrm{L}^{(1)}$ is the line group itself. For families $F = 2, 3, \ldots, 8$ it is a halving subgroup ($N_F = 2$), for the remaining families $F = 9, \ldots, 13$ the first family subgroup $\mathrm{L}^{(1)}$ is a subgroup of index four ($N_F = 4$). The coset representatives $l_i^{(F)}$ are given in Table C.1 [3].

In the theory of line groups the 1st family, being one of the simplest, plays nevertheless the most important role. The reason is in the structure of axial groups P in (2.22): any such group contains C_n as its subgroup and, consequently, admits decomposition in cosets of C_n.

The main result concerning the line groups of the 1st family may be formulated as follows [3]:

For a fixed translation period *a commensurate* line groups of the 1st family are parametrized by triplets $(\tilde{q}, n, r) \in \mathbb{N}^+ \times \mathbb{N}^+ \times K$

$$\mathrm{L} = \mathrm{T}_{\tilde{q}n}^r (\frac{a}{\tilde{q}}) \mathrm{C}_n = \mathrm{T}(a)\mathrm{F} \tag{2.26}$$

where $K = \{r : 0 \leq r \leq \tilde{q}\ \&\ \mathrm{GCD}(\tilde{q}, r) = 1\}$, GCD is the abbreviation for the greatest common divisor, and $\mathbb{N}^+$ is the set of positive natural numbers. Here

$$\mathrm{F} = \bigcup_{t=0}^{\tilde{q}-1} \left(C_q^{rt} | \frac{a}{\tilde{q}} t \right) \mathrm{C}_n, \quad q = \tilde{q}n \tag{2.27}$$

Note that, by definition, $\mathrm{GCD}(l, 0) = 1 \Leftrightarrow l = 1$ and, consequently, $r = 0$ corresponds to the case $\mathrm{T}_n^0(a) = \mathrm{T}(a)$. It is pertinent to emphasize as well that a (for fixed $(\tilde{q}, n, k)$) is a translation period of the maximal free 1-periodic subgroup $\mathrm{T}(a)$ of the line group (2.26). The analogous subgroup of the generalized group Z of translations has, in general, greater period ([3]).

Table C.1 shows that some line groups can be given with different factorizations. Rotations around the z-axis and translations along it commute, which implies that all the helical operations $(C_Q|f)$ (Q- is the rotation axis order, f is a partial translation) commute with pure rotations C_n around the z-axis i.e. rotations from the point group P_n. Therefore any group P_n is compatible with any group $T_Q(f)$ for any Q. Their products $T_Q(f)C_n$ comprise first family line groups $\mathrm{L}^{(1)}$ which are subgroups of all the other line groups. Similarly, all $T_Q(f)$ are compatible with groups D_n since $U(C_Q|f)^t = (C_Q|f)^{-t}U$. The products $\mathrm{T_Q(f)} \wedge \mathrm{D}_n$ comprise the fifth family groups $\mathrm{L}^{(5)}$. Other compatibility relations are as follows [3]. Mirror planes of intrinsic symmetry can be retained only if Q is rational, i.e. $Q = r/q$, where r and q are integers. It means that only commensurate helical groups allow a mirror plane. These helical groups are $T(f = a)$ and T_{2q}^1 $(f = a/2)$, where q is the order of the principal axis of a point group. On the other hand, the glide plane group T' is compatible with all axial point groups. The only requirement when a point group contains mirror planes or U-axes is that the glide plane should either coincide with them or bisect them, and different groups are obtained in these two cases. As a glide plane is commensurate, so are all the resulting groups. All the products of the point factor P and the generalized translation group Z define 11 remaining line group families, given in Table C.1. Thus one gets 13 infinite families of line groups. Each family includes all groups (with various parameters Q, f, n) with a fixed type of Z and P. Incommensurate line groups are either from the first or from the fifth family, while in all the other families the generalized translation group is either the glide plane reflections group T′, the pure translation group T, or the zigzag group T_{2n}^1. The products L = ZP are weak direct, Z is a cyclic group, the intersection of Z and P can only be the identity element. If one or both subgroups are invariant, this product becomes semi-direct (with the first factor invariant) or direct, respectively. It is well-known that some subgroups of the group of Euclidean transformations admit different geometric realizations. For example, group $\mathrm{C}_{qv}(\alpha) = \mathrm{C}_q \cup \sigma_\alpha \mathrm{C}_q$, where σ_α is a reflection in the vertical plane passing through z-axis and a line in the xy-plane with the direction vector $(\cos\alpha, \sin\alpha, 0)$ is a geometric realization of C_{qv} group defined by the setting angle α. Usually the setting angle is taken equal to zero which corresponds to choosing xz as a benchmark reflection plane. In particular, in the theory of line groups the setting angle is usually chosen equal to zero [3]. On the other hand, groups C_q stipulate a unique geometric realization as soon as the axis and direction of rotations are chosen.

Not being subgroups of space groups (unlike rod groups), line groups are a much wider class of symmetries. While rod groups describe only translationally periodical objects, line groups include symmetries of incommensurate structures. In the limit $q = \infty$ each family gives a continuous group P_∞. These limiting groups correspond to the symmetry of linear molecules and also behave as the isogonal

groups of incommensurate systems. Axial point groups P_I are descrete subgroups of the cylindrical point group P_∞.

When used to describe the symmetry of polymer molecules line groups can also be factorized as a weak direct product of the intrinsic point symmetry P of monomer and the group of generalized translations Z, arranging these monomers along the direction of periodicity, see [3] and references therein. The product of two subgroups is a group if and only if these subgroups commute, i.e. PZ = ZP(it does not mean that $Z_j P_i$ is equal to $P_i Z_j$). The symmetry operations of polymers are defined as geometrical transformations leaving the compound unchanged. These operations occur in two different ways: as periodicity of the regular arrangement of monomers (comprise group Z) and as the intrinsic symmetry P of a single monomer. However, the intrinsic symmetry of the monomer P_n is the symmetry of the whole polymer only if it leaves simultaneously all the monomers unchanged, i.e. if it is compatible with the periodical arrangement [3]. This fact was used in [27] for a line group classification: after an independent classification of all the possible arrangements and their symmetries, as well as of the symmetries of monomers, these two were combined in all possible compatible ways to get all the possible line groups. Such an approach allows one to consider the symmetry of both commensurate (one-periodic) and incommensurate (non-periodic) systems. Moreover, in such a way one can directly obtain important information on the specific structure of line groups and can use it to explore many significant physical consequences.

Under the standard approach any commensurate line group may be presented in the form

$$\mathrm{L} = \mathrm{T}(a)\mathrm{F} = \sum_{\mathrm{i}=1}^{\mathrm{n_p}} (\mathrm{R_i}|\mathrm{v_i})\mathrm{T(a)} \tag{2.28}$$

The choice of coset representatives $(R_i|v_i)$ in the standard factorization in not unique and any specific set F is, in general, not a subgroup of L. In (2.28) R_i and n_p are the operation and order of the isogonal point group P_I, respectively. Improper translations v_i appear only in nonsymmorphic line groups. Such a factorization of the line group is the same as that of rod groups. However in the former the rotation axis order q is any positive integer number, in the latter q = 1, 2, 3, 4, 6.

The first family commensurate line groups are represented in the standard factorization as $\mathrm{L} = q_p$ and as $\mathrm{L} = \mathrm{T}_q^r \times \mathrm{C}_n$ in factorization (2.22). In the standard factorization $L = (C_q^1|\frac{p}{q})$ where C_q^1 is the rotation by the angle $\frac{2\pi}{q}$ around the translation axis. Evidently $L = (C_q^r|\frac{rp}{q})$ so that $rp = n + lq$ (l is integer, $n = \mathrm{GCD}(q, r)$). These relations allow the two factorizations of the same line group to be written.

As an example we consider the line group $\mathrm{L} = q_{28}^{22}$ with q = 28, n = 2, p = 22. Therefore $22r = 2 + 28l$ and for l = 7 we obtain r = 9 so that in the factorization (2.22) this group is written as $T_{28}^9 C_2$. It will be seen later that such a line group is the symmetry group of the nanotube with the chirality (4,2) rolled up from the hexagonal lattice.

2.5.2 Rod Groups and their Settings as a Special Geometric Realizations of Line Groups

75 rod groups (RG) are known in crystallography as subperiodic subgroups of space groups (SG) [5] and form the finite subset of an infinite number of line groups as the order q of rotation or screw axis can only be 1, 2, 3, 4, 6. By analogy with a space (three-periodic) and layer (two-periodic) groups rod groups are factorized RG = TF as an extension of the one-dimensional translations group T (invariant subgroup of RG) by the factor group F = RG/T. A subperiodic rod group RG can contain the following elements [28]: translations $\boldsymbol{a}$ in one direction which by convention is designated as z-axis; a two-, three-, four- or sixfold rotation or screw axis pointed in this direction; the rotation U around twofold axes perpendicular to it; reflection planes containing translation vector (vertical planes σ_v) and reflection planes perpendicular to it (horizontal planes σ_h). Every RG is in correspondence with some three-periodic space group SG: it is a subgroup of SG and has the same point symmetry group F. To obtain RG, it is sufficient to keep translations only in one direction in a related SG. The related RG and SG groups have the same international notations.

Table D.1 (see Appendix D) gives the correspondence between rod and space groups—their international notation, the number of the corresponding SG and its Schönflis symbol. This Table can be compared with Table B.1 from Appendix B, where correspondence between three-dimensional two-periodic (DG) layer groups and three-dimensional three-periodic space groups (SG) is given. Screw axes in layer groups only can be the second-order axes, lying in the layer plane. Screw axes in rod groups are oriented along the translation direction and therefore can be axes of orders 2, 3, 4, 6. One can find information about rod groups on the Bilbao Crystallographic Server [8]. These groups are specified by their number or by international symbols. The first symbol P (primitive) is the same for all rod groups as the translations are made along the principal symmetry axis, formally forming primitive one-periodic lattice. Then the information about symmetry elements is given. The screw axis of the order q has subscript p (p = 0, 1, 2, …, $q-1$). The corresponding symmetry operations are rotations through $2\pi p/q$ about the z-axis. The reflection planes are denoted by m (mirror planes) and c (vertical glide planes containing the translation axis). The factor groups F of rod groups (called in crystallography by crystal classes) are isomorphic to axial point groups C_q, D_q, S_{2q}, C_{qv}, C_{qh}, D_{qd}, D_{qh}. For q = 1, 2, 3, 4, 6 there are 31 different axial point groups, defining the crystal class of the related space and rod groups. The point groups D_1, D_{1d}, D_{1h} are isomorphic to the point groups C_2,C_{2h}, C_{2v}, respectively; the point groups C_{1h}, C_{1v} are isomorphic to the point group C_s. This isomorphism is used in crystallographic description of rod groups distributed over 27 crystal classes. The corresponding space groups are given in their Schönflis notation in the second column in Table D.1. As can be seen from Table D.1, some rod groups are related to two different space groups as two possible RG settings can be chosen. For example, RG 46 (with the third order rotation axis along z) is related to the space groups D_3^2 and D_3^1 when the second order axis U is

directed along the x- and y-coordinate axes, respectively. However, two different rod groups 15 (Pmm2) and 18 (Pm2m) are subgroups of the same SG 25. Whereas, in RG 15 the second order rotation axis is directed along the translation direction z, in RG 18 the second order rotation axis is orthogonal to z. As in the latter case this axis can be directed along both the x and y Cartesian axes, RG 18 has two settings −P2mm and Pm2m, respectively. 75 rod groups can be distributed over 13 families, as is shown in Table D.2 (see Appendix D).

Family 1 consists of rod groups belonging to classes C_q and containing rotations q or q_p, p = 0, 1, ..., $q-1$ (in international notations) around q-order ($q = 2, 3, 4, 6$) rotation or screw axis. Family 5 consists of rod groups belonging to classes D_q and containing rotations q or q_p around the q-order rotation or screw axis and rotations U. The symmorphic rod groups of classes S_{2q}, C_{qh}, C_{qv}, D_{qd} and D_{qh} are related to families 2, 3, 6, 9 and 11, respectively. The remaining 6 families are formed by nonsymmorphic rod groups and include rotations around screw axes $(2q)_q$ with $q = 1, 2, 3$ (families 4, 8, 13) or reflections in vertical glide planes (families 7, 10, 12). As can be seen from Table D.2, rod groups 15 and 18 refer to families 6 (crystal class C_{2v}) and 11 (crystal class D_{1h}), respectively.

Table D.3 (see Appendix D) is taken from [3] and presents rod groups in the form accepted for a line group classification.

For the symmorphic RG a crystallographic factorization RG = TF coincides with that used for line groups (RG = TP_I). For nonsymmorphic RG difference appears: compare Tables D.2 and D.3.

The first family rod groups ($T_q^r C_n$) are represented in the standard factorization as q_p, q = 1, 2, 3, 4, 6; p = 0, 1, ..., $q-1$. In the standard factorization $L = (C_q^1|\frac{p}{q})$ where C_q^1 is the rotation by the angle $\frac{2\pi}{q}$ around the translation axis. Evidently $L = (C_q^r|\frac{rp}{q})$ so that $rp = n + lq$ (l is integer, $n = \mathrm{GCD}(q, r)$). These relations allow the two factorizations of the same rod group to be written. As an example we consider the rod group 57 ($L6_4$) of the first family: q = 6, n = 2, p = 4. Therefore $4r = 2 + 6l$, $r = 2$ (for l = 1) and the rod group 57 in the factorization (2.22) is written as $T_6^2 C_2$, see Table D.3.

Let us consider now rod groups belonging to family 4. In the crystallographic factorization these groups belong to classes C_{qh}, q = 1, 2, 3, see Table D.3. However, the factor group F contains rotations around the screw axis of the order $(2q)_q$ i.e. rotations around the translation axis are in fact rotohelical operations, including the rotation and improper translation by a half of the translation vector. The rod groups of family 4 can be factorized in such a way that the rotohelical operations are included in the cyclic group of the generalized translations Z (pure translations form the subgroup T of the group Z) and pure rotations are included in the point group P_n, see Table D.3. In this case rod groups of family 4 are written in the form ZP, where $Z = T_q^1$ and $P_n = C_{nh}$. Next we consider the example of the rod groups of family 12, belonging to crystallographic class D_{qh} and containing reflections in the vertical glide planes, see Table D.3. Now Z = T′ and contains all the pure translations and reflections in glide planes while $P_n = C_{nh}$, see Table D.3.

Rod groups being a special case of the line groups, arise as 1-periodic subgroups of space groups and it comes as no surprise that space groups may contain different geometric realizations of the same line group. Rod groups settings as a special geometric realizations of line groups are considered in [26]. For each of the 8 families of non-symmorphic line groups the explicit correspondence between rod groups and relevant geometric realizations of the corresponding line groups is established. The settings of rod groups and line groups are taken into account.

In crystallography different realizations of the same rod group are called *settings*. In the theory of line groups crystallographic settings manifest themselves as geometric realizations with specially chosen setting angles. Besides infinitely many geometric realizations of line groups containing reflections in vertical planes or Umklapp transformations there exist realizations which differ in the choice of a horizontal reflection plane. For example, instead of the point group $\mathrm{C}_{nh} = \mathrm{C}_n \cup \sigma_h \mathrm{C}_n$ it is possible to take the group $\mathrm{C}'_{nh} = \mathrm{C}_n \cup (\sigma_h|\frac{a}{2})\mathrm{C}_n$ which corresponds to selection as the reflection plane the affine plane parallel to the xy-plane but passing through the point $(0, 0, \frac{a}{4})$.

As we already mentioned, the rod groups are distinguished among general line groups by the orders q of principal axes of the isogonal groups which can take the values $q = 1, 2, 3, 4, 6$. For $q = 3, 6$ in tables of rod groups [5] the hexagonal coordinate system is used. The hexagonal coordinate system is obtained by the rotation of the y axis counter-clockwise by $\frac{\pi}{6}$ angle in the xy-plane. Basis vectors of the hexagonal coordinate system are connected with the Cartesian ones by the relations:

$$h_1 = e_1, \quad h_2 = -\frac{1}{2}e_1 + \frac{\sqrt{3}}{2}e_2, \quad h_3 = e_3 \tag{2.29}$$

To compare line and rod group realizations one should be able to proceed from the usual mathematical notation of affine transformations to that accepted in crystallography [5]. Symmetry elements (reflexion planes, axes, etc.) are defined in crystallography *parametrically*. For example, in Cartesian coordinates a triplet $x, 0, z$ defines a plane as a locus $\{xe_1 + ze_3 : x, z \in \mathbb{R}\}$. It is clear that the normal vector of this plane is $e_2 = (0, 1, 0)$. A triplet $x + s, -x, z$ defines the affine plane $\{(x + s)e_1 - xe_2 + ze_3 : x, z \in \mathbb{R}\}$ passing through the point $(s, 0, 0)$ and with the normal vector $e_1 + e_2 = (1, 1, 0)$. A triplet $x, -x, 0$ defines a line $\{xe_1 - xe_2 : x \in \mathbb{R}\}$ in the xy-plane. A triplet $x, -x, \frac{a}{4}$ is a line in the affine plane passing through the point $(0, 0, \frac{a}{4})$ in parallel with the xy-plane. The analogous convention is used in the case when the hexagonal coordinate system is used. For example, lines in the xy-plane having with the x-axis angles $-\frac{\pi}{3}, -\frac{\pi}{6}, 0, \frac{\pi}{6}, \frac{\pi}{3}, \frac{\pi}{2}, \frac{2\pi}{3}$ and passing through the origin have the following parametric presentation in hexagonal coordinate system: $0, y, 0$; $x, -x, 0$; $x, 0, 0$; $2x, x, 0$; $x, x, 0$; $x, 2x, 0$; $0, y, 0$.

Basic symmetry operations of rod groups in crystallography have the following designation: rotation $(C_{\pm n}|0)$ around the z-axis is designated as $n^{\pm}\, 0, 0, z$, screw rotation $(C_{\pm n}|f)$—as $n^{\pm}(f)\, 0, 0, z$, reflection $(\sigma_0|0)$ with respect to the xz-plane—as $m\, x, 0, z$, reflection $(\sigma_{\frac{\pi}{4}}|0)$—as $m\, x, x, z$, reflection $(\sigma_h|0)$—as $m\, x, y, 0$. Glide plane reflections of the type $(\sigma_0|\frac{a}{2})$ are encoded as $c\, x, 0, z$, transformations $(\sigma_h|\frac{a}{2})$—as

$m\ x, y, \frac{a}{4}$. Umklapp transformations are interpreted as rotations: for example, transformation $(U_{\frac{\pi}{2}}|0)$ is designated as $2\,0, y, 0$, and transformation $(U_{\frac{\pi}{2}}|\frac{a}{2})$—as $2\,0, y, \frac{a}{4}$. The notation for transformations of the type $(\sigma_h C_{\pm n}|f)$ is slightly more cumbersome and not unique: operation $(\sigma_h C_{\pm n}|0)$ is designated as $\bar{n}^{\pm}\,0, 0, z; 0, 0, 0$, and operation $(\sigma_h C_{\pm n}|\frac{a}{2})$—either as $\bar{n}^{\pm}(\frac{a}{2})\,0, 0, z; 0, 0, 0$ or as $\bar{n}^{\pm}\,0, 0, z; 0, 0, \frac{a}{4}$. In the last example ambiguity is connected with existence of two equivalent presentation of the transformation under consideration: $(\sigma_h C_{\pm n}|\frac{a}{2}) = (\sigma_h|\frac{a}{2})(C_{\pm n}|0) = (C_{\pm n}|\frac{a}{2})(\sigma_h|0)$. Inversion at the origin is encoded as $\bar{1}\,0, 0, 0$.

Line groups of the first family do not depend on the setting angle because their geometric realization is uniquely defined by the choice of the rotation axis and a convention about the direction of rotation (normally counter-clockwise). Therefore, each rod group of the first family should appear in the unique setting.

For each of the seven families of nonsymmorphic line groups the explicit correspondence between rod groups and relevant geometric realizations of the corresponding line groups is established in [29]. The settings of rod groups and line groups are taken into account. The results are presented in a table of 75 rod groups listed (in international and factorized notation) by families of the line groups according to the order of the principal axis q (q = 1, 2, 3, 4, 6) of the corresponding isogonal point group.

2.5.3 Orbits with Respect to Line and Rod Groups

Orbits are useful both in theory of molecules, polymers, and solids. Indeed, for arbitrary group G its orbit G.**x** contains points that should be occupied by atoms of the same element if at least one point, say **x**, is occupied by an atom of this type. In theory of molecules implicit subdivision of space into the union of orbits is performed as the first step in construction of symmetry adapted basis functions. Actual construction is performed either by application of certain projection operators or by diagonalization of specially selected matrices. It is normally assumed that irreducible matrix representations are tabulated and ready for use. Therefore the conception of stabilizer is not very fruitful here. The situation is different in line group theory. Stabilizers are used for site symmetry analysis and for construction of Frobenius induced representations. Line groups operate on the cylindrical (Cyl) surfaces of fixed radius and the corresponding orbits also lie on these surfaces. Type, or symmetry of orbit is defined by the set of stabilizers of its points: orbits of the same type have *identical* sets of stabilizers. Such orbits are called equivalent. Since non-degenerate cylindrical surfaces with fixed $\rho \neq 0$ are of dimension 2, sets of equivalent orbits as topological spaces can be of dimensions 2, 1, and 0 (isolated orbits). For $\rho = 0$ sets of equivalent orbits may be of dimension 1 and 0. It is convenient to introduce the notation $\mathbf{x}_\rho(\alpha+\beta, z) = (\rho\cos(\alpha+\beta), \rho\sin(\alpha+\beta), z)$ for general point belonging to Cyl_ρ where α will play the role of the *setting angle* and β angle will be used for orbit parametrization (along with the z- coordinate).

L-orbits and their types can not depend upon line group factorization. But it is possible to construct in a certain sense minimal sets of representatives of line group orbits which (i) uniquely define the orbit type, and (ii) can be used for *easy* generation of the whole L-orbit. These sets may depend on the line group factorization. It is clear that F-orbits can play a role of such sets of representatives in the case when the standard factorization is used. If the factorization $\mathrm{L} = \mathrm{ZP}$ is exploited then, as can be shown [3], either P or P^+-orbits satisfy the aforementioned requirements (i) and (ii) in *almost all* situations. Here P^+ is a subgroup of group P formed by orthogonal transformations leaving unchanged z- coordinate of any point. Ambiguity may arise in the case when the type of $\mathrm{P}(\mathrm{P}^+)$-orbit depends on the parity of n but the corresponding L-orbits turn out to be equivalent for all values of n. For example, if $\mathrm{P} = \mathrm{C}_{nv}(\alpha)$ then $\mathrm{C}_{nv}(\alpha)$ - orbits $\mathrm{C}_{nv}(\alpha)\mathbf{x}_\rho(\alpha, z)$ and $\mathrm{C}_{nv}(\alpha)\mathbf{x}_\rho(\alpha + \frac{\pi}{n}, z)$ are equivalent for odd and non-equivalent for even values of n. But the corresponding $\mathbf{T}^1_{2n}(a)\mathrm{C}_{nv}(\alpha)$-orbits (line groups of family 8) are equivalent without dependence on the parity of n. The analogous situation takes place for the line groups of family 13. And the second nuance is connected with the fact that even for symmorphic groups there may exist P^+-orbits whose actual type (symmetry) is determined by subgroups including transformations with *non-zero translational parts*. In more rigorous terms, if $\mathbf{x}$ is a point of P^+-orbit then it is possible that the stabilizer $\mathrm{P}^+_{\mathbf{x}}$ turns out to be only a proper subgroup of the full stabilizer $\mathrm{L}_{\mathbf{x}}$.

It is easy to see that $\mathrm{P}(\mathrm{P}^+)$-orbits are always the subsets of the corresponding F-orbits. The major difference between them is the following. L-orbit is obtained from the corresponding F-orbit by application to its points all possible pure translations along the z-axis. If the factorization (2.22) is used then either the screw axis group or the glide plane group must be applied to the points of the $\mathrm{P}(\mathrm{P}^+)$-orbit to get the whole L-orbit. Unfortunately in general there is no one-to-one correspondence between symmetry labels of orbits with respect to Line and Rod groups.

2.5.4 Nanotube Rolling Up from 2D Systems

The simplest description of nanotube symmetry and structure is based on so-called layer folding. Let $\mathbf{a}$ and $\mathbf{b}$ be the primitive translation vectors $\mathbf{a}_1$ and $\mathbf{a}_2$ of the two-periodic (2D) lattice of the layer and γ-the angle between them. Layer folding means the construction of the cylindrical surfaces of nanotubes by rolling up 2D crystalline layers. To specify the symmetry of nanotubes as monoperiodic (1D) systems, it is necessary to define the finite 1D translation vector $\mathbf{L} = l_1\mathbf{a} + l_2\mathbf{b}$ along the nanotube axis and normal to the chiral vector $\mathbf{R} = n_1\mathbf{a} + n_2\mathbf{b}$ (l_1, l_2, n_1 and n_2 are integers). The nanotube of the chirality (n_1, n_2) is obtained by folding the layer in a way that the chiral vector $\mathbf{R}$ becomes circumference of the tube. The orthogonal vectors $\mathbf{R}$ and $\mathbf{L}$ are connected with the 2D lattice translation vectors $\mathbf{a}$ and $\mathbf{b}$ by the transformation

$$\begin{pmatrix} \mathbf{R} \\ \mathbf{L} \end{pmatrix} = \mathbf{Q} \begin{pmatrix} \mathbf{a} \\ \mathbf{b} \end{pmatrix} \tag{2.30}$$

The determinant $q = \begin{vmatrix} n_1 & n_2 \\ l_1 & l_2 \end{vmatrix}$ of the matrix $\mathbf{Q} = \begin{pmatrix} n_1 & n_2 \\ l_1 & l_2 \end{pmatrix}$ is equal to the number of 2D lattice points in the plane lattice supercell formed by the chirality $\mathbf{R}$ and translation $\mathbf{L}$ vectors. The orthogonality relation $\mathbf{RL} = 0$ can be written in the form:

$$\frac{l_1}{l_2} = -\frac{n_2 b^2 + n_1 ab\cos\gamma}{n_1 a^2 + n_2 ab\cos\gamma} \tag{2.31}$$

where $a = |\mathbf{a}|$ and $b = |\mathbf{b}|$. If n is the greatest common devisor of n_1 and n_2 ($\tilde{n}_1 = n_1/n, \tilde{n}_2 = n_2/n$), one can introduce the reduced chirality vector $\tilde{\mathbf{R}}$ along the direction of the vector $\mathbf{R}$:

$$\tilde{\mathbf{R}} = \frac{1}{n}\mathbf{R}; \quad \begin{pmatrix} \tilde{\mathbf{R}} \\ \mathbf{L} \end{pmatrix} = \tilde{\mathbf{Q}} \begin{pmatrix} \mathbf{a} \\ \mathbf{b} \end{pmatrix}; \quad \tilde{\mathbf{Q}} = \begin{pmatrix} \tilde{n}_1 & \tilde{n}_2 \\ l_1 & l_2 \end{pmatrix}; \quad \tilde{q} = \det(\tilde{\mathbf{Q}}) \tag{2.32}$$

The comparison of (2.31), (2.32) shows that $q = n\tilde{\mathrm{q}}$ where $\tilde{q}$ is the number of the lattice points in the supercell formed by the reduced chirality $\tilde{\mathbf{R}}$ and translation $\mathbf{L}$ vectors.

Commensurate nanotubes, being monoperiodic systems, have a line group symmetry $\mathbf{L} = \mathbf{ZP}$ [30, 31], where $\mathbf{P}$ is the point factor and $\mathbf{Z}$ is the generalized translation group. The point factor $\mathbf{P}$ is a subgroup of the axial point group $\mathbf{P_I}$ belonging to one of the axial symmetry point groups. The group $\mathbf{Z}$ is infinite and cyclic, describing either the glide plane reflections $T' = (\sigma_v|\frac{1}{2})$ or the screw axis rotations by $\frac{2\pi}{n\tilde{q}}$ (for $\tilde{q} > 1$) generated by helical operations $T_q^r = (C_q^r|\frac{1}{\tilde{q}})$ where $r = 0, 1, \ldots, n-1$. For $n > 1$, pure rotations appear and form a subgroup of the point symmetry group $\mathbf{P_I}$. The smallest helical vector $\mathbf{H}$ is defined as $\mathbf{H} = h_1\mathbf{a} + h_2\mathbf{b} = \frac{r}{n\tilde{q}}\mathbf{R} + \frac{1}{\tilde{q}}\mathbf{L}$ and satisfies the following conditions: $\tilde{n}_1 h_2 - \tilde{n}_2 h_1 = 1$; $h_1 l_2 - h_2 l_1 = r$. The projections of the helical vector $\mathbf{H}$ on the chiral vector $\mathbf{R}$ and translation vector $\mathbf{L}$ (Fig. 2.24) define the rotational and translational parts of the helical rotation T_q^r, respectively. It is evident that the translational part of the helical vector $\mathbf{H}$ is the same for the ray of the nanotubes $(n_1, n_2) = n(\tilde{n}_1, \tilde{n}_2)$, differing by n.

The symmetry of a nanotube is defined by: (i) the nanotube chirality (n_1, n_2), (ii) translation vector components (l_1, l_2) found from the orthogonality relation (2.31), (iii) the point symmetry of the rolled 2D lattice (see below).

The orthogonality relation has different forms for different 2D lattices:

-rectangular primitive ($\cos\gamma = 0; a \neq b$);

$$\frac{l_1}{l_2} = -\frac{n_2 a^2}{n_1 b^2}, \quad \text{or} \quad l_1 n_1 b^2 = -l_2 n_2 a^2; \tag{2.33a}$$

- rectangular centered ($\cos\gamma \neq 0, \frac{1}{2}; a = b$);

$$\frac{l_1}{l_2} = -\frac{n_2 + n_1\cos\gamma}{n_1 + n_2\cos\gamma}; \tag{2.33b}$$

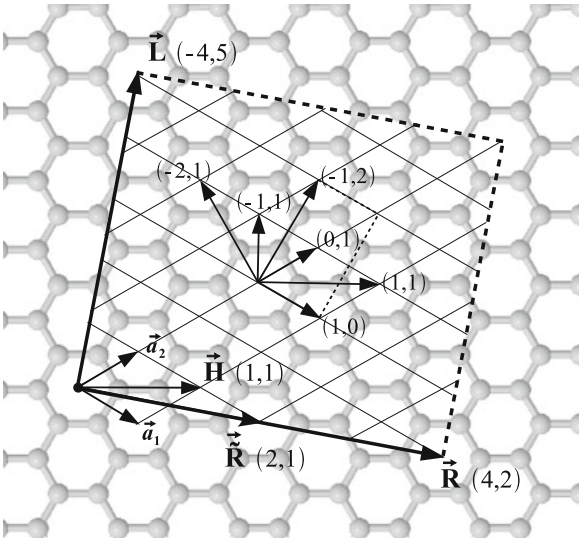

Fig. 2.24 Chirality vectors of the nanotubes from graphene layer

- square ($\cos\gamma = 0; a = b$);

$$\frac{l_1}{l_2} = -\frac{n_2}{n_1} \quad \text{or} \quad l_1 n_1 + l_2 n_2 = 0; \tag{2.33c}$$

- hexagonal ($\cos\gamma = \frac{1}{2}; a = b$);

$$\frac{l_1}{l_2} = -\frac{2n_2 + n_1}{2n_1 + n_2}. \tag{2.33d}$$

It is readily seen from (2.33) that the translational symmetry of the nanotube can exist for any arbitrary chirality (n_1,n_2) if the nanotube is obtained by folding the layer with square or hexagonal 2D lattices. However, there are restrictions on the possible chiralities for rectangular lattices: (n,0), (0,n) for rectangular primitive and ($-n$,n), (n,n) for rectangular centered ones.

The translations of the layer become rotohelical operations T_q^r on the nanotube, giving the first family subgroup $\mathbf{L}^{(1)} = \mathbf{ZP}(\mathbf{P} = \mathbf{C}_q)$ of the nanotube line group $\mathbf{L}$. The latter has the same parameters for the ray of the nanotubes $(n_1, n_2) = n(\tilde{n}_1, \tilde{n}_2)$, differing by n.

Apart from the translational invariance, the layer groups have rotational symmetry generated by the rotations around the z-axis perpendicular to the layer. For rectangular, square and hexagonal lattices the order of these rotation axes is 2, 4 and 6, respectively. In addition, non-oblique 2D lattices have both vertical mirror and glide planes. In the layer groups some of the 2D lattice symmetry operations are absent.

The symmetry operations matrices $G^{(3)} = (F^{(3)}|\mathbf{t}^{(2)})$, corresponding to the layer group, consist of orthogonal $F^{(3)}$ and translational $\mathbf{t}^{(2)}$ parts. Let the Cartesian axes x, y and z be directed along the chiral vector $\mathbf{R}$, the nanotube translation vector $\mathbf{L}$ and the layer principal axis perpendicular to the layer, respectively.

During the folding procedure after the transformation described by (2.30) of the 2D lattice the orthogonal symmetry operations survive if they do not change the z-coordinate (the layer is rolled up to the tube) and do not mix or interchange the x and y coordinates (chirality and translation vectors are assumed to be fixed). It means that after folding the layer, only those layer group symmetry operations survive which had the diagonal 2×2 submatrices

$$F^{Q} = \begin{pmatrix} \pm 1 & 0 \\ 0 & \pm 1 \end{pmatrix}$$

$$E = \begin{pmatrix} 1 & 0 \\ 0 & 1 \end{pmatrix}, \quad U = \begin{pmatrix} -1 & 0 \\ 0 & -1 \end{pmatrix}, \quad \sigma_v = \begin{pmatrix} -1 & 0 \\ 0 & 1 \end{pmatrix}, \quad \sigma_h = \begin{pmatrix} 1 & 0 \\ 0 & -1 \end{pmatrix} \tag{2.34}$$

The transformations (2.34) include the rotation U by π around the second order axis, normal to the tube, and reflections in planes, orthogonal to the 2D lattice plane and parallel to the tube axis, directed along the translation vector $\mathbf{L}(\sigma_v)$ or orthogonal to it (σ_h). In particular among the normal-to-layer rotation axes only the two-fold U-axes survive, being compatible with the monoperiodic symmetry. Therefore whenever the order of the principal axis of the layer is 2, 4 or 6, the symmetry of the nanotube is at least the fifth family line group $\mathbf{L}^{(5)} = \mathbf{ZP}(\mathbf{P} = \mathbf{D}_q)$.

The transformed translations $\mathbf{t}^{Q}$ can be written in the components of the vectors $\mathbf{R}$ and $\mathbf{L}$ as:

$$\mathbf{t}^{Q} = (0\ 0), \quad \left(\tfrac{1}{2n}\ 0\right), \quad \left(0\ \tfrac{1}{2}\right), \quad \left(\tfrac{1}{2n}\ \tfrac{1}{2}\right) \tag{2.35}$$

where $n = 1$ for the reduced chirality vector $\tilde{\mathbf{R}}$, while 1/2 in the second position produces the non-symmorphic line groups containing the helical rotation $T^1_{2n} = (C^1_{2n}|\frac{1}{2})$ or the reflection in glide plane $T' = (\sigma_v|\frac{1}{2})$. The nanotube symmetry groups are formed by the point symmetry operations (2.34) and translations (2.35) survive the folding and combined in such a way that they form the line group $\mathbf{L} = \mathbf{ZP}$.

The procedure described can be applied for finding the nanotube symmetry if the symmetry of the layer group used for folding is known [31]. A helical axis and pure rotations are always present in the line group of a nanotube, while mirror and glide planes appear only for special chiral vectors of rectangular, square and hexagonal lattices. Table 2.10 presents the rolling up correspondence of the line and diperiodic (layer) groups. For each family F of the line groups the roto-helical subgroup $\mathrm{L}^{(1)}$ and the isogonal group P^{I}_{q} (for irrational Q in families 1 and 5, q is infinite)are given in columns 2 and 3. The corresponding diperiodoc groups enumerated according to [5] follow: for an arbitrary chiral vector the rolling gives either the first or the fifth family line group (when the order of the orthogonal to the lattice plane axis is

Table 2.10 Rolling up correspondence of the line and diperiodic (layer) groups

F	$L^{(1)}$	P_q^I	Diperiodic groups
1	$T_Q C_n$	C_q	1,2,4,5,8,9,10,11,12,13,14,15,16,17,18,27,28,29,30, 31,32,33,34,35,36,65,66,67,68,69,70,71,72,74,78,79
5	$T_Q C_n$	D_q	3,6,7,19,20,21,22,23,24,25,26,37,38,39,40,41,42,43,44,45,46,47,48, 49,50,51,52,53,54,55,56,57,58,59,60,61,62,63,64,73,75,76,77,80
2	TC_q	S_{2q}	**a**:17,33,34; **b**:12,16,29,30
3	TC_q	C_{qh}	**a**:11,14,15,27,31,32; **b**:28
4	$T^1_{2q}C_q$	C_{2qh}	**e**:13,18,35; **d**:36; **h**:69,72,78; **g**:70,71,79
6	TC_q	C_{qv}	**a**:28; **b**:11,14,15,27,31,32
7	TC_q	C_{qv}	**a**:12,16,29,30; **b**: 17,33,34
8	$T^1_{2q}C_q$	C_{2qv}	**e**:36; **d**:13,18,35; **h**:70,71,79; **g**:69,72,78
9	TC_q	D_{qd}	**a**:42,45; **b**:24,38,40
10	TC_q	D_{qd}	**c**:25,39,43,44,56,60,62,63
11	TC_q	D_{qh}	**c**:23,37,41,46,55,59,61,64
12	TC_q	D_{qh}	**a**:24,38,40; **b**:42,45
13	$T^1_{2q}C_q$	D_{2qh}	**f**:26,47,48,55,56,57,58,61,62,63,64; **i**:77,80

2, 4, 6). The underlined diperiodic groups (following after the corresponding special chiral vectors) give other line group families below. The corresponding special chiral vectors are the following: $a = (n, 0)$, $b = (0, n)$, $c \in \{(n, 0), (0, n)\}$, $d = (n, n)$, $e = (-n, n)$, $f \in \{(n, n), (-n, n)\}$, $g \in \{(n, 0), (0, n), (-n, n)\}$, $h \in \{(n, n), (-n, 2n), (-2n, n)\}$, $i \in \{(n, 0), (0, n), (-n, n), (n, n), (-n, 2n), (-2n, n)\}$.

2.5.5 Hexagonal and Square Lattices

Different types of nanotubes can be rolled up from layers with a hexagonal plane lattice. We call them nanotubes with hexagonal morphology. Figure 2.25 shows the supercells of a graphene layer defining armchair (3,3), zigzag (3,0) and chiral (6,3) nanotubes.

The first reports on synthesis of carbon nanotubes [32] were followed by extensive symmetry investigation [3, 33] of the nanotubes with hexagonal morphology. Equation (2.33d) ensures the orthogonality of the chiral and translation vectors. From (2.32) we find the matrix $\tilde{\mathbf{Q}}$, its determinant $\tilde{q}$, the components h_1, h_2 of the smallest helical vector $\mathbf{H}$ and $r = h_1 l_2 - h_2 l_1$ for the special chiral vectors $\mathbf{R}$.

$$\mathbf{R}(n, n) : l_1/l_2 = -1; \quad \tilde{\mathbf{Q}} = \begin{pmatrix} 1 & 1 \\ -1 & 1 \end{pmatrix}; \ \tilde{q} = 2; \quad \mathbf{H}(0, 1), \ r = 1 \tag{2.36a}$$

$$\mathbf{R}(-n, n) : l_1/l_2 = 1; \quad \tilde{\mathbf{Q}} = \begin{pmatrix} -1 & 1 \\ -1 & -1 \end{pmatrix}; \ \tilde{q} = 2; \quad \mathbf{H}(-1, 0), \ r = 1 \tag{2.36b}$$

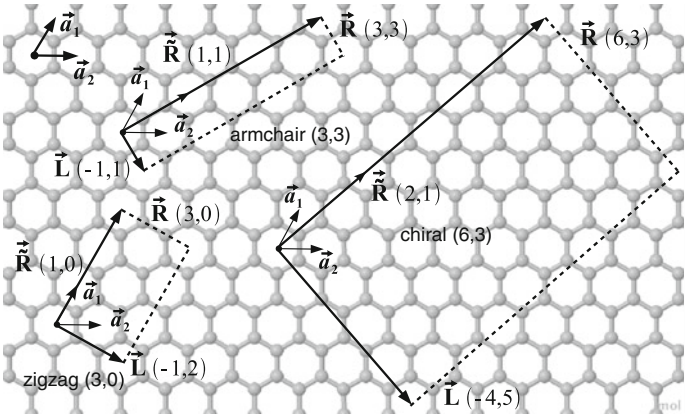

Fig. 2.25 Supercells of graphene layer defining armchair (3,3), zigzag (3,0) and chiral (6,3) nanotubes

$$\mathbf{R}(n,0): l_1/l_2 = -1/2; \quad \tilde{\mathbf{Q}} = \begin{pmatrix} 1 & 0 \\ -1 & 2 \end{pmatrix}; \ \tilde{q} = 2; \quad \mathbf{H}(0,1), \ r = 1 \tag{2.36c}$$

$$\mathbf{R}(-n,2n): l_1 = 1, \ l_2 = 0; \quad \tilde{\mathbf{Q}} = \begin{pmatrix} -1 & 2 \\ -1 & 0 \end{pmatrix}; \ \tilde{q} = 2; \quad \mathbf{H}(-1,1), \ r = 1 \tag{2.36d}$$

$$\mathbf{R}(-2n,n): l_1 = 0, \ l_2 = -1; \quad \tilde{\mathbf{Q}} = \begin{pmatrix} -2 & 1 \\ 0 & -1 \end{pmatrix}; \tilde{q} = 2; \quad \mathbf{H}(-1,1), \ r = 1 \tag{2.36e}$$

As $\tilde{q} = 2$ for all the special chiral vectors, the rototranslational part of the corresponding line group is $T^1_{2n} = (C^1_{2n}|\frac{1}{2})$ while $q = n\tilde{q}$ and $\mathbf{L} = \mathbf{T}^1_{2n}\mathbf{P}_n$. For the general chiral vector $\mathbf{R}(n_1, n_2)(n_1 \neq 0, n_2 \neq 0; n_2 \neq \pm n_1, -2n_1, -\frac{1}{2}n_1)$ we have

$$\tilde{\mathbf{Q}} = \begin{pmatrix} \tilde{n}_1 & \tilde{n}_2 \\ -(2\tilde{n}_2 + \tilde{n}_1) & (2\tilde{n}_1 + \tilde{n}_2) \end{pmatrix}, \ \tilde{q} = 2(\tilde{n}_1^2 + \tilde{n}_1\tilde{n}_2 + \tilde{n}_2^2); \ \tilde{n}_1 h_2 - \tilde{n}_2 h_1 = 1;$$
$$(2\tilde{n}_1 + \tilde{n}_2)h_1 + (2\tilde{n}_2 + \tilde{n}_1)h_2 = r$$

In this case the rotohelical operations are $T^r_q = (C^r_q|\frac{\tilde{r}}{\tilde{q}})$, $q = n\tilde{q}$ is the order of the screw axis, $r = 0, 1, 2 \ldots, q - 1$.

Keeping in mind these results let us analyze Table 2.10. The hexagonal lattice defines layer groups 65–80 (see Table in Chap. 11). In groups 65–68 and 74 the order 3 axes are orthogonal to the lattice plane and mirror planes are absent. Therefore these groups belong to Family one and the tubes rolled up from the corresponding layers have the same symmetry for any chiral vector $\mathbf{R}(n_1, n_2)$. The tubes rolled up from layers with diperiodic groups 69, 72, 78, 70, 71, 79 belong to families 4, 8 depending on the setting of the special chiral vector relative to the mirror planes.

In all these groups the mirror planes appear that are orthogonal to the x- or y-axis appear. Finally, the tubes rolled up from the layers with diperiodic groups 77, 80 belong to Family 13: in these layer groups there are mirror planes orthogonal both to the x- and y-axes.

Perovskite $SrTiO_3$, $BaTiO_3$ nanotubes are synthesized by a low temperature hydrothermal reaction [34]. These nanotubes have a square morphology, i.e. can be rolled up from layers with a square plane lattice ($\cos\gamma = 0; a = b$) [35]. From (2.33c) it follows that $l_1 n_1 + l_2 n_2 = 0$. Applying (2.32) we have

$$\mathbf{R}(n,0) : l_1 = 0,\ l_2 = 1;\quad \tilde{\mathbf{Q}} = \begin{pmatrix} 1 & 0 \\ 0 & 1 \end{pmatrix};\ \tilde{q} = 1;\quad \mathbf{H}(0,1),\ r = 0 \tag{2.37a}$$

$$\mathbf{R}(0,n) : l_1 = -1,\ l_2 = 0;\quad \tilde{\mathbf{Q}} = \begin{pmatrix} 0 & 1 \\ -1 & 0 \end{pmatrix};\ \tilde{q} = 1;\quad \mathbf{H}(-1,0),\ r = 0 \tag{2.37b}$$

As in (2.37a), (2.37b) $r = 0$, no screw axis appears either for $\mathbf{R}(n,0)$ or $\mathbf{R}(0,n)$ special chiral vectors.

$$\mathbf{R}(n,n) : l_1 = -1,\ l_2 = 1;\quad \tilde{\mathbf{Q}} = \begin{pmatrix} 1 & 1 \\ -1 & 1 \end{pmatrix};\ \tilde{q} = 2;\quad \mathbf{H}(0,1),\ r = 1 \tag{2.37c}$$

$$\mathbf{R}(-n,n) : l_1 = -1,\ l_2 = -1;\quad \tilde{\mathbf{Q}} = \begin{pmatrix} -1 & 1 \\ -1 & -1 \end{pmatrix};\ \tilde{q} = 2;\quad \mathbf{H}(-1,0),\ r = 1 \tag{2.37d}$$

As in (2.37c), (2.37d) $\tilde{q} = 2$, the rototranslational part of the corresponding line groups is $T^1_{2n} = (C^1_{2n}|\frac{1}{2})$ while $q = n\tilde{q} = 2n$ and $\mathbf{L} = \mathbf{T}^1_{2n}\mathbf{P}_n$.

For the general chiral vector $\mathbf{R}(n_1, n_2)$, $(n_1 \neq 0, n_2 \neq 0; n_2 \neq \pm n_1)$ we have

$$\tilde{\mathbf{Q}} = \begin{pmatrix} \tilde{n}_1 & \tilde{n}_2 \\ -\tilde{n}_2 & \tilde{n}_1 \end{pmatrix},\ \tilde{q} = \tilde{n}_1^2 + \tilde{n}_2^2;\ \tilde{n}_1 h_2 - \tilde{n}_2 h_1 = 1;\ \tilde{n}_1 h_1 + \tilde{n}_2 h_2 = r;$$
$$h_1 = \frac{1}{\tilde{q}}(r\tilde{n}_1 - \tilde{n}_2);\ h_2 = \frac{1}{\tilde{q}}(r\tilde{n}_2 + \tilde{n}_1) \tag{2.37e}$$

In this case the rotohelical operations are $T^r_q = (C^r_q|\frac{1}{\tilde{q}})$, $q = n\tilde{q}$ is the order of the screw axis, $r = 0, 1, 2, \ldots, q-1$.

Now let us analyze Table 2.10 for layer groups 49–64 with a square lattice. In all these groups the order four axis is orthogonal to the lattice plane. Therefore the tubes with the general chiral vector $\mathbf{R}(n_1, n_2)$ belong to the fifth family. In groups 49–54 there are no mirror planes orthogonal to the lattice plane. Therefore the line group of the corresponding nanotubes belong to the fifth family. As no screw axis appears for the tubes with the special chiral vectors $\mathbf{R}(n,0)$ and $\mathbf{R}(0,n)$, see (2.37a), (2.37b), the corresponding line groups 56, 60, 62, 63 and 55, 59, 61, 64 are symmorphic and belong to families ten and eleven, respectively. These two sets of groups differ in the type of the mirror plane: in the former the orthogonal to the x-axis plane is a glide plane, in the latter this plane is a mirror plane. In layer groups 57, 58 there are no

mirror or glide planes orthogonal to the x-axis. The special chiral vectors $\mathbf{R}(n, n)$ and $\mathbf{R}(-n, n)$, see (2.37c), (2.37d) generate tubes with line groups belonging to Family 13 with a rotochelical tube axis of the order $q = 2n$.

2.5.6 Rectangular Lattices

The layers with rectangular lattices are used for inorganic TiO_2 nanotube modeling [36–38].

For the primitive rectangular lattice ($\cos\gamma = 0; a \neq b$) we have $l_1 n_1 b^2 = -l_2 n_2 a^2$, see (2.33a). For commensurate nanotubes a/b has to be a rational number as it defines l_1/l_2 (l_1, l_2 are integers). It means that the nanotubes are commensurate only for the special chiral vectors.

$$\mathbf{R}(n,0) : l_1 = 1,\ l_2 = 0;\quad \tilde{\mathbf{Q}} = \begin{pmatrix} 1 & 0 \\ 0 & 1 \end{pmatrix};\ \tilde{q} = 1;\quad \mathbf{H}(0,1),\ r = 0 \tag{2.38a}$$

$$\mathbf{R}(0,n) : l_1 = 0,\ l_2 = 1;\quad \tilde{\mathbf{Q}} = \begin{pmatrix} 0 & 1 \\ -1 & 0 \end{pmatrix};\ \tilde{q} = 1;\quad \mathbf{H}(-1,0),\ r = 0 \tag{2.38b}$$

It is seen that for a primitive rectangular lattice the screw axis is absent ($r = 0$).

For the rectangular centered lattice ($cos\gamma \neq 0, 0.5; a = b$), see (2.33b), we have:

$$\frac{l_1}{l_2} = -\frac{n_2 + n_1 \cos\gamma}{n_1 + n_2 \cos\gamma};$$

The corresponding nannotubes are commensurate for the following special chiral vectors:

$$\mathbf{R}(n,n) : l_1 = -1,\ l_2 = 0;\quad \tilde{\mathbf{Q}} = \begin{pmatrix} 1 & 1 \\ -1 & 1 \end{pmatrix};\ \tilde{q} = 2;\quad \mathbf{H}(0,1),\ r = 1 \tag{2.39a}$$

$$\mathbf{R}(-n,n) : l_1 = -1,\ l_2 = -1;\quad \tilde{\mathbf{Q}} = \begin{pmatrix} -1 & 1 \\ -1 & -1 \end{pmatrix};\ \tilde{q} = 2;\quad \mathbf{H}(-1,0),\ r = 1 \tag{2.39b}$$

In this case the rotohelical operations are $T_q^r = (C_q^r | \frac{1}{\tilde{q}})$, $q = 2n$ is the order of the screw axis, $r = 0, 1, 2, \ldots, q-1$.

Now let us analyze Table 2.10 for layer groups 8–48 with rectangular primitive and centered lattices. In groups 8–10 there are no U axis or mirror planes and these groups generate nanotubes belonging to the first family. The two-fold axis orthogonal to the layer plane appears in layer groups 19–22, so that the corresponding nanotube symmetry belongs to the fifth family. The line groups generated by the rolling vectors $\mathbf{R}(n, 0)$ and $\mathbf{R}(0, n)$ are both symmorphic (families 2,3,6,9) or contain a glide plane (families 7,9,12). The line groups generated by the rolling vectors $\mathbf{R}(n, n)$ and $\mathbf{R}(-n, n)$ are nonsymmorphic (families 4,8,13).

For arbitrary single-walled nanotubes, the algorithm of rolled up nanotubes construction, described here theoretically within the formalism of line groups, is also implemented for composition of inputs in CRYSTAL code [14, 39] and is now actively used in LCAO calculations of the different inorganic nanotubes. Nanotubes of any size and order of symmetry can be built automatically by rolling up a 2D slab [40]. That is done by specifying a pair of integers to define a roll-up vector in terms of the slab unit vector components. The rolling vector is perpendicular to the nanotube axis and its modulus is the nanotube circumference.

2.5.7 Symmetry of Double and Multiwall Nanotubes

The symmetry groups of doublewall and multiwall nanotubes are considered in [3, 30, 41]. The symmetry of SW NTs is described by line group $\mathbf{L} = \mathbf{ZP}$, which is a product of axial point group $\mathbf{P}$ and the infinite cyclic group $\mathbf{Z}$ of generalized translations (see Subsection 2.5.1). The latter consists of rotations by $2\pi r/q$ around the q-order screw axis, translations $(n/q)a$ (a denotes the translational period) or reflections in the glide plane $(\sigma_v|a/2)$. Here $n = G(n_1, n_2)$ is the greatest common divisor and (n_1, n_2) define the chiral vector of SW NT.

The line symmetry group of a double-wall nanotube can be found as the intersection $\mathbf{L_2} = \mathbf{Z_2P_2} = (\mathbf{L} \cap \mathbf{L}')$ of the symmetry groups $\mathbf{L}$ and $\mathbf{L}'$ of its single-wall constituents [41]. The intersection $\mathbf{P_2} = (\mathbf{P} \cap \mathbf{P}')$ of the point groups is chosen independently of the generalized translational factor $\mathbf{Z_2}$ [30].

Let (n_1, n_2) and (n_1', n_2') define the chiral vectors of the single-wall constituents of a double-wall nanotube. Its axial point group $\mathbf{P}_2 = \mathbf{C}_N$ is the principal axis subgroup of the DW NT line group $\mathbf{L}_2$ with $N = G(n, n') = G(n_1, n_2, n_1', n_2')$. Only nanotubes composed exclusively of either (n, n) (armchair) or $(n, 0)$ (zigzag) SW constituents can have additional mirror or glide planes, as well as a rotoreflectional axis. The translational factor $\mathbf{Z}_2$ is completely absent for incommensurate DW NT, i.e. when the ratio a/a' is not rational [30]. As an example, we can mention DW NT formed from the hexagonal SW NTs with different types of chirality, both armchair and zigzag, i.e., $(n_1, n_1)@(n_2, 0)$, where the ratio $a/a' = \sqrt{3}$ (a, a' are lengths of the translation vectors of SW constituents).

The coaxial hexagonal DW NTs with $(n_1, n_1)@(n_2, n_2)$ and $(n_1, 0)@(n_2, 0)$ chiralities are commensurate: their translation period is the same as for the constituents: $\mathbf{L} = -\mathbf{a} + \mathbf{b}$ ((n,n)-chirality), $\mathbf{L} = -\mathbf{a} + \mathbf{2b}$ ((n,0)-chirality), as described by (2.33d). For the square lattice period of such DW NTs is the same as for the constituents: $\mathbf{L} = \mathbf{a} - \mathbf{b}$ ((n,n)-chirality), $\mathbf{L} = \mathbf{b}$ ((n,0) chirality), as described by (2.33c). For the commensurate DWNT the translational factor $\mathbf{Z}_2$ contains rotations around the screw axis, common to both SW components. Two possibilities for periodic DW NTs have been considered in [30]: (i) both n_1/N and n_2/N are odd—$\mathbf{L}_2$ contains the screw axis $(2N)_N$; (ii) either one or both n_1/N and n_2/N are even—$\mathbf{L}_2$ contains the rotation axis of order the N. As an example of the first possibility one has hexagonal DW NT $(6, 6)@(10, 10)$: $N = 2$, $n_1/N = 3$, $n_2/N = 5$, the screw axis 4_2.

For DW NT (12, 0)@(18, 0), we have $N = 6$, $n_1/N = 2$, $n_2/N = 3$, the rotation axis of order 6.

In the particular case of commensurate armchair $(n_1, n_1)@M(n_1, n_1)$ and zigzag $(n_1, 0)@M(n_1, 0)$ DW nanotubes with hexagonal morphology (i.e., $n_2 = Mn_1$), the symmetry group can be found from the results obtained in [30] for the full symmetry of multiwall nanotubes. For armchair and zigzag DW NTs with odd M, the line symmetry groups are the same as for their SW constituents—$(2n)_n/m$ (Family 4, point symmetry $\mathbf{C}_{2nh}$) and $(2n)_n mc$ (Family 8, point symmetry $\mathbf{C}_{2nv}$), respectively. For an even M, the rotations about the screw axis of the order $2n$ are replaced by rotations around the pure rotation axis of the order n so that DW NT line symmetry groups become n/m (family 3, point symmetry $\mathbf{C}_{nh}$) and nm (family 6, point symmetry $\mathbf{C}_{nv}$), for armchair and zigzag chiralities, respectively.

For each SW NT, the coordinate system can be chosen with its origin fixed in the initial nanosheet (slab) which the folding procedure has to be applied to. The normal to the slab plane passing through the origin can be defined as x axis in the SW NT coordinate system. Because of the coaxiality, the two parameters completely determine the relative positions of SW constituents in DW NT: the angle φ and length Δz by which the outer tube is rotated around z and translated along z, respectively (in regard to the initial configuration with the coinciding x and x′ axes of both shells) [30, 41]. Thus, the initial position of both SW constituents in DW NTs is characterized by $\varphi = 0$ and $\Delta z = 0$. In this case the maximum possible number of symmetry elements for both SW NTs coincide, and the symmetry of the initial DW NT structure is described by one of the line groups considered above. After atomic relaxation the values of φ and Δz can differ from zero. Presumably, the roto-translational part of DW NT symmetry group (independent of the relative SW NT positions) is not changed after the relaxation. However, other common symmetry elements of SW NTs (second-order U axes normal to the translation vector, reflection and glide planes) can be lost. Thus, the total symmetry of DW NT is reduced. The symmetry of DWNT with hexagonal and square morphology is considered in more detail in next subsections dealing with for BN, TiO_2 and $SrTiO_3$ nanotubes.

For multiwall nanotubes the following symmetry can be found [30]. If at least one of the single-wall constituents is chiral, there are two possibilities in the commensurate case: $\mathbf{T}_q^r \mathbf{C}_N$, corresponding to the general mutual position; and $\mathbf{T}_q^r \mathbf{D}_N$ in the special mutual positions with the common U axis. Similarly, the tube built of incommensurate components has a symmetry described by the point groups $\mathbf{C}_N$ or $\mathbf{D}_N$. If the nanotube is built of either single-wall $(n, 0)$,$(n', 0)$…tubes or single wall (n, n), (n', n'),…tubes, the order of the principal rotational axis is $N = G(n, n' \ldots)$. If the tube contains single-wall tubes of both types, no translational periodicity appears and its symmetry is described by a point group. On the other hand, for a tube composed of components of the same type, the translational period is equal to that of the components. Two different situations can occur: if all the integers n/N, n'/N,…are odd ("odd" case), the translations are refined by the screw axis $\mathbf{T}_{2N}^1$; otherwise, if at least one of these integers is even ("even" case), no screw axis emerges. Note that owing to the various arrangements of the components, any of the line and axial point groups can be the resulting symmetry for the commensurate and incommensurate

Table 2.11 Symmetry of the multiwall $(n, 0)$ (zigzag) and (n, n) (armchair) tubes

Relative position	Line group				Isogonal group		Point group
	Odd		Even		Odd	Even	
General	$\mathbf{T}^1_{2n}\mathbf{C}_N$	(1)	$\mathbf{TC}_N$	(1)	$\mathbf{C}_{2N}$	$\mathbf{C}_N$	$\mathbf{C}_N$
σ_h	$\mathbf{T}^1_{2n}\mathbf{C}_{Nh}$	(4)	$\mathbf{TC}_{Nh}$	(3)	$\mathbf{C}_{2Nh}$	$\mathbf{C}_{Nh}$	$\mathbf{C}_{Nh}$
σ_v	$\mathbf{T}^1_{2n}\mathbf{C}_{Nv}$	(8)	$\mathbf{TC}_{Nv}$	(6)	$\mathbf{C}_{2Nv}$	$\mathbf{C}_{Nv}$	$\mathbf{C}_{Nv}$
σ'_v	$\mathbf{T}^1_{2n}\mathbf{C}_{Nv}$	(8)	$\mathbf{T}_c\mathbf{C}_{Nv}$	(7)	$\mathbf{C}_{2Nv}$	$\mathbf{C}_{Nv}$	$\mathbf{C}_N$
(U, U')	$\mathbf{T}^1_{2n}\mathbf{D}_N$	(5)	$\mathbf{TD}_N$	(5)	$\mathbf{D}_{2N}$	$\mathbf{D}_N$	$\mathbf{D}_N$
σ_h, σ_v	$\mathbf{T}^1_{2n}\mathbf{D}_{Nh}$	(13)	$\mathbf{TD}_{Nh}$	(11)	$\mathbf{D}_{2Nh}$	$\mathbf{D}_{Nh}$	$\mathbf{D}_{Nh}$
σ_h, σ'_v	$\mathbf{T}^1_{2n}\mathbf{D}_{Nh}$	(13)	$\mathbf{T}_c\mathbf{C}_{Nh}$	(12)	$\mathbf{D}_{2Nh}$	$\mathbf{D}_{Nh}$	$\mathbf{C}_{Nh}$
(σ_h, σ'_h)	$\mathbf{T}^1_{2n}\mathbf{C}_{Nh}$	(4)	$\mathbf{TS}_{2N}$	(2)	$\mathbf{C}_{2Nh}$	$\mathbf{S}_{2N}$	$\mathbf{S}_{2N}$
$(\sigma_h, \sigma'_h), \sigma_v$	$\mathbf{T}^1_{2n}\mathbf{D}_{Nh}$	(13)	$\mathbf{TD}_{Nd}$	(9)	$\mathbf{D}_{2Nh}$	$\mathbf{D}_{Nd}$	$\mathbf{D}_{Nd}$
$(\sigma_h, \sigma'_h), \sigma'_v$	$\mathbf{T}^1_{2n}\mathbf{D}_{Nh}$	(13)	$\mathbf{T}_c\mathbf{S}_{2N}$	(10)	$\mathbf{D}_{2Nh}$	$\mathbf{D}_{Nd}$	$\mathbf{S}_{2N}$

components, respectively. The analysis of the special arrangements of constituents with common horizontal axes, mirror or glide planes, that increase the symmetry of the total system is summarized in Table 2.11. For periodic tubes, the line groups (and families) and the isogonal groups are in the "odd" columns if all the ratios n/N, $n'/N, \ldots$ are odd, and in the "even" columns otherwise. The point groups of the tubes with both zigzag ($(n, 0)$—chiralities) and armchair ((n, n)—chiralities) components are in the last column. In the first column the relative positions of the component tubes are characterized by coinciding symmetry elements (beside the common principal axis in the general position). Here (U, U') denotes the horizontal axis, which is the U axis in some of the constituents, and the U' axis in the remaining ones (thus, additional mirror or glide planes are excluded). Also, (σ_h, σ'_h) is a plane which is σ_h in some of the constituents (with n necessarily even) and σ'_h in the remaining tubes; in the incommensurate case, the same groups are obtained when they have commom σ'_h planes.

A single-wall MeS_2 nanotube is three layer sandwich and a building block for a multi-wall tubes. The symmetry analysis of these nanotubes is given in [42]. Depending on chirality, the symmetry group of NT belongs to one of three different families: chiral (n_1, n_2)-$T^r_q(f)C_n$; achiral(n, n)-$T^1_{2n}(f)C_{nh}$; achiral $(n, 0)$-$T^1_{2n}(f)C_{nv}$. Regardless of chirality, single-wall MeS_2 nanotube is a three-orbit system:each S-Me-S sheet is generated by the action of the transformations from the group $T^r_q(f)C_n$ on a single atom arbitrary chosen to represent the orbit. For achiral tubes this is the halving subgroup of the symmetry group, while for the chiral ones it is a complete group.

2.5.8 The Nanowires Construction

The symmetry of a nanowire is described by one of 75 rod groups (RG) considered above. As we have seen the order of the main rotation or screw axis in line groups can be any integer number while in RGs this order can only be the same as in a

bulk crystal, i.e., 1, 2, 3, 4, and 6. This circumstance causes specific conditions of NW geometry construction depending on morphology and symmetry of crystalline lattice. The NW symmetry is defined both by the structure of the prototype bulk crystal and by the direction of the one-dimensional translation periodicity.

The geometric constructions of possible atomic arrangments for inorganic nanowires are suggested in [43]: the nanowires are considered as fragments of bulk crystals (nanocrystalline nanowires). The basic idea of this approach is (1) choose a maximally linear, charge-neutral, and (if possible) dipole-free atomic cluster containing a single formula unit, and (2) using if possible the symmetry axis of this linear cluster as the nanowire growth axis, distributed by translations and screw rotations the atomic clusters to give a stoichiometric nanowire with some symmetry around the growth axis and minimal surface polarity. This approach is demonstrated in [43] for: (1) wurtzite structure (which occurs in [001] nanowires based on GaN and ZnO); (2) fluorite structure CaF_2 based nanowires, growing in [111] orientation; (3) rutile based nanowires growing in [001] and [110] directions and anatase based nanowires oriented along [001] direction. In both cases the charge neutral and dipole free linear TiO_2 units are chosen to construct the nanowire; (4) based on perovskite $BaTiO_3$ structure nanowires oriented along [111] direxion.

Since nanowires can be described as infinite prisms of different diameters, their stability depends on stability of lateral facets, according to Wulff's construction formalism [44]. Lateral facets of nanowire can be constructed basing on the two-periodic slab model used in the surface calculations. There are two approaches to such a construction: (1) choosing the slab in such away that its surface is normal to the chosen NW periodicity direction with subsequent removal of the slab translations and restoring the translation for NW; (2) choosing the nanowire periodicity along the one of the slab 2D translation vectors with subsequent removal of the second translation vector. The first approach is considered in Chap. 7 for the rutile TiO_2 based nanowires construction. Let us consider in more detail the second approach.

Let the nanowire periodicity direction **L** is defined by the set of integer numbers [l_1,l_2,l_3] in units of the bulk lattice translations $\mathbf{a}_1$, $\mathbf{a}_2$, and $\mathbf{a}_3$. One constructs the slab with the nanowire periodicity along the one of the slab 2D translation vectors with subsequent removal of the second translation vector. The rod symmetry group of such a nanowire is subgroup of the slab layer group. The slab surface becomes a facet of the rod obtained, being parallel to the nanowire periodicity direction **L**. All the possible slab surfaces (possible nanowire facets), parallel to **L**, are defined by the integer solutions of the equation

$$l_1k_1 + l_2k_2 + l_3k_3 = 0 \tag{2.40}$$

where the integer numbers k_1, k_2, k_3 are Miller indexes of the slab surface and equal to 0, ± 1 for the low index surfaces. In this case the reciprocal lattice vectors have only two independent integer components m and n for each of seven possible nanowires directions [l_1, l_2, l_3] : [001]→(m,n,0), [010]→(n,0,m), [100]→(0,m,n), [110]→(m,−m,0), [101]→(−m,n,m), [011]→(n,m,−m), [111]→(m,n,−m−n).

Table 2.12 Low index facets of nanowires cut from triclinic, monoclinic and orthorhombic lattices

Nanorod direction	Facets, **k**		Orthogonality, (±)		
	A	B	Triclinic	Monoclinic	Orthorhombic
[001]	(100)	(010)	−	+	+
	(110)	$(\bar{1}10)$	−	−	−
[010]	(001)	(100)	−	−	+
	(101)	$(10\bar{1})$	−	−	−
[100]	(010)	(001)	−	+	+
	(011)	$(0\bar{1}1)$	−	−	−
[110]	(001)	$(\bar{1}10)$	−	−	+
	$(\bar{1}11)$	$(1\bar{1}1)$	−	−	−
[101]	(010)	$(10\bar{1})$	−	+	+
	$(11\bar{1})$	$(\bar{1}11)$	−	−	−
[011]	(100)	$(0\bar{1}1)$	−	−	+
	$(1\bar{1}1)$	$(11\bar{1})$	−	−	−
[111]	$(\bar{1}10)$	$(11\bar{2})$	−	−	−
	$(10\bar{1})$	$(1\bar{2}1)$	−	−	−
	$(0\bar{1}1)$	$(\bar{2}11)$	−	−	−

The existence of (2.40) solutions depends on the nanowire periodicity direction and Miller indexes of the surfaces in consideration. The sign + in Tables 2.12 and 2.13 means that for a given nanowire direction and the crystal system chosen the orthogonality (2.40) is satisfied for A and B low index surfaces (facets). For monoclinic lattice $\beta \neq 90$. These tables allow to construct the nanowire models for the crystals with the different Bravais lattices.

Let us consider the NWs facets for the rutile TiO_2 structure with the primitive tetragonal lattice [45]. For the [001]-oriented NWs one can expect the {110} facets

Table 2.13 Low index facets of nanowires cut from tetragonal, hexagonal and cubic lattices

Nanorod direction	Facets, **k**		Orthogonality, (±)		
	A	B	Tetragonal	Hexagonal	Cubic
[001]	(100)	(010)	+	−	+
	(110)	$(\bar{1}10)$	+	+	+
[100]	(010)	(001)	+	+	
	(011)	$(0\bar{1}1)$	−	−	
[110]	(001)	$(\bar{1}10)$	+	+	+
	$(\bar{1}11)$	$(1\bar{1}1)$	−	−	−
[101]	(010)	$(10\bar{1})$	+	−	
	$(11\bar{1})$	$(\bar{1}11)$	−	−	
[111]	$(\bar{1}10)$	$(11\bar{2})$	+	+	+
	$(10\bar{1})$	$(1\bar{2}1)$	−	−	+
	$(0\bar{1}1)$	$(\bar{2}11)$	−	−	+

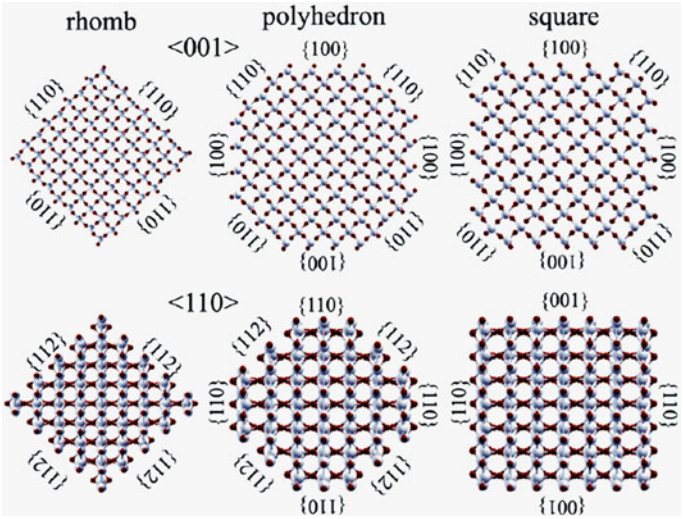

Fig. 2.26 Cross sections of the [001]-oriented TiO_2 NWs with diameters of about 3.9 nm (the *top* panel) and of the [110]-oriented TiO_2 NWs with diameters of 2.9 nm (the *bottom* panel) displaying three possible morphology (the rhomb, the polyhedron, and the square). The large, *light-blue* (*gray*) *balls* stand for Ti atoms, the small, *red* (*dark*) *balls* represent O atoms. All facets are indicated (Reprinted figure with permission from Migas et al. [45], Copyright (2010) by the American Chemical Society)

to characterize their surface (the rhomb case in Fig. 2.26) and this morphology has been observed experimentally [46]. One can also consider NWs in which the {110} and {100} facets are close in size (the polyhedron case in Fig. 2.26) and where the {100} facets dominate with small in size {110} facets playing the role of edges (the square case in Fig. 2.26). The unit cell parameter along the NWs axis ($a_{||}$) is equal to c_{bvlk}.

In the case of NWs with axis along the [110] directions, the facets the {110} and {001} are predicted to appear (the square case in Fig. 2.26). Some other possible morphology can be the polyhedron (the {110}, {001}, and {112} facets are close in size) and the rhomb (only the {112} facets are present), which are also shown in Fig. 2.26. Unfortunately, there is no information about the (112) surface and it is quite possible that such a surface is unstable as far as it has not been observed experimentally.

As a next example let us consider the construction of the nanowire with the periodicity direction $\mathbf{L} = [101]$ for the primitive tetragonal lattice. It is seen that the Miller indexes of the surfaces (010) and $(10\bar{1})$ satisfy (2.40). As the next step we construct the slab parallel to the surface $(10\bar{1})$ and after this remove the periodicity along the direction [010]. For the body centered tetragonal lattice the preliminary supercell transformation has to be made to obtain the teragonal direct lattice unit cell.

All the models in consideration are characterized by the TiO_2 stoichiometry.

The computer code CRYSTAL-14 [39] contains the option which allows the nanowire construction basing on the described above approach. To build nanowire starting from the corresponding 3D bulk structure one needs give in the code input the information about the crystal plane, termination and thickness of the two crystal planes defining the nanowire. The corresponding NW direction is then easily defined from the two tables given above [40]. At this stage, a nanowire can exhibit sharp and unphysical edges that can be smoothed out by further cutting the rod along additional crystal planes parallel to the periodic direction. The origin of the nanowire cell is shifted automatically to maximize symmetry of the rod group.

The NANOCUT code used recently for construction of TiO_2 nanowires with anatase and rutile structures [47] requires to introduce the cut-off radii along the cutting directions orthogonal to direction of NW periodicity. The choice of the cutting distance used as a parameter in that code could be simplified if the preliminary slab consideration is made.

2.6 Symmetry of Crystalline Orbitals in Periodic Systems: Space, Layer and Line Groups

2.6.1 Symmetry of Molecular and Crystalline Orbitals

The aim of the first-principles approaches in quantum chemistry is to calculate the properties of molecules and crystals without the use of empirical parameters. In principle, all the particles—electrons and nuclei—should be involved in such calculations. In fact, the solution of this complicated task is simplified in the Born–Oppenheimer approximation (also called the adiabatic approximation). In the first stage the electronic subsystem is studied for different nuclear configurations to calculate the potential-energy surface and to find the optimized atomic positions corresponding to the minimal total energy per primitive cell. The nuclear motion can be studied *a posteriori*, by considering the electronic energy surface as an external potential.

Quantum chemistry of solids concerns mainly those physical and chemical properties of solids that depend on the electronic structure. The problem of nuclear motion is solved in approaches using molecular-dynamics method. The calculations of the electronic subsystem in the adiabatic approximation are always connected with the choice of the electronic Hamiltonian. Formally, the symmetry of the electronic Hamiltonian may differ from the symmetry of the nuclear configuration. However, in the case of crystalline solids the approximate electronic Hamiltonians are usually chosen in such a way that the translational and point symmetry of a crystal is maintained. In this chapter we consider in more detail two of the mostly popular approximate methods of many-electron systems description—Hartree-Fock method and the density-functional theory. In both approaches the approximate many-electron function is introduced in such a way that the electron subsystem calculations are made for one-electron wavefunctions. The latter are known as molecular orbitals in molecules and crystalline orbitals in crystals.

The symmetry of the electronic Hamiltonian $\hat{\mathrm{H}}$ ensures that orbitals (one-electron functions for many-electron systems) can be classified according to the irreducible representations of point groups for molecules and space groups for crystals.

In the symmetry-adapted basis the diagonalizing of the Hamiltonian matrix H is reduced to the diagonalizing of its diagonal blocks. Every eigenvalue of the matrix $H^{(\alpha)}$ is repeated n_α times in the total list of the eigenvalues of the operator $\hat{\mathrm{H}}$. The eigenfunctions of the Hamiltonian $\hat{\mathrm{H}}$ corresponding to the same eigenvalue are the basis functions of an irrep of the symmetry group G of $\hat{\mathrm{H}}$ (in the absence of accidental degeneracy that is not due to the symmetry) and the degeneracies of eigenvalues are equal to dimensions of the irreps of G (also in the absence of accidental degeneracy). Thus, the eigenstates $\varphi(\boldsymbol{r})$ and their eigenvalues may be labeled by the irreps of the symmetry group G of the Hamiltonian $\hat{\mathrm{H}}$.

The symmetry properties of molecular orbitals and the degeneracy of the corresponding eigenvalues are defined by the irreducible representations of the point groups. The tables of these irreps characters are published in many books and their notations are well known and as a rule unambiguous. The energy-level degeneracy is usually 1 (a, b irreps), 2 (e irreps) and 3 (t or f irreps). As an exclusion, the icosahedral point symmetry group of the fullerene molecule C_{60} has 4- and 5-dimensional representations (g and h irreps, respectively).

For crystalline solids the translation symmetry of the Hamiltonian is taken into account in any electronic-structure calculations as it allows calculations to be made for the basis connected only with the primitive unit cell. In the translation-symmetry-adapted basis the matrix H has a quasidiagonal structure with identical blocks related to an irrep $\boldsymbol{k}$ of the translation symmetry group T. As the latter is Abelian its irreps are one-dimensional. The translation symmetry adapted functions are known as Bloch functions and numbered by wavevector $\boldsymbol{k}$. Use of the point symmetry of a crystal allows the number of Bloch functions calculated to be decreased and further block-diagonalization of Hamiltonian of a crystal to be made.

The numbering of the translation symmetry adapted functions (Bloch functions) remains when the trnslations become two-dimensional (layer groups) or one-dimensional (line groups).

The space symmetry of crystalline orbitals is defined by irreducible representations of space, layer or line groups. The structure of these irreps is more complicated than in the case of point groups. The dimensions of the space, layer and line group irreps and the corresponding degeneracy of energy levels are also different from those for point groups.

The time-reversal symmetry of the crystalline Hamiltonian introduces an additional energy-level degeneracy. Let the Hamiltonian operator $\hat{\mathrm{H}}$ be real. The transition in the time-dependent Schrodinger equation to a complex-conjugate equation with simultaneous time-inversion substitution

$$\mathrm{i}\frac{\partial\varphi(\boldsymbol{r},t)}{\partial t} = \hat{\mathrm{H}}\varphi(\boldsymbol{r},t),\ \mathrm{i}\frac{\partial\varphi^*(\boldsymbol{r},-t)}{\partial t} = \hat{\mathrm{H}}\varphi^*(\boldsymbol{r},-t) \tag{2.41}$$

shows that the functions $\varphi(\boldsymbol{r}, t)$ and $\varphi^*(\boldsymbol{r}, -t)$ are solutions of the same time-dependent Schrodinger equation. This combined operation (complex conjugation + time inversion) is called the time-reversal transformation. Applying this operation to the time-independent Schrödinger equation for the time-independent part of stationary-state wavefunctions

$$\hat{\mathrm{H}}\varphi(\boldsymbol{r}) = E\varphi(\boldsymbol{r}),\ \hat{\mathrm{H}}\varphi^*(\boldsymbol{r}) = E\varphi^*(\boldsymbol{r}) \tag{2.42}$$

we see that $\varphi(\boldsymbol{r})$ and $\varphi^*(\boldsymbol{r})$ are the eigenfunctions of the same real operator $\hat{\mathrm{H}}$ belonging to the same eigenvalue E. So with respect to the time-independent part of stationary states $\varphi(\boldsymbol{r})$ the time-reversal operator reduces to a simple complex conjugation

$$\hat{\mathrm{K}}\varphi(\boldsymbol{r}) = \varphi^*(\boldsymbol{r}) \tag{2.43}$$

Let φ_i $(i = 1, 2, \ldots, n)$ be eigenfunctions of a real Hamiltonian $\hat{\mathrm{H}}$ belonging to an eigenvalue E and also be the basis of a unitary irrep $D(g)$ of its symmetry group $G(g \in G)$. The functions $\hat{\mathrm{K}}\varphi_i = \varphi_i^*$ are also eigenfunctions of $\hat{\mathrm{H}}$ belonging to the same eigenvalue E, but transforming according to the irrep $D^*(g)$. The irreps $D(g)$ and $D^*(g)$ may be either equivalent or inequivalent. The functions φ_i and φ_i^* may be linearly dependent or linearly independent. There are three cases: (1) the functions φ_i and φ_i^* are linearly dependent and are bases of equivalent irreps ; (2) the functions φ_i and φ_i^* are linearly independent and transform according to inequivalent irreps; (3) the functions φ_i and φ_i^* are linearly independent and are bases of equivalent irreps. In cases 2 and 3 the eigenvalue E belongs to $2n$ states φ_i and φ_i^*. They form a basis of the rep of the group G that is the sum of two irreps $D(g)$ and $D^*(g)$ of the same dimension n. Thus, the degeneracy of the eigenvalue E doubles with respect to that caused by the symmetry group in the space. In case 1, there is no additional degeneracy. In tables of irreps of space, layer and line groups the complex conjugate irreps are usually united in one so-called physically irreducible rep. When analyzing the degeneracy of one-electron energy levels in crystals it is necessary to take into account the time-reversal symmetry. In particular, even in the case when the point-symmetry group F of a crystal does not include inversion the complex conjugated crystalline orbitals with wavevectors $\boldsymbol{k}$ and $-\boldsymbol{k}$ correspond to the same energy eigenvalue.

2.6.2 *Irreducible Representations of Space Groups. Symmetry of Crystalline Orbitals of Bulk Crystals*

The group T of pure translations $t_{\boldsymbol{a}}$ of an infinite lattice is a group of infinite order. By introducing cyclic boundary conditions one assumes that the infinite crystal consists of equivalent blocks in the form of parallelepipeds having sides $\boldsymbol{A}_1 = N_1\boldsymbol{a}_1, \boldsymbol{A}_2 = N_2\boldsymbol{a}_2, \boldsymbol{A}_3 = N_3\boldsymbol{a}_3$. It is assumed that the points of different

blocks connected by translations are physically equivalent, i.e. $t_{\boldsymbol{A}_j}^{N_j} = t_{\boldsymbol{0}}$. The large positive number $N = N_1N_2N_3$ defines the size of each block, also called the main region of a crystal (this block contains N primitive unit cells in the cyclic model of a crystal). Only the finite-order group $\mathrm{T}^{(N)}$ (modulo translations $\boldsymbol{A}_l, \boldsymbol{A}_2, \boldsymbol{A}_3$) of N translations $\boldsymbol{a}_n = \sum_{i=1}^{3} n_i \boldsymbol{a}_i$ inside the main region is considered when generating the irreps of the translation group. Because this group is Abelian all its irreps are one-dimensional. Moreover, the group $\mathrm{T}^{(N)}$ is a direct product of groups $\mathrm{T}^{(N_1)}$, $\mathrm{T}^{(N_2)}$ and $\mathrm{T}^{(N_3)}$, as all the translations $t_{\boldsymbol{a}_n}$ commute. Each group $\mathrm{T}^{(N_i)}$ of N_i translations $t_{n_i\boldsymbol{a}_i}$ has N_i one-dimensional irreps $D^j(t_{n_i\boldsymbol{a}_i})$, $j = 1, 2, \ldots, N_i$, satisfying the condition $\left[D^j(t_{\boldsymbol{a}_n})\right]^{N_j} = D^j(t_{N_j\boldsymbol{a}_n}) = D^j(t_{\boldsymbol{0}}) = 1$. Taking $D^j(t_{\boldsymbol{a}_i}) = \exp(-2\pi \mathrm{i} p_j/N_j)$ (where p_j is an integer) one satisfies this condition. The integer $p_j = 0, 1, \ldots, N_j - 1 (i = 1, 2, 3)$ denotes different irreps of the translation group $\mathrm{T}^{(N_i)}$. The irrep $D^{(p_1p_2p_3)}(t_{\boldsymbol{a}_n})$ of the translation group $\mathrm{T}^{(N)}$ can be written as

$$D^{(p_1p_2p_3)}(t_{\boldsymbol{a}_n}) = \exp\left[-2\pi \mathrm{i}(p_1n_1/N_1 + p_2n_2/N_2 + p_3n_3/N_3)\right] \tag{2.44}$$

There are $N = N_1N_2N_3$ sets of integers p_1, p_2, p_3 ($p_i = 0, 1, \ldots, N_i - 1$) that are used to label N different irreps of the translation group $\mathrm{T}^{(N)}$.

Introducing the primitive translation vectors $\boldsymbol{B}_1, \boldsymbol{B}_2, \boldsymbol{B}_3$ of the reciprocal lattice by

$$(\boldsymbol{a}_i \cdot \boldsymbol{B}_j) = 2\pi\delta_{ij}, \quad (i, j = 1, 2, 3) \tag{2.45}$$

one may define allowed $\boldsymbol{k}$ vectors (wavevectors) by $\boldsymbol{k} = \kappa_1\boldsymbol{B}_1 + \kappa_2\boldsymbol{B}_2 + \kappa_3\boldsymbol{B}_3$, where $\kappa_i = p_i/N_i (i = 1, 2, 3)$. Thus

$$(\boldsymbol{k} \cdot \boldsymbol{a}_n) = 2\pi(n_1p_1/N_1 + n_2p_2/N_2 + n_3p_3/N_3) \tag{2.46}$$

so that

$$D^{(\boldsymbol{k})}(t_{a_n}) = \exp(-\mathrm{i}\boldsymbol{k} \cdot \boldsymbol{a}_n) \tag{2.47}$$

The N irreps of $\mathrm{T}^{(N)}$ are now labeled by the N allowed $\boldsymbol{k}$ vectors. The point symmetry of reciprocal lattice coincides with that of the direct one. However, the type of reciprocal lattice may differ from that of the direct lattice.

Adding the reciprocal lattice vector

$$\boldsymbol{B}_{\boldsymbol{m}} = \sum_i m_i \boldsymbol{B}_i \tag{2.48}$$

to the allowed $\boldsymbol{k}$ vector we have

$$\begin{aligned} \exp(-\mathrm{i}(\boldsymbol{k} + \boldsymbol{B}_{\boldsymbol{m}}) \cdot \boldsymbol{a}_{\boldsymbol{n}})) &= \exp(-\mathrm{i}\boldsymbol{k} \cdot \boldsymbol{a}_{\boldsymbol{n}}) \exp(-\mathrm{i}\boldsymbol{B}_{\boldsymbol{m}} \cdot \boldsymbol{a}_{\boldsymbol{n}}) \\ &= \exp(-\mathrm{i}\boldsymbol{k} \cdot \boldsymbol{a}_{\boldsymbol{n}}) \end{aligned} \tag{2.49}$$

A pair of vectors $\boldsymbol{k}$ and $\boldsymbol{k}' = \boldsymbol{k} + \boldsymbol{B}_m$ is said to be equivalent since the irrep of $\mathrm{T}^{(N)}$ described by $\boldsymbol{k}$ can be equally well described by $\boldsymbol{k}'$. Therefore, the label $\boldsymbol{k}$ is determined up to within a reciprocal lattice vector and can be changed by vectors $\boldsymbol{B}_m$ of the reciprocal lattice.

The basis functions for the irreps of the translation group $\mathrm{T}^{(N)}$ are known as Bloch functions $\varphi(\boldsymbol{k}, \boldsymbol{r})$ and may be written in the form

$$\varphi(\boldsymbol{k}, \boldsymbol{r}) = \exp(\mathrm{i}\boldsymbol{k} \cdot \boldsymbol{r}) U(\boldsymbol{k}, \boldsymbol{r}) \tag{2.50}$$

where $U(\boldsymbol{k}, \boldsymbol{r}) = U(\boldsymbol{k}, \boldsymbol{r} + \boldsymbol{a}_n)$. Indeed

$$\begin{aligned} t_n \varphi(\boldsymbol{k}, \boldsymbol{r}) &= \exp(-\mathrm{i}\boldsymbol{k} \cdot \boldsymbol{a}_n) \exp(\mathrm{i}\boldsymbol{k} \cdot \boldsymbol{r}) U(\boldsymbol{k}, \boldsymbol{r} - \boldsymbol{a}_n) \\ &= \exp(-\mathrm{i}\boldsymbol{k} \cdot \boldsymbol{a}_n) \varphi(\boldsymbol{k}, \boldsymbol{r}). \end{aligned} \tag{2.51}$$

The Bloch functions are also called the $\boldsymbol{k}$ basis.

Applying a space group operator $g \equiv t_v R (g \in G)$ to the Bloch function $\varphi(\boldsymbol{k}, \boldsymbol{r})$ we obtain a Bloch function $\tilde{\varphi}(\boldsymbol{k}, \boldsymbol{r})$. Indeed

$$\begin{aligned} t_{a_n} t_v R \varphi(\boldsymbol{k}, \boldsymbol{r}) &= t_v R t_{R^{-1} a_n} \varphi(\boldsymbol{k}, \boldsymbol{r}) \\ &= \exp(-\mathrm{i}\boldsymbol{k} \cdot R^{-1} \boldsymbol{a}_n) t_v R \varphi(\boldsymbol{k}, \boldsymbol{r}) \\ &= \exp(-\mathrm{i} R\boldsymbol{k} \cdot \boldsymbol{a}_n) t_v R \varphi(\boldsymbol{k}, \boldsymbol{r}) \end{aligned} \tag{2.52}$$

i.e.

$$t_v R \varphi(\boldsymbol{k}, \boldsymbol{r}) = \tilde{\varphi}(R\boldsymbol{k}, \boldsymbol{r}) \tag{2.53}$$

As follows from (2.49) from the point of view of determining all the irreducible representations of a space group it is only necessary to consider the wavevectors in one unit cell of reciprocal space ($\boldsymbol{k}$ space) and the unit cell that is chosen is referred to as the first Brillouin zone (BZ). For most space groups it is not a primitive unit cell in $\boldsymbol{k}$ space. Instead, the unit cell of $\boldsymbol{k}$ space is the Wigner–Seitz unit cell. The latter is defined as consisting of all those points of $\boldsymbol{k}$ space that lie closer to $\boldsymbol{k} = \boldsymbol{0}$ than to any other reciprocal lattice point. Its boundaries are therefore the planes that are the perpendicular bisectors of the lines joining the point $\boldsymbol{k} = \boldsymbol{0}$ to the nearest and sometimes to the next-nearest reciprocal lattice nodes (the planes bisecting the line from $\boldsymbol{k} = \boldsymbol{0}$ to $\boldsymbol{k} = \boldsymbol{B}_m$ have the equation $\boldsymbol{k}\boldsymbol{B}_m = |\boldsymbol{B}_m|^2/2$). For some direct lattices (simple cubic, for example, see Fig. 2.27) only nearest-neighbor reciprocal lattice points are involved in the construction of the Brillouin zone but for others next-nearest neighbors are involved as well, see Fig. 2.28.

The advantage of this choice is that the Wigner–Seitz unit cell manifests the point-group symmetry F^0 of the appropriate crystal system. The disadvantage is that for certain Bravais lattices the appearance of BZ may be different for different values of lattice parameters. For all Bravais lattices except those of extremely low symmetry the advantage of this definition outweighs the disadvantage [48]. For monoclinic and triclinic space groups the problem of drawing of Brillouin zones for all possible

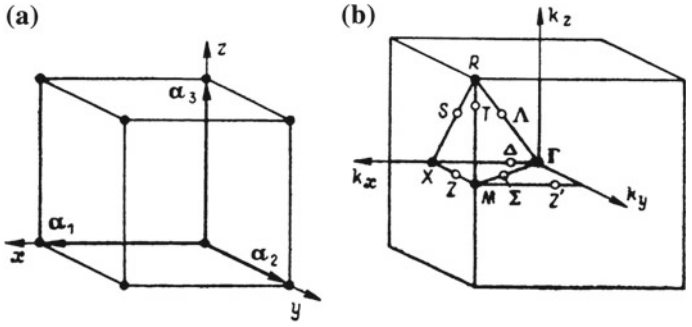

Fig. 2.27 Primitive unit cell (**a**) and Brillouin zone (**b**) for simple cubic lattice

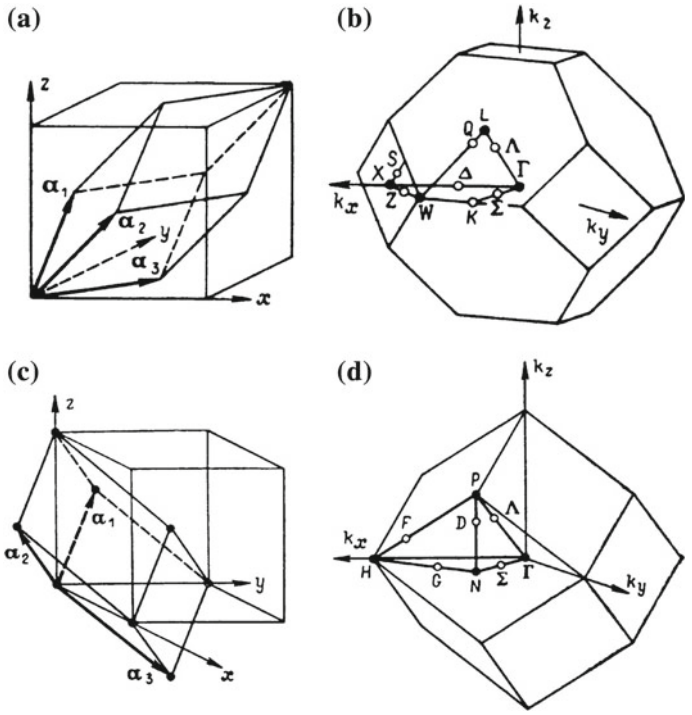

Fig. 2.28 Primitive unit cells (**a, c**) and Brillouin zones (**b, d**) for face-centered and body- centered cubic lattices

relative values of lattice parameters is so complicated that the primitive unit cell of the reciprocal lattice is used for the Brillouin zone. In [49] one can find Brillouin zones representations for all the Bravais lattices and for each set of possible restrictions on the lattice parameters. For cubic, hexagonal, simple tetragonal and simple orthorhombic lattices the shape of the Brillouin zone is unique, while for trigonal, body-centered tetragonal, body-, base- and face-centered orthorhombic lattices there

are two or more possible shapes depending on the relative lengths of the primitive translations and the angles between them.

By construction, the BZ contains N allowed $\boldsymbol{k}$ vectors when N primitive unit cells are included in the main region of a crystal. As the number N is assumed to be arbitrarily large, in the limiting case of $N = \infty$ the allowed $\boldsymbol{k}$ vectors take all values inside the BZ. In the electronic- structure calculations of crystals finite (and relatively small) numbers of $\boldsymbol{k}$ points are considered. However, the interpolation procedure used after calculation allows the one-electron energies to be shown as continuous functions of wavevectors (see, for example, Figs. 2.29 and 2.30 for band structures of $SrZrO_3$ and silicon, respectively).

Two vectors $\boldsymbol{k}$ and $\boldsymbol{k}'$ are said to be equivalent if $\boldsymbol{k}' = \boldsymbol{k} + \boldsymbol{B}_m$. By definition, no two interior points of a Brillouin zone can be equivalent; but every point on the surface of the Brillouin zone has at least one equivalent also on the surface of the Brillouin zone. For each BZ there is a basic domain Ω such that $\sum_R R\Omega$ is equal to the whole BZ, where R are the elements of the holosymmetric point group F^0 (F^0 is the point- symmetry group of the Bravais lattice and defines the appropriate crystal system). For each space group there is a representation domain Φ of the appropriate BZ (it is also called the irreducible part of the Brillouin zone), such that $\sum_R R\Phi$ is equal to the whole BZ, where the sum over R runs through the elements of the point-symmetry group $F \subseteq F^0$ (F is also called the isogonal point group and is obtained

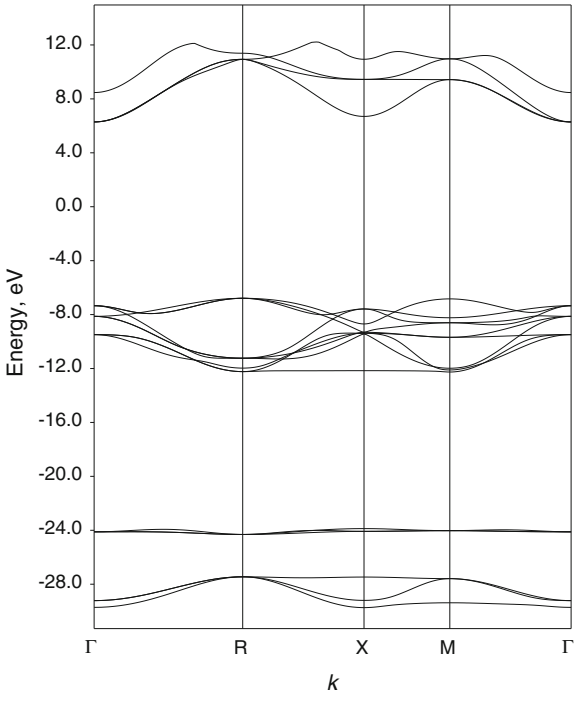

Fig. 2.29 Hartree-Fock energy bands for $SrZrO_3$ crystal

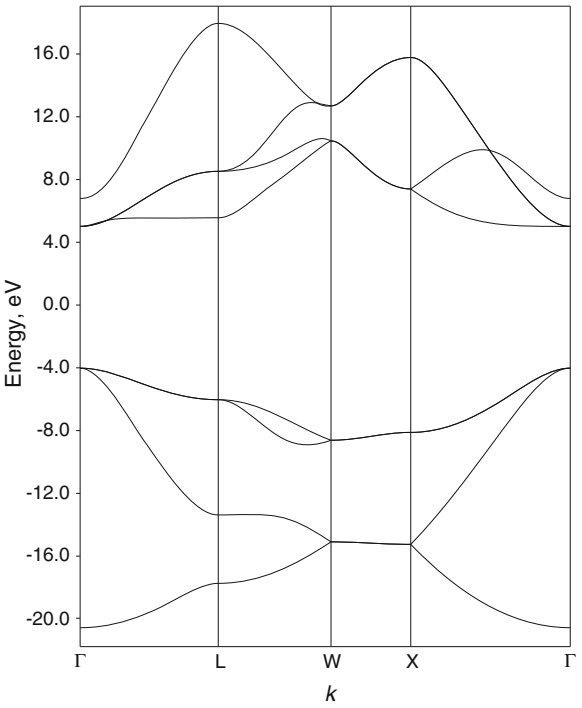

Fig. 2.30 Hartree-Fock energy bands for silicon crystal

by taking all the distinct elements R that are found in the elements $t_v R$ of space group G). For each holosymmetric space group (for which the set of all the distinct rotational parts of the space-group symmetry operations forms the holosymmetric point group F^0 of the appropriate crystal system) Φ can be taken to be identical with Ω. But for the remaining space groups the volume of Φ is some small-integer multiple of the volume of Ω. This multiple is equal to n_{F^0}/n_F, i.e. is defined by orders n_{F^0} and n_F of the holosymmetric point group n_{F^0} and crystal structure point group F. The majority of crystal structures considered in Sect. 2.3 have holosymmetric point groups. The exclusions refer to the structures of sphalerite and wurtzite with point groups T_d and C_{6v} being subgroups of cubic and hexagonal lattices point groups O_h and D_{6h}. In two cases under consideration (BZ for face-centered and hexagonal lattices, Figs. 2.28 and 2.31) the basic domain volumes are equal to 1/48 and 1/24 of the Brillouin-zone volume, the representation domains are two times larger.

Those elements of the point-symmetry group F^0 of the reciprocal lattice that transform a point $\boldsymbol{k}$ into itself or into some equivalent $\boldsymbol{k}$ point form the wavevector point-symmetry group $F_{\boldsymbol{k}} \subset F^0$. For example, for the direct face-centered cubic lattice ($F^0 = O_h$) BZ points Γ(0,0,0), X (1/2,1/2,0), L(1/2,1/2,1/2),W(1/4,1/2,3/4) (see Fig. 2.28) have point symmetry groups O_h, D_{4h}, D_{3d}, D_{2d}, respectively. The point group $F_{\boldsymbol{k}}$ of the $\boldsymbol{k}$ vectors F, Z, M, A (Fig. 2.32) for a simple tetragonal lattice

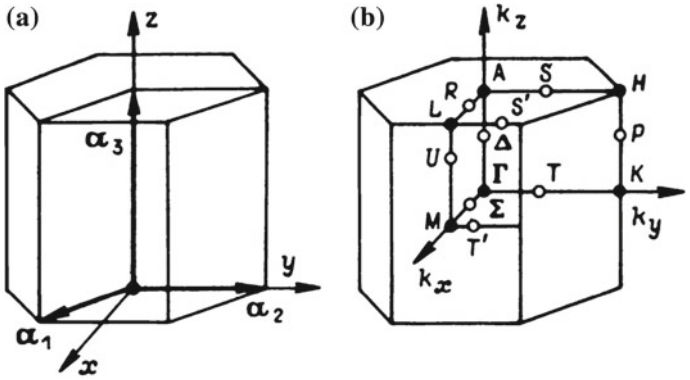

Fig. 2.31 Primitive unit cell (**a**) and Brillouin zone (**b**) for hexagonal lattice

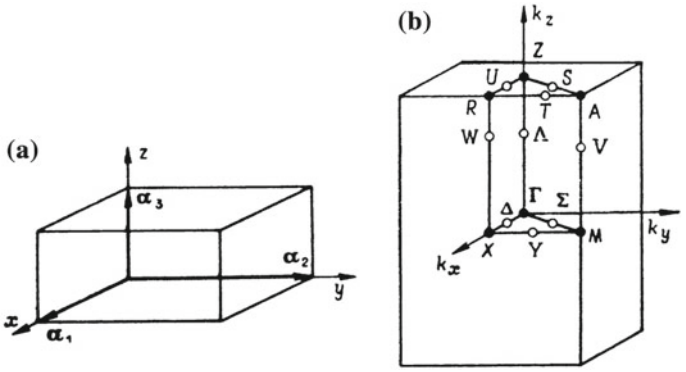

Fig. 2.32 Primitive unit cell (**a**) and Brillouin zone (**b**) for simple tetragonal lattice

coincides with the D_{4h} point group of the tetragonal lattice itself; the point group D_{2h} of the $\boldsymbol{k}$ vectors X and R is a subgroup of D_{4h}.

All the mentioned points of the BZ are called points of symmetry. By definition, $\boldsymbol{k}$ is a point of symmetry if there exists a neighborhood of $\boldsymbol{k}$ in which no point $\boldsymbol{k}'$ has the same symmetry group $\mathrm{F}_{\boldsymbol{k}}$ and $\mathrm{F}_{\boldsymbol{k}'} \subset \mathrm{F}_{\boldsymbol{k}}$. The Γ ($\boldsymbol{k} = \boldsymbol{0}$) point of the Brillouin zone is usually a symmetry point; exceptions here are the space groups of the crystallographic classes C_s, C_{nv}, C_n. All the other symmetry points are situated on the surface of the Brillouin zone and are usually denoted in a more or less unique way by capital Roman letters as in Fig. 2.32 for a simple tetragonal lattice.

If, in any sufficiently small neighborhood of $\boldsymbol{k}$, there is a line (plane) of points passing through $\boldsymbol{k}$ and having the same point group $\mathrm{F}_{\boldsymbol{k}}$ then $\boldsymbol{k}$ is said to be on a line (plane) of symmetry. The lines of symmetry are denoted both by Roman (on the surface of the Brillouin zone) and Greek (inside the Brillouin zone) capital letters. A symmetry line may be denoted by two symmetry points at the ends of this line: $\Lambda - \Gamma L(C_{3v})$, $\Sigma - \Gamma M(C_{2v})$, $\Delta - \Gamma X(C_{2v})$ (Fig. 2.28a); the corresponding

$F_{\boldsymbol{k}}$ groups are in parentheses. It is evident that the point groups C_{2v} of different wavevectors, being isomorphic to each other, do not coincide for all symmetry lines. For example, the second-order symmetry axis C_2 is along the X-coordinate axis for the ΓX line and along the XY symmetry axis for the ΓM line.

Tables of $\boldsymbol{k}$ vector types for BZ symmetry points and symmetry lines can taken from the site [8]. In fact, for all the space groups referring to the same crystal class and the same lattice type the $\boldsymbol{k}$ vector types are the same. This follows from the fact that in reciprocal space only the point-symmetry operations R transform the $\boldsymbol{k}$ vectors.

The representation theory of space groups uses a theorem that the translation group T is an invariant subgroup of G. Therefore, the little-group method [6] may be used for the generation of irreps of space group G from irreps of translation subgroup T. The one-dimensional irreps of translation group T transform under point-symmetry operations R of space group G according to relation (2.53) i.e. the Bloch function with wave vector $\boldsymbol{k}$ transforms to a Bloch function with wavevector $R\boldsymbol{k}$.

Let us suppose that $\mathrm{D}(g)$ is an irrep of G acting in a space L of dimension n. The operators $\mathrm{D}(g)$ for $g = t_{\boldsymbol{a}} \in \mathrm{T}$ form a rep of T that is in general reducible. Let it contain irreps of T characterized by the vectors $\boldsymbol{k} = \boldsymbol{k}_1, \boldsymbol{k}_2, \ldots, \boldsymbol{k}_n$. Therefore a basis can be found in space L that consists of Bloch functions $\varphi(\boldsymbol{k}_1, \boldsymbol{r}), \ldots, \varphi(\boldsymbol{k}_n, \boldsymbol{r})$. With respect to this basis, the elements of T are represented in the irrep $\mathrm{D}(g)$ by diagonal matrices with elements $\exp(-\mathrm{i}\boldsymbol{k}_p\boldsymbol{a})$, $p = 1, 2, \ldots, n$. The fact that $\mathrm{D}(g)$ is a rep of G implies that if we start with $\varphi(\boldsymbol{k}, \boldsymbol{r})$ and generate the Bloch functions $t_{\boldsymbol{v}}R\varphi(\boldsymbol{k}, \boldsymbol{r}) = \tilde{\varphi}(R\boldsymbol{k}, \boldsymbol{r})$, where $t_{\boldsymbol{v}}R \in \mathrm{G}$ then we obtain some linear combination of n Bloch functions of the initial basis. This means that $R\boldsymbol{k}$ is one of the vectors $\boldsymbol{k}, \boldsymbol{k}_2, \ldots, \boldsymbol{k}_n$.

In n-dimensional space L there are no nonzero subspaces invariant with respect to $\mathrm{D}(g)$ for all $g \in \mathrm{G}$.

Therefore, as we run over all elements of G operating on $\varphi(\boldsymbol{k}, \boldsymbol{r})$ by $\mathrm{D}(g)$, we generate the entire space L, i.e. each of the vectors $\boldsymbol{k}_1, \ldots, \boldsymbol{k}_n$ appears as the transform of $\boldsymbol{k}$ under some element of the point group F (point group of the space group G). It may be that the vectors $\boldsymbol{k}_1, \ldots, \boldsymbol{k}_n$ are not all different. A set of n_s distinct (non-equivalent) $\boldsymbol{k}$ vectors chosen from the set $\boldsymbol{k}_1, \ldots, \boldsymbol{k}_n$ is called the star of wavevector $\boldsymbol{k}$ and is denoted as ${}^*\boldsymbol{k}$. A star can be generated from one of its members by operating on it by elements of point group F. The Γ point of BZ forms one-ray star for any space group as it is a coordinate system origin for all the point- symmetry group F transformations in reciprocal space. The stars ${}^*X$, ${}^*L$ and ${}^*W$ (see Fig. 2.28 of the Brillouin zone for the fcc direct lattice) consist of 3, 4 and 6 rays, respectively.

The point group of the wavevector $\boldsymbol{k}$ (little cogroup of $\boldsymbol{k}$) $F_{\boldsymbol{k}} \subseteq F$, by definition, consists of all the rotations or reflections $R\boldsymbol{k}(i = 1, 2, ..., n_k)$ that rotate $\boldsymbol{k}$ into itself or an equivalent vector $R\boldsymbol{k} = \boldsymbol{k} + \boldsymbol{B}_m$.

By definition, the basic and representation domains in Brillouin zone include one representative of all wave vector stars defined by point groups F^0 and $\mathrm{F} \subset \mathrm{F}^0$, respectivelly.

The space-group irreps generation is described, for example, in [7, 26, 49]. It is shown that the dimension of a space-group representation (degeneracy of energy

levels in a crystal) for a given $\mathbf{k}$ is equal to the product of the number of rays in the star $\mathbf{k}^*$ and the dimension of the point group $F_{\mathbf{k}}$ irreducible representation (ordinary for symmorphic space groups or projective for nonsymmorphic space groups at the points on the surface of Brillouin zone). As to each of the degenerated states corresponds the same one-electron energy it is enough to identify energy levels only for one ray of the wavevector star as it is made in the figures showing the electronic band structure. To identify the one-electron energies at the symmetry lines the group-subgroup compatibility relations are used.

When the space group is realized in a crystalline structure the atomic states included in the LCAO basis define the symmetry of crystalline orbitals appearing in the electronic-structure calculations. The symmetry connection of atomic and crystalline orbitals is given by induced representations of space groups.

2.6.3 Site Symmetry and Induced Representations of Space Groups

In the previous section we examined the use of space-group irreducible representations for the classification of the delocalized (Bloch-type) crystalline states. In this traditional approach the crystal is considered as a whole system and the symmetry properties of the environment of constituent atoms are ignored. This results in a loss of information about the connection between the atomic and crystalline states. This information is widely used in the quantum chemistry of solids as it allows the crystalline properties to be explained from the knowledge of the chemical nature of the constituent atoms and their interactions. In the plane-waves methods of electronic-structure calculations the Bloch-type delocalized states are not directly connected with the states of the separate atoms. However, in the LCAO methods the Bloch-type delocalized functions are represented as the linear combination of the functions of separate atoms. Therefore, the symmetry connection between the delocalized Bloch and localized atomic states appears to be important. If we use not only the space symmetry of a crystal as a whole but also the site symmetry of different groups of constituent atoms we can considerably extend the possibilities of the group-theory applications. To study this in more detail the reader is referred to our previous book [6] where we examined the theory and the applications of the site-symmetry approach to the electron, phonon, magnetic properties of crystals and in the theory of phase transitions. In this section, we examine only those theoretical aspects of the site-symmetry approach that concern the electron states and allow analysis of the symmetry connection between the delocalized Bloch-type and localized Wannier-type electron states in crystals. This symmetry connection is described using representations of space groups induced by the irreps β of the site-symmetry subgroup $\mathrm{G}_{\mathbf{q}}$ of point $\mathbf{q}$ in the direct lattice space ($\beta \uparrow \mathrm{G}$). This type of induced rep of space groups was considered in [6].

All elements of the space group G can be written in the form $t_{\mathbf{v}_R+\mathbf{a}_n} R$, where $\mathbf{v}_R$ is a fractional lattice translation associated with the F point-group element R and $\mathbf{a}_n$ is a direct lattice translation vector.

The elements of the site-symmetry group $G_{\mathbf{q}} \subseteq G$ of the point $\mathbf{q}$ in the direct lattice space are those elements of G for which $g_{\boldsymbol{q}}\boldsymbol{q} = t_{\boldsymbol{v}_R+\boldsymbol{a}_n} R_{\boldsymbol{q}}\mathbf{q} = \boldsymbol{q}$. The space-group elements $g_{\mathbf{q}}$ are supposed to be given in the coordinate system whose origin is at one of the Wyckoff positions. The site-symmetry group elements for the other Wyckoff positions are mapped by the space-group elements with the point-symmetry operators R. Thus the site-symmetry group $G_{\mathbf{q}} \subseteq G$ is isomorphic with the point group $F_{\mathbf{q}}$ formed by $R_{\mathbf{q}}$. When the coordinate system origin is moved to the other Wyckoff position $\mathbf{q}_1$ the site-symmetry group elements of this new origin are elements of the point group $F_{\mathbf{q}_1}$ but the site-symmetry group elements $g_{\mathbf{q}}$ of the former origin $\mathbf{q}$ contain translations. As an example we consider the space group O_h^7 for the two origin choices given in the International Tables for Crystallography [2]. The site-symmetry group of Wyckoff position a(000) is mapped to the pure point-symmetry operations of the group for the first origin choice and to the set of operations with the translational part for the second origin choice.

Let the representatives $g_{jn} (j = 1, 2, \ldots, n_q = n_G/n_F)$ in the decomposition

$$G = \sum_{j,\mathbf{n}} g_{jn} G_{\mathbf{q}}, \quad g_{j\mathbf{n}} = t_{\mathbf{v}_j+\mathbf{a}_n} R_j \tag{2.54}$$

be chosen so that the points

$$\mathbf{q}_j = t_{\mathbf{v}_j} R_j \mathbf{q} \tag{2.55}$$

occupy the positions within the smallest unit cell (primitive or Wigner–Seitz). The operations $g_{j\mathbf{n}}$ generate from the point $\mathbf{q}$ sublattices $\mathbf{q}_j + \mathbf{a}_n (j = 1, 2, \ldots, n_q)$.

Let the local functions $W_{i1}^{(\beta)}(\mathbf{r}) \equiv W_i(\mathbf{r} - \mathbf{q}), (i = 1, 2, \ldots, n_\beta)$ be centered at point $\mathbf{q}$ of the direct lattice and span the space of the irrep β of the site-symmetry group $G_{\mathbf{q}} \subset G$ with matrices $d^{(\beta)}(g_{\mathbf{q}})$ and characters $\chi^{(\beta)}(g_{\mathbf{q}})(g_{\mathbf{q}} \in G_{\mathbf{q}})$. The nature of these functions depends on the physical problem under consideration. In the electron-band theory of crystals $W_i^{(\beta)}(\mathbf{r} - \mathbf{q}_A)$ are atomic functions of atom A. In phonon spectroscopy applications $W_i^{(\beta)}(\mathbf{r} - \mathbf{q}_A)$ mean the components of atomic displacements of an atom A, in magnetically ordered crystals these functions are the magnetic moments of atoms [6].

To specify the induced rep $\beta \uparrow G$ in the basis of local functions $W_{ij}^{(\beta)}(\mathbf{r} - \mathbf{a}_n)$ one has to indicate the symmetry center $\mathbf{q}$ of local functions by its Wyckoff position and the irrep β of the site-symmetry point group $G_{\mathbf{q}}$. Thus, in the $\boldsymbol{q}$ basis the induced rep $\beta \uparrow G$ is specified by the index $(\mathbf{q}, \beta)$.

As an example, we consider oxygen atom $2s$ functions in the perovskite $CaTiO_3$ structure. The oxygen atoms occupy Wyckoff position c of the space group O_h^1 with the site-symmetry D_{4h}. The $2s$-functions of an oxygen atom transform over a_{1g} irrep of the point group D_{4h}. Thus, the induced representation in $\mathbf{q}$ basis (c, a_{1g}) is three-dimensional at each $\mathbf{k}$ point $(d^{(\beta)} = a_{1g}, n_\beta = 1, n_{\mathbf{q}} = 3)$.

The labels of the induced rep $(\boldsymbol{q}, \beta)$ can be given in the $\boldsymbol{k}$ basis corresponding to those in the $\boldsymbol{q}$ basis, i.e. the results of the reduction of the induced rep over irreps of the group $G_{\boldsymbol{k}}$. All the information obtained can be specified by listing the symmetry

(the labels of irreps) of the Bloch states with wavevectors $\boldsymbol{k}$ corresponding only to a relatively small number of $\boldsymbol{k}$ points in the Brillouin zone forming a set K. The set K contains the inequivalent symmetry points of the Brillouin zone and one representative point from each inequivalent symmetry element (symmetry line or symmetry plane) if the latter does not contain the points of higher symmetry [26].

The symmetry properties of basis functions with other vectors $\boldsymbol{k}$ can be determined with the use of the compatibility relations.

Reducing the induced rep requires the characters of the irreps of the little group $G_{\boldsymbol{k}}$ (tabulated in [48] and on site [8]) and gives the induced rep index in the $\boldsymbol{k}$-basis. At the site [8] this procedure is programmed so that user can find the induced rep index in the $\boldsymbol{k}$-basis for any Wyckoff positions of 230 space groups.

Let us consider the induced representation (c, a_{1g}) of the space group O_h^1 formed by $2s$ functions of oxygen atoms in the perovskite structure. Using the site-symmetry option at the site [8] one obtains the induced band representation (c, a_{1g}) in the $\boldsymbol{k}$ basis in the form $\Gamma(1^+3^+)\mathrm{R}(5^+)\mathrm{M}(4^+5^-)\mathrm{X}(1^+3^-4^-)$. The labels of the small irreps of the little groups are taken from [48].

The theory of induced representations of space groups gives the answer to the question of whether it is possible to generate in the space of states of a given energy band the basis of localized functions? The answer to this question allows the symmetry connection between delocalized Bloch-type and localized Wannier-type crystalline orbitals to be obtained.

The following qualitative discussion should explain some features of band reps corresponding to real energy bands in crystals. Let a crystal be formed from isolated constituent atoms by decreasing the interatomic distances from very large ones to those corresponding to real crystalline structure. The crystal field may split the degenerate one-electron atomic levels due to symmetry requirements, leading to quite narrow energy bands, because of the interatomic interactions. The interatomic distances are sufficiently large that the crystalline orbitals corresponding to these bands are localized quite well at the atomic sites and are close to atomic functions. The Bloch states of these narrow energy bands span the spaces of some band reps that certainly have $\boldsymbol{q}$ basis, i.e. are induced representations. These reps are induced by those irreps of site-symmetry groups of atoms that describe the transformation properties of atomic states generating the energy bands. The further decrease of the interatomic distances may considerably transform the energy bands (join them together into more complicated ones and later split them up again into other simple ones) but a new electronic state of arbitrary symmetry cannot arise nor can any state disappear. At the same time, the wavefunctions of all possible symmetry types may change and corresponding one-electron energies may shift along the energy scale. Thus, an energy band corresponding to a band rep without a $\boldsymbol{q}$ basis (i.e. that is not an induced rep) may arise. However, this band, in joining with one or several neighboring ones, forms an energy band corresponding to a composite induced rep with $\boldsymbol{q}$ basis. In the joint space of these band states one can generate the basis of localized functions. Thus, the calculated one-electron energy band spectra of crystals may always be divided into bands connected with some simple or composite induced reps. When the interatomic distances are decreased to those in a real crystal

the atomic functions undergo more or less extensive modifications and become the Wannier functions of a crystal. When the latter arise directly from atomic functions one can use for them the same notation (s, p, d and so on). Let the atoms be at Wyckoff positions with the site symmetry group $G_{\boldsymbol{q}}$. Localized functions transforming according to irreps of the group $G_{\boldsymbol{q}}$ correspond to the bands arising from atomic levels split by a crystalline field. If, when the interatomic distances are decreased, the energy bands cross one another then the states of the resultant composite band also span the space of a composite induced rep. However, it may happen that this new band splits into several subbands related to localized functions that have centers of localization somewhat displaced from the atomic positions for further decreases in the interatomic distances. This case is typical for the electronic structure of crystals with covalent chemical bonding.

The space symmetry of crystalline orbitals generated by atomic orbitals of the LCAO basis can be found from induced representations of space groups. The knowledge of space symmetry of crystalline orbitals allows the pictures of electronic bands given as a result of electronic-structure calculations to be understood. It is also useful in localized crystalline orbitals generation. As an example, we show the energy bands for MgO (Fig. 2.33), silicon (Si) (Fig. 2.30) and $SrZrO_3$ crystals (Fig. 2.29). The LCAO calculations of these crystals were made using the Hartree-Fock LCAO method (see Chap. 3). MgO crystal has rocksalt structure

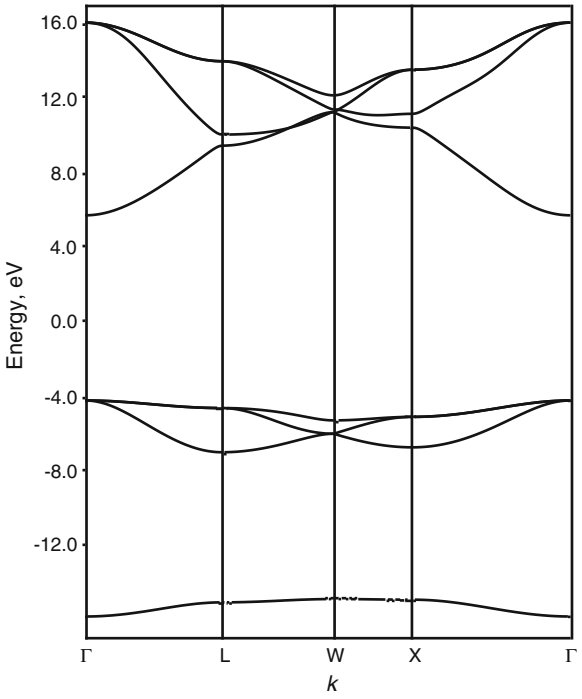

Fig. 2.33 Hartree-Fock energy bands for MgO crystal

with symmorphic space group O_h^5, Si crystal has diamond structure with nonsymmorphic space group O_h^7 and $SrZrO_3$ crystal has perovskite structure with symmorphic space group O_h^1, see Sect. 2.3. The translation symmetry of the first two crystals is described by the same face-centered cubic lattice, of the third one—by the simple cubic lattice. The point group $F = O_h$ of all the three crystals is holosymmetric (coincides with point group F^0 of the cubic lattice). For the first two crystals the wavevector belongs to the same Brillouin zone (Fig. 2.28), the representation domain coincides with the basic domain, the symmetry points of BZ are the same: $\Gamma(0, 0, 0)$, $X(1/2, 1/2, 0)$, $L(1/2, 1/2, 1/2)$ and $W(1/4, 1/2, 3/4)$ with the wavevector point groups O_h, D_{4h}, D_{3d} and D_{2d}, respectively. For the third crystal, the wavevector belongs to the simple cubic lattice Brillouin zone (Fig. 2.27), the representation domain also coincides with basic domain, the symmetry points of BZ are: $\Gamma(0, 0, 0)$, $R(1/2, 1/2, 1/2)$, $X(1/2, 0, 0)$ and $M(1/2, 1/2, 0)$ with the wavevector point groups O_h, O_h, D_{4h} and D_{4h}, respectively. For the symmorphic space groups O_h^5 and O_h^1 the small representations of little groups of symmetry points of BZ coincide with the ordinary (vector) irreducible representations of the corresponding wavevector point groups. For nonsymmorphic space group O_h^7 and the Γ and L the corresponding small representations are p-equivalent to ordinary representations of point groups O_h and D_{3d}. For the X and W points the small representations are not p-equivalent to ordinary irreducible representations of point groups D_{4h} and D_{2d}, respectively.

Let us connect the pictures of the calculated band structures with the symmetry of crystalline orbitals. As for MgO and silicon crystals the dimensions of the corresponding small representations are different at the X and W points, the splitting of the valence band to one-sheet and three-sheet subbands takes place for MgO, but for Si crystal the valence band is not split. In the symmetry directions of the Brillouin zone the compatibility relations are used to explain the energy-level splittings.

For the symmetry directions in the Brillouin zone $\Delta(\Gamma X)$, $\Lambda(\Gamma L)$, Σ (see Fig. 2.28) the small representations of both space groups are p-equivalent to ordinary irreducible representations of point groups C_{4v}, C_{3v} and C_{2v}. The notations of these representations are taken from [48]. For symmetry directions on the surface of the Brillouin zone $Z(XW)$, S small representations of space group O_h^5 are p-equivalent to ordinary irreducible representations of point group C_{2v}, for the symmetry direction Q – to ordinary irreducible representations of group C_s. For the nonsymmorphic space group O_h^7 small representations in the symmetry direction Z are not p-equivalent to ordinary irreducible representations of point group C_{2v}.

In Tables 2.14 and 2.15 we give the notations of induced representations in $\boldsymbol{k}$-basis for symmetry points of the Brillouin zone. We include only the band representations for upper valence bands of all the crystals under consideration.

These bands are induced by the oxygen atom $2s$, $2p$ states in MgO, by the silicon atom $3s$, $3p$ states in silicon, by the strontium atom $4p$ states and oxygen atom $2s$, $2p$ states in $SrZrO_3$. For all three crystals the short symbol of the band representation in $\mathbf{k}$-basis contains only the indices of the small IR s for the most symmetrical points of the BZ, because the indices for all other IR s contained in the BR are determined with the help of compatibility relations. These are the states responsible

Table 2.14 Band representations of space groups O_h^5 and O_h^7 for upper valence bands of MgO and Si crystals

	Γ	X	L	W	
MgO $- O_h^5$					
$b(1/2, 1/2, 1/2)$	a_{1g}	1^+	1^+	2^-	4
	t_{1v}	5^-	2^-5^-	1^+3^+	1 5
Si $- O_h^7$					
$a(0\,0\,0)$	a_1	1^+2^-	1	1^+2^-	1
	t_2	4^-5^+	1 3 4	$1^+2^-3^+3^-$	1 2 2

Table 2.15 Band representations for upper valence bands in $SrZrO_3$ crystal induced from Sr $4p-$, O $2s-$ and O $2p-$ atom-like states

Atom states	**q**-basis	Γ	R	M	X
Sr $4p-$	(b, t_{1v})	4^-	5^+	2^-5^-	1^+5^+
O $2s-$	(d, a_{1g})	1^+3^+	4^-	1^+5^-	$1^+2^+3^-$
O $2p_z-$	(d, a_{2v})	4^-	1^+3^+	$1^+2^+3^-$	1^+5^-
O $2p_{x,y}-$	(d, e_v)	4^-5^-	4^+5^+	$3^+4^+5^\pm$	$3^-4^-5^\pm$

for four-sheet valence bands in the first two crystals (Figs. 2.33 and 2.30) and for the 6- and 9-sheet valence bands in $SrZrO_3$ crystal (Fig. 2.29)

Due to the considered symmetry difference of crystalline orbitals in MgO and Si crystals the nature of chemical bonding in these crystals is also different. Indeed, in ionic MgO crystal the splitting of the valence band allows the crystalline orbitals localized on an oxygen atom to be generated and transformed over a_{1g} and t_{1v} irreducible representations of the oxygen site-symmetry group O_h. In covalent Si crystal all four sheets of the valence band have to be included in localization so that the localized orbitals found are centered at the middle of the Si $-$ Si bond.

In $SrZrO_3$ crystal oxygen $2s$ functions transform according to $\beta = a_{1g}$ IR of the oxygen site-symmetry group $G_{\mathbf{q}} = D_{4h}$ and generate a 3-sheeted BR. The symmetry of states in this band is fully determined by the $2s$ function of one of three oxygens in the primitive cell and may be labeled by the symbol (d, a_{1g}) as oxygen atoms occupy Wyckoff position d in space group O_h^1. In Table 2.15 this band, with the symbol of the BR (d, a_{1g}), is given in $\boldsymbol{k}$-basis (Γ, R, M, X are the symmetry points of the BZ).

Analysis of the space symmetry of crystalline orbitals is used to consider the possible centers of localization of chemical bonding in crystals.

2.6.4 *Irreducible Representations of Layer Groups. Symmetry of Crystalline Orbitals*

It can be shown that all the irreps of DG are contained in the irreps of the related space group G. The simple connection between the irreps of G and DG may be established using (2.15), i.e. isomorphism DG $\leftrightarrow$ G$/T_3$: every irrep of DG is related to a definite

irrep of G (of the same dimension). In these irreps of G all the elements of the coset $(R_i|\boldsymbol{v}_i + \boldsymbol{a}_n)T_3$ are mapped by the same matrix. In particular, all the translations in T_3 (coset $(E|\boldsymbol{0})T_3$) are mapped by unit matrices. We refer the reader to Chap. 6 in [6] for details. The same approach can be used to connect irreps of space group G with those of subperiodic rod group RG $\leftrightarrow$ G/$T^{(2)}$ ($T^{(2)}$ is the two-dimensional group of translations in a plane that does not contain the one-dimensional translations of a rod group), [28]. The two-dimensional plane groups and the corresponding layer groups are isomorphic (see Table B.2) and therefore have the same sets of irreps. The theory of induced reps described above for triperiodic space groups G may be easily applied to diperiodic groups DG. The tables of simple induced reps of DG may be directly constructed by using this theory [6]. The induced reps of layer groups are useful when analyzing electron-density localization on a crystal surface. Such analysis is important in the study of chemisorption of atoms and molecules.

In order to understand the principal features of the origin of surface states it is important to know how the energy bands of a crystal look in terms of the diperiodic specification. The comparison of bulk and surface states according to the symmetry is based on the relation between the irreps of the corresponding tri- and diperiodic groups G and DG. The bulk states are specified by the wavevector $\boldsymbol{k}^{(3)}$ in the three-dimensional BZ (BZ-3) for the group G. The surface states are classified by $\boldsymbol{k}^{(2)}$ in the two-dimensional BZ (BZ-2) of the layer (plane) group DG. The choice of the translation vectors $\boldsymbol{a}_1$ and $\boldsymbol{a}_2$ in the surface plane defines its orientation relative to the primitive translation vectors $\boldsymbol{a}_i^{(3)} (i = 1, 2, 3)$ of the corresponding space group G. The surface is identified by three integers (hkl)—Miller indices, specifying the atomic planes in the crystal by means of the components of a vector perpendicular to that plane. Planes perpendicular to crystallographic axes X, Y, Z are indicated $(h00)$, $(0k0)$ and $(00l)$, respectively. In particular, the planes closest to the origin are identified with indices (100), (010) and (001). Planes parallel to one of the three axes X, Y, Z are indicated $(0kl)$, $(h0l)$ and $(hk0)$, respectively. When the surface reconstruction effects (change of the surface plane translational symmetry with respect to that of the perfect crystal) may be neglected, the symmetry group DG of a crystal with a surface is a subgroup of the bulk crystal group G. However, the BZ-2 depends on the indices of the surface plane.

Consider, for example, crystals with face-centered cubic Bravais lattices. For the (001), (110) and (111) sections the plane lattices are square, rectangular and hexagonal, respectively. The basic translation vectors of the direct and reciprocal lattices for these three cases are given in Table 2.16 ($\boldsymbol{a}_1$ and $\boldsymbol{a}_2$ are given in units $a/2$, $\boldsymbol{B}_i$ in units $2\pi/a$, where a is the cubic lattice parameter). Note that for a cubic lattice the planes (100), (010) and (001) are equivalent. The equivalence takes place also for (110), (101), and (011) planes. We see that the vectors $\boldsymbol{B}_i (i = 1, 2)$ are now not the translation vectors of the three-dimensional reciprocal lattice. Therefore, the boundaries of BZ-2 do not coincide with those of BZ-3.

Figure 2.34 shows the Brillouin zones corresponding to the surface (001), (110) and (111) inscribed in the three-dimensional Brillouin zone for a face-centered cubic lattice.

Note that some nonequivalent points of BZ-3 become equivalent in BZ-2 (for example, the points X for the surface (001) and the points L for the (110) surface).

Table 2.16 Vectors of basis translations for three sections of a face-centered cubic Bravais lattice

Surface translation vectors	(001)	(110)	(111)
$\mathbf{a}_1$	110	−110	1 − 10
$\mathbf{a}_2$	1–10	002	10 − 1
$\mathbf{B}_1$	110	−110	2/3, −4/3, 2/3
$\mathbf{B}_2$	1–10	001	2/3, 2/3, −4/3

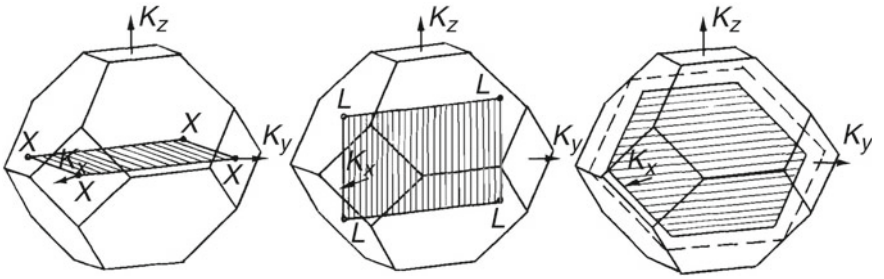

Fig. 2.34 Brillouin zones for a face-centered cubic lattice and surfaces **a** (001), **b** (110), **c** (111)

Some points of BZ-2 have higher symmetry than in BZ-3 (for example, the vertices of BZ-2 for the (111) surface). These properties of BZ-2 arise because the unit-cell vectors in the two-dimensional reciprocal space $\boldsymbol{B}_i$ are not the lattice vectors of the three-dimensional reciprocal lattice.

To obtain the crystal energy band structure in terms of a diperiodic specification it is necessary to represent the dispersion law $E = E_n(\boldsymbol{k}^{(3)})$ in the form

$$E_n^s(\boldsymbol{k}_\parallel^s) = E_n(\boldsymbol{k}_\parallel^s + \boldsymbol{k}_\perp - \boldsymbol{B}_n) \tag{2.56}$$

where $\boldsymbol{k}_\parallel^s$ is a projection of the three-dimensional wavevector $\boldsymbol{k}^{(3)}$ onto the surface and $\boldsymbol{k}_\perp$ is its component perpendicular to the surface. The vector $\boldsymbol{B}_n$ is assumed to be chosen so that the wavevector $\boldsymbol{k}_\parallel^s = \boldsymbol{k}_\parallel + \boldsymbol{B}_n$ takes values in the limits of BZ-2. In the projection of the energy bands of the three-dimensional crystal on the two-dimensional Brillouin zone forbidden energy lacunas can appear. When the surface is taken into account, a band of surface states appears inside the energy lacuna. These surface states are analogous to the local energy levels of point defects that appear in the forbidden energy gap of a perfect crystal. The energy levels of surface states may arise in the continuous energy spectrum of a bulk three-dimensional perfect crystal. These are the so-called resonance surface states. They are analogous to the point defect states in the spectrum of bulk-crystal states.

2.6.5 Irreducible Representations of Line Groups

The consideration the triperiodic translation group and its irreducible representations can easily be extended to the monoperiodic groups.

The one dimensional direct **a** and reciprocal **B** lattice translations are now one-dimensional vectors, satisfying the orthogonality relation $(\mathbf{aB}) = 2\pi$. Let the one-dimensional translations $t_{\mathbf{a}}$ be directed along z Cartesian axis.

In the standard factorization $L = TF$ the translations form the invariant subgroup of L and the factor group $P_I = L/T$ (isogonal point group) is isomorphic to one of the axial point groups C_q, $S_{2q} \leftrightarrow C_{2q}$, D_q,C_{qv},C_{qh},D_{qd},D_{qh}. In Line groups the rotation axis order q is any integer number (for Rod groups q = 1, 2, 3, 4, 6). The point groups P_I (isogonal point groups) of monoperiodic nanostructures can be considered as an analog of the crystal class introduced for the space and layer groups. The line groups from families 2, 3, 6, 9, 11 are symmorphic as these groups do not contain helical rotations or the reflections in the glide planes. The Line groups of families 1 and 5 can be both symmorphic and nonsymmorphic. For the symmorphic Line groups P_I are axial point groups; for nonsymmorphic Line groups P_I is isomorphic to the factor group L/T.

As in the case of the space groups the little-group method may be used for the generation of irreps of line group L from one-dimensional irreps of the translation subgroup T.

As in the case of 3D translations the Bloch function with wave vector $\boldsymbol{k}$ transforms to a Bloch function with wavevector $R\boldsymbol{k}$. Here R is the operation of the isogonal point group.

The point group of the wavevector $\boldsymbol{k}$ (little cogroup of $\boldsymbol{k}$) $F_{\boldsymbol{k}} \subseteq F$, by definition, consists of all the rotations or reflections $R\boldsymbol{k}(i = 1, 2, \ldots, n_k)$ that rotate $\boldsymbol{k}$ into itself or an equivalent vector $R\boldsymbol{k} = \boldsymbol{k} + \boldsymbol{B}$. The number of rays in the wave vector star is equal to n_F/n_k where n_F is the number of the elements in the group F.

The one-dimensional Brillouin zone is the segment connecting the reciprocal lattice points π/a and $-\pi/a$. The symmetry points of BZ are $\Gamma(0)$ and Z(1/2) (in units $2\pi/a$) with the one ray in the wave vector star. The number of rays in the star of other (general) **k**-points depends on the axial point group. The general **k**-points form one-ray stars for the isogonal point groups C_n, C_{nv} which do not contain the operations transforming **k** to $-\mathbf{k}$. For all the rest axial point groups the general **k**-points form two-rays stars, including both **k** and $-\mathbf{k}$ -points.

By definition, the little group $\mathrm{L}_{\boldsymbol{k}}$ of wavevector $\boldsymbol{k}$ consists of all elements $l_j^{\boldsymbol{k}} = t_{\boldsymbol{v}_j^{(k)}+\boldsymbol{a}} R_j^{(\boldsymbol{k})}$, $j = 1, 2, \ldots, n_k$, where $R_j^{(\boldsymbol{k})} \in \mathrm{F}_{\boldsymbol{k}}$. The group $\mathrm{L}_{\boldsymbol{k}} \subseteq \mathrm{L}$ is a group of order $N \cdot n_{\boldsymbol{k}}^j$ where N is the number of one-dimensional translations in the main region of a monoperiodic crystal.

The dimension of a Line group full representation (degeneracy of energy levels in a monoperiodic structure) for a given **k** is equal to the product of the number of rays in the star $\mathbf{k}^*$ and the dimension of the axial point group $F_{\mathbf{k}}$ irreducible representation (ordinary or projective).

The ordinary irreps of axial point groups are well known, the characters of their irreps can be found on the site [50]. These representations are one and two-dimensional. The projective irreps of these groups are not tabulated, their knowledge is necessary only for $Z(1/2)$ point of the one-dimensional BZ for the line group families 4, 5, 10, 12, 13.

The irreducible representations of the commensurate line groups are found and tabulated in [51–53] using the standard factorization. In order to obtain a complete set of non-equivalent representations of any line group of L^+ type it is sufficient to know all the reps of the corresponding isogonal point group C_q or C_{qv}, q = 1,2,... The representations of line group of L^- type are induced from those of its invariant subgroup L^+. The factorization (2.22) is used in [3] for the construction of irreps both for the commensurate and noncommensurate line group irreps. The construction of the line groups irreps starts with the first family group. In this case the line group is the direct product L = Z × P, both factors Z and P = C_n are the cyclic groups with the one-dimensional irreps $\exp(ilx)$, lx is a multiple of 2π, l is the order of the cyclic group.

The helical group Z irreps are classified with the help of the helical quasimomentum $\tilde{k}$ changing in the helical Brillouin zone - the segment connecting the reciprocal lattice points π/f and $-\pi/f$ where f is the partial translation. For the commensurate line groups the partial translation $f = \frac{ra}{q}$, r = 1,2,...q−1, so that the helical Brillouin zone is $\frac{q}{r}$ times larger than that of the quasimomentum k introduced in the standard line group factorization. Analogously, for the rotational subgroup C_n there are n different one-dimensional irreducible representations, given by the integer $\tilde{m}$. Thus the irreps of the first family line groups have the form

$$_{\tilde{k}}A_{\tilde{m}} = \exp(\mathbf{i}\tilde{k}f)\exp(\frac{\mathbf{i}\tilde{m}2\pi}{n}) \tag{2.57}$$

In the both classifications the irreducible representations are grouped into the so called bands, the property which will be inherited by all the other families. Namely, for fixed $\tilde{m}$, representations differ only by $\tilde{k}$. When $\tilde{k}$ varies within the helical Brillouin zone one obtains a series of representations to be referred to as a helical or $\tilde{m}$-band. Analogously, for commensurate groups, fixing m one gets series of the representations with k from the Brillouin zone, which is called linear or m-band [3]. The representations of the first family line groups have been used in [3] to construct the irreps of other groups. It is seen from Table D.2 that the first family group $L^{(1)}$ is the halving subgroup of the line groups of the families 2,...8. Therefore the induction procedure from a halving subgroup was used in [3] to construct the representations of the families 2,...,8. In the third step the representations of the families 9,...13 have been found using the reps of the positive families 6,7,8 and the induction procedure from a halving subgroup.

As an example we briefly describe how to construct irreducible representations of line groups belonging to the families 4 and 8. But to begin with, we remind the definition of a conjugate representation. If H is a normal subgroup of a group G and ρ is some matrix representation of H then for any $s \in$ G the representation $\rho^s(h) = \rho(s^{-1}hs)$ is called s - conjugate of ρ.

Family 4. L = $T^1_{2n}(\frac{a}{2})C_{nh}$ = H ∪ sH where H = $T^1_{2n}(\frac{a}{2})C_n$ is a zigzag group with generators $(C_{2n}|\frac{a}{2})$, $(C_n|0) \in$ H, and $s = (\sigma_h|0)$. Irreps of the normal subgroup H are 1-dimensional:

$$ {}_kA_m(C_{2n}|\frac{a}{2}) = e^{\mathbf{i}k\frac{a}{2}}e^{\mathbf{i}m\frac{\pi}{n}}, \quad {}_kA_m(C_n|0) = e^{\mathbf{i}m\frac{2\pi}{n}} \tag{2.58} $$

where $k \in \left(-\frac{\pi}{a}, \frac{\pi}{a}\right]$ and $m \in (-n, n]$. It is easy to ascertain that s-conjugate irreps of H are

$$ {}_kA^s_m(C_{2n}|\frac{a}{2}) = {}_{-k}A_m(C_{2n}|\frac{a}{2}) = e^{-\mathbf{i}k\frac{a}{2}}e^{\mathbf{i}m\frac{\pi}{n}}, \quad {}_kA^s_m(C_n|0) = e^{\mathbf{i}m\frac{2\pi}{n}} \tag{2.59} $$

In the case under discussion irrep of H is identical to its s-conjugate if and only if

$$ e^{\mathbf{i}k\frac{a}{2}} = e^{-\mathbf{i}k\frac{a}{2}} \Leftrightarrow k\frac{a}{2} = -k\frac{a}{2} + 2\pi l \tag{2.60} $$

and relevant solution of this equation is $k = 0$. Thus, 1-dimensional irreps of L are

$$ {}_kA^{\pm}_m(C_{2n}|\frac{a}{2}) = e^{\mathbf{i}k\frac{a}{2}}e^{\mathbf{i}m\frac{\pi}{n}}, \quad {}_kA^{\pm}_m(C_n|0) = e^{\mathbf{i}m\frac{2\pi}{n}}, \quad {}_kA^{\pm}_m(\sigma_h|0) = \pm 1 \tag{2.61} $$

For $k \neq 0$ irreps ${}_kA_m$ and ${}_kA^s_m$ of H are non-equivalent and the induced representations ${}_kE_m = Ind^{\mathrm{L}}_{\mathrm{H}}({}_kA_m)$ are irreducible:

$$ \begin{aligned} {}_kE_m(C_{2n}|\frac{a}{2}) &= \begin{pmatrix} e^{\mathbf{i}(k\frac{a}{2}+m\frac{\pi}{n})} & 0 \\ 0 & e^{\mathbf{i}(-k\frac{a}{2}+m\frac{\pi}{n})} \end{pmatrix} \\ {}_kE_m(C_n|0) &= \begin{pmatrix} e^{\mathbf{i}m\frac{2\pi}{n}} & 0 \\ 0 & e^{\mathbf{i}m\frac{2\pi}{n}} \end{pmatrix} \\ {}_kE_m(\sigma_h|0) &= \begin{pmatrix} 0 & 1 \\ 1 & 0 \end{pmatrix} \end{aligned} \tag{2.62} $$

It is easy to see that for $k \in (-\frac{\pi}{a}, \frac{\pi}{a})$ the induced irreps with k and $-k$ are equivalent and therefore the range of k reduces to $(0, \frac{\pi}{a})$ with $m \in (-n, n]$ for each k. The case $k = \frac{\pi}{a}$ requires special attention because for this value of k the interval of m values reduces to $(0, n]$.

Family 8. $\mathrm{L} = \mathrm{T}^1_{2n}(\frac{a}{2})\mathrm{C}_{nv} = \mathrm{H} \cup s\mathrm{H}$ where $\mathrm{H} = \mathrm{T}^1_{2n}(\frac{a}{2})\mathrm{C}_n$ is a zigzag group with generators $(C_{2n}|\frac{a}{2})$, $(C_n|0) \in \mathrm{H}$, and $s = (\sigma_v|0)$. Irreps of normal subgroup H are 1-dimensional and are given by (2.58). In this case s-conjugate irreps are

$$ \begin{aligned} {}_kA^s_m(C_{2n}|\frac{a}{2}) &= {}_kA_{-m}(C_{2n}|\frac{a}{2}) = e^{\mathbf{i}k\frac{a}{2}}e^{-\mathbf{i}m\frac{\pi}{n}} \\ {}_kA^s_m(C_n|0) &= {}_kA^s_{-m}(C_n|0) = e^{-\mathbf{i}m\frac{2\pi}{n}} \end{aligned} \tag{2.63} $$

and irrep of H is identical to its s-conjugate if and only if

$$ m\frac{\pi}{n} = -m\frac{\pi}{n} + 2\pi l \tag{2.64} $$

It is easy to see that the relevant solutions of this equation are $m = 0, n$ and 1-dimensional irreps of the line group under discussion are

$$
\begin{aligned}
&{}_kA_m(C_{2n}|\frac{a}{2}) = e^{\mathbf{i}k\frac{a}{2}}e^{\mathbf{i}m\frac{\pi}{n}}, \quad {}_kA^s_m(C_n|0) = 1, \quad {}_kA^s_m(\sigma_v|0) = 1 \\
&{}_kB_m(C_{2n}|\frac{a}{2}) = e^{\mathbf{i}k\frac{a}{2}}e^{\mathbf{i}m\frac{\pi}{n}}, \quad {}_kB^s_m(C_n|0) = 1, \quad {}_kB^s_m(\sigma_v|0) = -1
\end{aligned} \tag{2.65}
$$

where $k \in (-\frac{\pi}{a}, \frac{\pi}{a}]$ and $m = 0, n$. It seems pertinent to note that due to tradition 1-dimensional irreps which accept values $+1$ or -1 at the element $(\sigma_v|0)$ are denoted by capital letters A and B, respectively. For the remainder values of k and m we should induce to get

$$
\begin{aligned}
{}_kE_m(C_{2n}|\frac{a}{2}) &= \begin{pmatrix} e^{\mathbf{i}(k\frac{a}{2}+m\frac{\pi}{n})} & 0 \\ 0 & e^{\mathbf{i}(k\frac{a}{2}-m\frac{\pi}{n})} \end{pmatrix} \\
{}_kE_m(C_n|0) &= \begin{pmatrix} e^{\mathbf{i}m\frac{2\pi}{n}} & 0 \\ 0 & e^{-\mathbf{i}m\frac{2\pi}{n}} \end{pmatrix} \\
{}_kE_m(\sigma_v|0) &= \begin{pmatrix} 0 & 1 \\ 1 & 0 \end{pmatrix}
\end{aligned} \tag{2.66}
$$

where $k \in (-\frac{\pi}{a}, \frac{\pi}{a}]$ and $m \in (0, n)$. Note that here the range of m reduces to $(0, n)$ since 2-dimensional irreps with labels m and $-m$ are equivalent.

2.6.6 Site Symmetry for Line Groups of Families 4 and 8

The site symmetry approach used for the space and layer groups can be extended to the line groups using the induction procedure from the irreps of the orbit representative stabilizer being the subgroup of the line group. The other possibility is to use the restriction of Line group irreps to orbit stabilizers. As an example we apply the restriction procedure for the construction of the induced irreps of families 8 and 13 of Line groups. As soon as the induced representations from the irreps of orbit stabilizers are obtained, it is easy to construct the so-called dynamical representations of line groups which are defined as representations induced from the vector representations of orbit stabilizers (probably with subsequent multiplication by a certain permutation matrix). The use of the site-symmetry approach in lattice dynamics allows one to make a quick group theoretical analysis of the phonon symmetry not only at the Brillouine zone center but in the entire Brillouine zone. The knowledge of the symmetry of phonons at K=0 is necessary for interpretation of second order infrared and Raman spectra. Furthermore, this information can be used in the symmetry assignment of vibrational mode branches calculated by numerical methods

General character of a point group F we denote by the symbol $\chi(\mathrm{F})$. If an irrep of F is labeled by the symbol m, its character will be denoted as $\chi_m(F)$.

For example, $\chi_m(\mathrm{C}_n)$ will stand for the irrep $C_n^l \mapsto e^{\mathbf{i}m\frac{2\pi}{n}l}$ of C_n group where integer $m \in (-\frac{n}{2}, \frac{n}{2}]$.

The symbol $\chi_m(\mathrm{S}_{2n})$ will stand for the irrep $\sigma_h C_{2n}^l \mapsto e^{\mathbf{i}m\frac{\pi}{n}l}$ of the group S_{2n} with integer $m \in (-n, n]$.

For characters of the groups $\mathrm{C}_{1v} = \mathrm{C}_s, \mathrm{C}_{1h}, \mathrm{C}_i$ we will use the symbol $\chi_0^{\pm}(\mathrm{F}) = \{1, \pm 1\}$. These groups are just different geometric realizations of the same abstract group of order 2, but their representations are traditionally labeled as

$$\begin{aligned} &\chi_0^+(\mathrm{C}_s) = a_1, \quad \chi_0^-(\mathrm{C}_s) = a_2, \quad \chi_0^+(\mathrm{C}_{1h}) = a', \\ &\chi_0^-(\mathrm{C}_{1h}) = a'', \quad \chi_0^+(\mathrm{C}_i) = a_g, \quad \chi_0^-(\mathrm{C}_i) = a_v \end{aligned} \tag{2.67}$$

For C_{nv} group with $n > 1$ 1-dimensional irreps are usually denoted

$$\begin{aligned} &\chi_0^+(\mathrm{C}_{nv}) = a_1, \quad \chi_0^-(\mathrm{C}_{nv}) = a_2 \\ &\chi_{\frac{n}{2}}^+(\mathrm{C}_{nv}) = b_1, \quad \chi_{\frac{n}{2}}^-(\mathrm{C}_{nv}) = b_2 \text{ (for even } n) \end{aligned} \tag{2.68}$$

The irrep $\chi_0(\mathrm{C}_1)$ of the trivial group C_1 is denoted by the symbol a.

The restriction of line group irreps to representations of orbit stabilizers is well-defined and easy procedure. Expressions for the induced from irreps of orbit stabilizers representations of line groups will include integration over linear Brillouine zone or summation over finite set of k values if the periodic boundary conditions are imposed on the translations along the z axis. Let us consider in more detail the Line groups of Family 8.

Line groups of the 8th family are $\mathrm{L} = \mathrm{T}_{2n}^1(a)\mathrm{C}_{nv} = \mathrm{T}(a)\left(\mathrm{C}_{nv} \bigcup (C_{\frac{\pi}{n}}|\frac{a}{2})\mathrm{C}_{nv}\right)$. The isogonal group is C_{2nv} and transversal $\mathrm{F} = \mathrm{C}_{nv} \bigcup (C_{\frac{\pi}{n}}|\frac{a}{2})\mathrm{C}_{nv}$ contains $4n$ elements being a group modulo pure translations.

For $n > 1$ line groups from this family generate orbits of 3 types. The number of types reduces to 2 for $n = 1$.

For orbits of the type a_1 (Rod group label c) their representatives may be taken as $\mathbf{x}_\rho(\alpha + \beta, z)$ with $\beta \in (0, \frac{\pi}{n})$ and arbitrary z value. The stabilizer of orbit points is trivial and the restriction rules are

$${}_kA_m \downarrow \mathrm{C}_1 = \chi_0(\mathrm{C}_1), \quad {}_kB_m \downarrow \mathrm{C}_1 = \chi_0(\mathrm{C}_1) \tag{2.69}$$

for $k \in (-\frac{\pi}{a}, \frac{\pi}{a}]$, $m = 0, n$, and

$${}_kE_m \downarrow \mathrm{C}_1 = 2\chi_0(\mathrm{C}_1) \tag{2.70}$$

for $k \in (-\frac{\pi}{a}, \frac{\pi}{a}]$, $m \in (0, n)$.

The induction rules give regular representation as could be expected:

$$\chi_0(\mathrm{C}_1)\uparrow \mathrm{L} = \bigoplus_{k\in(-\frac{\pi}{a},\frac{\pi}{a}]}\left[\left(2\bigoplus_{m\in(0,n)} {}_kE_m\right)\oplus {}_kA_0\oplus {}_kB_0\oplus {}_kA_n\oplus {}_kB_n\right] \tag{2.71}$$

The corresponding dynamical representation is just a threefold regular one.

Orbits with representatives $\mathbf{x}_\rho(\alpha, z)$ are of the type b_1 (Rod group label b) and these representatives have stabilizer $\mathrm{C}_{1v}(\alpha) = \{(0, e), (0, \sigma_\alpha)\}$. The restriction of the line group irreps to C_{1v} group gives

$${}_kA_m\downarrow \mathrm{C}_{1v} = \chi_0^+(\mathrm{C}_{1v}),\quad {}_kB_m\downarrow \mathrm{C}_{1v} = \chi_0^-(\mathrm{C}_{1v}) \tag{2.72}$$

where $k \in (-\frac{\pi}{a}, \frac{\pi}{a}]$, $m = 0, n$, and

$${}_kE_m\downarrow \mathrm{C}_{1v} = \chi_0^+(\mathrm{C}_{1v})\oplus\chi_0^-(\mathrm{C}_{1v}) \tag{2.73}$$

where $k \in (-\frac{\pi}{a}, \frac{\pi}{a}]$, $m \in (0, n)$.

The corresponding induction rules are

$$\begin{aligned}\chi_0^+(\mathrm{C}_{1v})\uparrow \mathrm{L} &= \bigoplus_{k\in(-\frac{\pi}{a},\frac{\pi}{a}]}\left[\left(\bigoplus_{m\in(0,n)} {}_kE_m\right)\oplus {}_kA_0\oplus {}_kA_n\right]\\ \chi_0^-(\mathrm{C}_{1v})\uparrow \mathrm{L} &= \bigoplus_{k\in(-\frac{\pi}{a},\frac{\pi}{a}]}\left[\left(\bigoplus_{m\in(0,n)} {}_kE_m\right)\oplus {}_kB_0\oplus {}_kB_n\right]\end{aligned} \tag{2.74}$$

Vector representation is $2\chi_0^+(C_{1v})\oplus\chi_0^-(C_{1v})$ and

$$\begin{aligned}\rho^{dyn}(\mathrm{L}) &= (2\chi_0^+(\mathrm{C}_{1v})\oplus\chi_0^-(\mathrm{C}_{1v}))\uparrow \mathrm{L}\\ &= \bigoplus_{k\in(-\frac{\pi}{a},\frac{\pi}{a}]}\left[2({}_kA_0\oplus_k A_n)\oplus_k B_0\oplus_k B_n\oplus\bigoplus_{m\in(0,n)} 3{}_kE_m\right]\end{aligned} \tag{2.75}$$

Points $(0, 0, z)$ represent two-point F-orbits $\{(0, 0, z), (0, 0, z + \frac{a}{2})\}$ with group C_{nv} as a stabilizer of their points. We have

$${}_kA_m\downarrow \mathrm{C}_{nv} = \chi_0^+(\mathrm{C}_{nv}),\quad {}_kB_m\downarrow \mathrm{C}_{nv} = \chi_0^-(\mathrm{C}_{nv}) \tag{2.76}$$

where $k \in (-\frac{\pi}{a}, \frac{\pi}{a}]$ and $m = 0, n$. For 2-dimensional irreps we have

$$kE_m\downarrow \mathrm{C}_{nv} = e_m(\mathrm{C}_{nv}), m \in (0, \frac{n}{2})$$

$$kE_m \downarrow \mathrm{C}_{nv} = e_{m-[\frac{n}{2}]}(\mathrm{C}_{nv}), m \in (\frac{n}{2}, n) \tag{2.77}$$

The induction rules are

$$\begin{aligned}
\chi_0^+(\mathrm{C}_{nv}) \uparrow \mathrm{L} &= \bigoplus_{k\in(-\frac{\pi}{a},\frac{\pi}{a}]} {}_kA_0 \oplus {}_kA_n \\
\chi_0^-(\mathrm{C}_{nv}) \uparrow \mathrm{L} &= \bigoplus_{k\in(-\frac{\pi}{a},\frac{\pi}{a}]} {}_kB_0 \oplus {}_kB_n \\
e_m(\mathrm{C}_{nv}) \uparrow \mathrm{L} &= \bigoplus_{k\in(-\frac{\pi}{a},\frac{\pi}{a}]} \left[{}_kE_m \oplus {}_kE_{m+[\frac{n}{2}]}\right]
\end{aligned} \tag{2.78}$$

where $m \in (0, \frac{n}{2})$. For even values of n and $m = \frac{n}{2}$

$${}_kE_{\frac{n}{2}} \downarrow \mathrm{C}_{nv} = \chi_{\frac{n}{2}}^+(\mathrm{C}_{nv}) \oplus \chi_{\frac{n}{2}}^-(\mathrm{C}_{nv}) \tag{2.79}$$

and the induction rules are

$$\chi_{\frac{n}{2}}^+(\mathrm{C}_{nv}) \uparrow \mathrm{L} = \bigoplus_{k\in(-\frac{\pi}{a},\frac{\pi}{a}]} {}_kE_{\frac{n}{2}}, \quad \chi_{\frac{n}{2}}^-(\mathrm{C}_{nv}) \uparrow \mathrm{L} = \bigoplus_{k\in(-\frac{\pi}{a},\frac{\pi}{a}]} {}_kE_{\frac{n}{2}} \tag{2.80}$$

Three cases should be analyzed when dynamical representations are constructed.

For $n = 1$ the vector representation is $2\chi_0^+(C_{1v}) \oplus \chi_0^-(C_{1v})$ and

$$\rho^{dyn}(\mathrm{L}) = (2\chi_0^+(\mathrm{C}_{1v}) \oplus \chi_0^-(\mathrm{C}_{1v})) \uparrow \mathrm{L} = \bigoplus_{k\in(-\frac{\pi}{a},\frac{\pi}{a}]} [2({}_kA_0 \oplus_k A_1) \oplus_k B_0 \oplus_k B_1] \tag{2.81}$$

For $n = 2$ the vector representation is $\chi_0^+(C_{1v}) \oplus \chi_1^+(C_{2v}) \oplus \chi_1^-(C_{2v})$ and

$$\rho^{dyn}(\mathrm{L}) = (\chi_0^+(\mathrm{C}_{1v}) \oplus \chi_1^+(\mathrm{C}_{2v}) \oplus \chi_1^-(\mathrm{C}_{2v})) \uparrow \mathrm{L} = \bigoplus_{k\in(-\frac{\pi}{a},\frac{\pi}{a}]} ({}_kA_0 \oplus_k A_2 \oplus 2_kE_1) \tag{2.82}$$

For $n > 2$ we have the vector representation $\chi_0^+(C_{nv}) \oplus e_1(C_{nv})$ and

$$\rho^{dyn}(\mathrm{L}) = (\chi_0^+(\mathrm{C}_{nv}) \oplus e_1(\mathrm{C}_{nv})) \uparrow \mathrm{L} = \bigoplus_{k\in(-\frac{\pi}{a},\frac{\pi}{a}]} ({}_kA_0 \oplus_k A_n \oplus_k E_1 \oplus_k E_{n-1}) \tag{2.83}$$

The case $n = 2$ is embraced by the last formula and its separate treatment is actually not required.

As an example we consider TiO_2-based nanotubes (NTs) of different morphology systematically synthesized and carefully studied as promising technological materials, see Chap. 7.

As we have seen above in most theoretical simulations on titanium nanotubes, the model $3D \longrightarrow 2D \longrightarrow 1D$ of structural transformations described was applied, i.e., the bulk ($3D$) phase first formed a lamellar product ($3D \longrightarrow 2D$) and then was bent and rolled to a nanotubular form ($2D \longrightarrow 1D$). The lamellar product is mainly formed by the anatase (101) surface, identified as prevailing in TiO_2. A further geometry optimization of the 3-sheet O–Ti–O layer for $2D \longrightarrow 1D$ transition results in the formation of titania nanotubes possessing hexagonal fluorite-like (111) morphology [26].

The three-layer nanosheets cut from the fluorite phase of the bulk TiO_2 (the space group 225 $Fm\bar{3}m$) have the symmetry of the layer group 72 $P\bar{3}m1$. Using the rolling up correspondence of the line and layer groups [31], one obtains line groups for special chiralities of TiO_2 nanotubes: (n,n)–Family 4, (n,0)–Family 8 with the isogonal point groups C_{2nh} and C_{2nv}, respectively. For n = 1,2,3 these line groups coincide with the crystallographic rod groups.

The symmetry of electron and phonon states for rod groups can be found using the site-symmetry approach [8] for the space groups as the Wyckoff positions of rod groups form subsets of those for space groups.

The site-symmetry approach described above can be applied to find the symmetry of phonon and electron d-states for (n,n) and (n,0) nanotubes rolled up from 3-sheet O–Ti–O layer (n = 1, 2, 3). The rod symmetry groups are $2n_n/m$ and $2n_nmc$ and belong to families 4 and 8, respectively. In this case the tube unit cell contains 6n atoms occupying three nonequivalent 2n-atom orbits (1 titanium orbit and 2 oxygen orbits), corresponding to Wyckoff positions d (stabilizer C_{1h}) and b (stabilizer C_{1v}) for families 4 and 8, respectively.

The corresponding general analytic expressions for the induced representations of all Line groups can be found in Tables published in [3] and are used in the computer code, generating the induced representations for any Wyckoff positions, belonging to Families 4 and 8 of Line groups. This code has been applied to the case of Rod groups and Wyckoff positions, described above for TiO_2 nanotubes. The results obtained by two different ways, coincide.

2.7 CRYSTAL Program. Use of Symmetry in First-Principles LCAO Calculations of 3D, 2D, 1D Systems

CRYSTAL is a general-purpose program for the study of crystalline solids, and the first which has been distributed publicly [39]. The first version was released in 1988 and then seven next versions have followed: CRYSTAL92, CRYSTAL95, CRYSTAL98, CRYSTAL03, CRYSTAL06, CRYSTAL09, CRYSTAL14.

The recent version of the CRYSTAL program -CRYSTAL14- [39] computes the electronic structure of periodic systems within Hartree-Fock, Density Functional or various hybrid approximations. The Bloch functions of the periodic systems are expanded as linear combinations of atom centred Gaussian functions

(LCAO). Powerful screening techniques are used to exploit real space locality. Restricted (Closed Shell) and Unrestricted (Spin-polarized) calculations can be performed with all-electron and valence-only basis sets with effective core pseudopotentials.

The program can automatically handle space symmetry of 230 space groups, 80 layer groups, 75 rod groups (99, if the different rod group settings are taken into account), 45 point groups. Point symmetries compatible with translation symmetry are provided for molecules. Helical symmetry of the polymers is available. Input tools allow the generation of a slab (2D system), or a cluster (0D system), from a 3D crystalline structure, or the creation of a supercell with a defect, nanotubes (1D system) from a single-layer slab model (2D system), nanorods (1D systems) from the bulk crystal (3D system).

The code may be used to perform consistent studies of the physical and chemical properties of molecules, polymers, nanotubes, nanorods, surfaces and crystalline solids: structural features, vibrational properties, electronic structure, magnetic properties, dielectric properties (linear and non-linear electric susceptibilities up to forth-order), elastic, piezoelectric and photoelastic properties [39].

The lack of the crystallographic restrictions for line groups makes translations just a small part of the full symmetry, in contrast to space and layer groups. While in the unit cell of a three-dimensional crystal there are typically several to hundred atoms, the unit cell of a typical nanotube includes hundreds or thousands of atoms. The majority of the existing ab initio numerical codes do not implement line group symmetry.

One of the first attempts of such an implementation was made in [54] to calculate the graphene nanotubes by the method of linear augmented cylindrical waves. Using the symmetry-adapted version of this method carbon nanotubes containing up to 118804 atoms per translational unit cell (the chiral vector $\mathbf{R}(100, 99)$, helical axis order 59402) were calculated. Even for the largest system with a huge unit cell, the band structure can be easily calculated and the results can be presented in the standard form of four curves for the valence band plus one curve for the low-energy states of the conduction band.

The rototranslational (helical) symmetry was implemented in CRYSTAL09 code, [14, 55] and used in the first-principles LCAO calculations of carbon nanotubes. To the best of our knowledge, this is the first complete, tested and documented implementation of helical point symmetry in a general purpose computer code. It has been shown that the use of the helical symmetry of nanotubes, usually quite high, permits one to drastically reduce the computational time and tackle large unit cell nanotubes with an extended basis set. The code permits one to pass from a 3D object (bulk crystal) to a 2D slab and then to a 1D nanotube in a fully automatic way.

In the direct space the helical symmetry is exploited for the calculation of mono- and bi-electronic integrals, so that only a small fraction (the irreducible wedge) of the Fock (Kohn-Sham) matrix F is explicitly computed. The saving factor in the computing time can be as large as N, where N is the number of point symmetry operators that characterize the system.

The symmetry in the reciprocal space is also exploited, as the matrices corresponding to each irreducible representation (IR) are individually diagonalized for the considered **k** points. By transforming the Bloch basis into a symmetry adapted basis the Fock matrix F(**k**) becomes block-diagonal, with each block corresponding to an irreducible representation (IR) of the point group. When the system is periodic only along one direction (z in our convention) and the rotation part of the symmetry operators acts on the Cartesian coordinates (x and y) orthogonal to the translation direction, the point group of each **k** point is the same, and contains the full set of point operators. The Fock matrix then factorizes in exactly the same way at each **k** point. As the cyclic group Z is Abelian, the number of IRs (and of blocks to be diagonalized) is equal to the number of rototranslation operators. In this case the saving factor is much larger than N, due to the third-to-fourth order scaling of the diagonalization process. As a matter of fact, the dimension of all the diagonalized matrices is $M = mN_{AO}$, where N_{AO} is the number of atomic orbitals describing each atom and m is the number of atoms in the layer unit cell.

Following [55] we consider the use of helical symmetry in the first-principles calculations of carbon nanotubes. The structure of a carbon nanotube is modelled by rolling up a single sheet of graphite (i.e. graphene) into a cylinder along the given translation vector $\mathbf{R}(n_1, n_2)$ in a plane hexagonal lattice with two carbon atoms in the primitive cell. The symmetry of graphene is given by layer group $80(P6/mmm)$. It is seen from Table 2.10 that this layer group generates nanotubes with the symmetry of the line group $\mathbf{L}^{(5)}$ (the fifth family) when the general chiral vector $\mathbf{R}(n_1, n_2)$ is used for rolling up the tube (chiral carbon nanotubes). Zigzag and armchair achiral nanotubes are obtained by rolling up the special chiral vectors $\mathbf{R}(n, 0)$ and $\mathbf{R}(n, n)$, respectively. The symmetry of these tubes is given by the line group $\mathbf{L}^{(13)}$, see Table 2.10. The isogonal point groups of the carbon chiral and achiral nanotubes are $\mathbf{D}_n$ and $\mathbf{D}_{2nh}$, with the helical symmetry axis orders equal to n and $2n$, respectively. The resulting nanotubes contain $2q$ and $4q$ atoms, respectively, i.e. dozens or hundreds of atoms in the unit cell, depending on the chiral vector choice. As an example, consider the (24,0) nanotube; with the basis set used for calculations in [55] (a 6-1111G^* contraction) the size of the Fock matrix in the AO basis is 2112 (22 AOs times 96 atoms); in the symmetry adapted basis there are 48 blocks, each containing 44 lines. Then 48 44×44 - matrices are diagonalized at each **k** point.

It is clear that the reduction in computational time due to this factorization is dramatic, in particular, in the case of highly symmetric systems with large unit cells, for which the diagonalization requires a large fraction of the overall computing time. Table 2.17 demonstrates the effect of using of the helical point symmetry in the simulation of carbon nanotubes of increasing size. The results are taken from [55]. The geometry of a set of carbon zigzag $(n, 0)$ nanotubes was optimized. Structure optimizations were performed by using analytical energy gradients with respect to atomic coordinates and unit-cell parameters. Convergence was checked on both gradient components and nuclear displacements. The hybrid B3LYP functional was adopted, together with a quite complete basis set containing $1s$, $4sp$, and $1d$ shells, that is 22 AOs per carbon atom (6-1111G^* contraction). The level of accuracy in evaluating the Coulomb and Hartree-Fock exchange series is controlled by

Table 2.17 Effect of the exploitation of point symmetry in the simulation of carbon nanotubes of increasing size [55]

	R	N_A	N_{AO}	N_R	$N_{\hat{S}}$	t_{SCF}	t_G	ΔE	δE
(8,0)	3.137	32	704	15.8	16	72.1	459.6	42.78	1.48
(9,0)	3.529	36	792	17.8	18	65.9	409.2	34.47	0.728
(10,0)	3.921	40	880	19.8	20	63.0	384.3	27.20	0.475
(11,0)	4.313	44	968	21.8	22	60.7	365.0	22.57	0.387
(12,0)	4.705	48	1,056	23.8	24	60.6	355.2	19.50	0.126
(13,0)	5.097	52	1,144	25.8	26	61.4	353.9	16.24	0.117
(14,0)	5.489	56	1,232	27.8	28	62.8	350.1	14.08	0.134
(15,0)	5.881	60	1,320	29.7	30	63.4	352.6	12.65	0.0518
(16,0)	6.273	64	1,408	31.7	32	65.2	346.9	10.88	0.0685
(17,0)	6.665	68	1,496	33.7	34	66.5	344.3	9.70	0.0750
(18,0)	7.058	72	1,584	35.7	36	67.9	341.0	8.93	0.0195
(19,0)	7.450	76	1,672	37.7	38	70.2	344.1	7.86	0.0320
(20,0)	7.842	80	1,760	39.6	40	72.5	344.6	7.14	0.0386
(21,0)	8.234	84	1,848	41.6	42	75.4	344.9	6.68	0.0151
(22,0)	8.626	88	1,936	43.6	44	78.4	347.1	5.97	0.0162
(23,0)	9.018	92	2,024	45.6	46	81.7	348.6	5.49	0.0243
(24,0)	9.410	96	2,112	47.6	48	85.6	351.5	5.20	8.63E-3

five parameters, [14] for which the 8 8 8 8 16 values were used. The threshold on the SCF energy was set to 10^{-8}Ha. The reciprocal space was sampled according to a regular sublattice with shrinking factor 10 (6 **k** vectors). The DFT exchange-correlation contribution was evaluated by numerical integration over the unit cell volume. In these calculations, a (75,974) grid was used which corresponds to a pruned grid with 75 radial and 974 angular points; the accuracy in the integration can be estimated by the error in the integrated electronic charge density in the unit cell ($\Delta_e = 810^{-4}|e|$ for a total of 576 electrons in the (24,0) nanotube).

Table 2.17 documents the effect of point symmetry use for a set of $(n, 0)$ nanotubes (all of them share the same rolling direction). In the first two columns, the (n_1, n_2) indices of the nanotubes and their radius, R (Å), are reported. N_A and N_{AO} are the number of atoms and atomic orbitals in $(6-1111G(d))$ basis set per unit cell, N_R is the ratio between the number of elements of the complete and irreducible Fock matrix, $N_{\hat{S}}$ is the number of symmetry operators. The cost of the calculation is documented in the t_{SCF} and t_G columns of Table 2.17; t_{SCF} and t_G are given in seconds and mean the time of a single SCF cycle and of the gradient calculation, respectively (single processor-Intel Xeon, 1.86 GHz, RAM 8 Gb). ΔE and δE (kJmol^{-1} per couple of C atoms) are the energy difference with respect to graphene and the relaxation energy after rigid rolling, respectively.

In going from (8,0) to (24,0), the number of atoms (N_A), basis functions (N_{AO}), and symmetry operators ($N_{\hat{S}}$) increase exactly by threefold (from 32 to 96, from 704 to 2112, and from 16 to 48, respectively). The complete Fock matrix for the largest

case is then about three times larger than for the (8,0) case, whereas the symmetry adapted matrix size is roughly constant. The (8,0) nanotube F matrix has about 11,500 elements that diminish to 10,000 for the (24,0) case. The number of elements N_R is extremely close to the number of symmetry operators $N_{\hat{S}}$. The time required for the calculation of bi-electronic integrals, the most expensive part of the SCF calculation, decreases for a while and then remains nearly constant. The same behavior is shown by the gradient, whose cost from (12,0) to (24,0) varies by less than 1 %. The overall cost of the SCF cycle increases (slowly) for three reasons. First, the diagonalization step scales linearly with N (i.e., with the number of symmetry operators and with the number of atoms). Second, the t_{SCF} and t_G AO $\rightarrow$ Bloch $\rightarrow$ symmetry adapted basis transformations, and the back transformations to the AO basis for building the density matrix, are matrix multiplications. In principle, AO $\rightarrow$ Bloch and Bloch $\rightarrow$ symmetry adapted basis transformations should scale as N_{AO}^2 and N_{AO}^3, respectively, with a low prefactor. In practice, the sparsity of all the involved matrices is exploited, so that the scaling of this stage is closer to N_{AO}^2 than to N_{AO}^3. Third, the overhead for the symmetry analysis increases with the number of symmetry operators. Overall, the total cost increases by less than 50 % for the SCF and remains constant for the gradient, whereas in a perfect linear scaling code, not exploiting the symmetry, the cost would increase by a factor of three. The last two columns provide the energy difference between the relaxed nanotube and graphene, $\Delta \mathrm{E} = \mathrm{E}_{\mathrm{relaxed}} - \mathrm{E}_{\mathrm{graphene}}$, and the relaxation energy after rigid rolling, δE (energy difference between unrelaxed and relaxed nanotubes). Roughly speaking, both ΔE and δE decrease regularly as n increases, as expected and in line with the previous findings. Actually, a finer analysis shows that δE data belongs to three different curves, describing the $(3n, 0)$, $(3n + 1, 0)$, and $(3n + 2, 0)$ cases; however, the differences are quite small and tend to disappear with the increase of the nanotube diameter. The stability of a nanotube family with respect to graphene calculated at the B3LYP level documents the feasibility of this kind of calculations, and the accuracy of the implementation [55].

The rototranslational symmetry subgroup of the line group was implemented in CRYSTAL09 code. The full line group symmetry was implemented in CRYSTAL14 code and gives the higher efficiency in the calculations of the nanotubes with the isogonal point groups C_{nv}, C_{nh}, D_{nd}, D_{nh}.

References

1. B.K. Vainstein, *Modern Crystallography: Fundamentals of Crystals, Symmetry and Methods of Structural Crystallography*, vol. 1 (Springer, Berlin, 1994) Kristallographia **4**, 842 (1959)
2. T. Hahn (ed.), *International Tables for Crystallography*. Space-group Symmetry, vol. A (Reidel, Dordrecht, 1983)
3. M. Damnjanović, I. Milošević, *Line Groups in Physics*. Lecture Notes in Physics, vol. 801 (Springer, Berlin, 2010)
4. M. Vujičić, I.B. Božović, F. Herbut, J. Phys. A: Math. Gen. **10**, 1271 (1977)

5. V. Kopsky, D.B. Litvin (eds.), *International Tables for Crystallography*. Subperiodic Groups, vol. E (Kluwer Academic Publishers, Dodrecht, 2002)
6. R.A. Evarestov, V.P. Smirnov, *Site Symmetry in Crystals: Theory and Applications*, 2nd edn. Springer Series in Solid State Sciences, vol. 108 (Springer, Berlin, 1997)
7. M.I. Petrashen, E.D. Trifonov, *Applications of Group Theory in Quantum Mechanics* (M.I.T. Press, Massachusetts, 1969)
8. *Bilbao Crystallographic Server. The Crystallographic Site at the Condensed Matter* (Physics Department of the University of the Basque Country), http://www.cryst.ehv.es/
9. L.L. Boyle, Acta Cryst. A **29**, 353 (1973)
10. http://cst-www.nrl.navy.mil/lattice/
11. http://cst-www.nrl.navy.mil/lattice/others.html
12. H.A. Jahn, E. Teller, Proc. R. Soc. Lond. A **161**, 220 (1937)
13. Inorganic Crystal Structure Database (ICSD), http://www.fiz-informationsdienste.de/en/DB/icsd/
14. R. Dovesi, V.R. Saunders, C. Roetti, R. Orlando, C.M. Zicovich-Wilson, F. Pascale, B. Civalleri, K. Doll, N.M. Harrison, I.J. Bush, P. D'Arco, M. Llunell, *CRYSTAL09 User's Manual* (University of Torino, Torino, 2010)
15. O.A. Graeve, Zirconia, in *Ceramic and Glass Materials: Structure, Properties and Processing*, ed. by J.F. Shackelford, R.H. Doremus (Springer Science, New York, 2008), p. 169
16. D. Vollath, F.D. Fischer, M. Hagelstein, D.V. Szabó, J. Nanopart. Res. **8**, 1016 (2006)
17. C.M. Wang, S. Azad, S. Thevuthasan, V. Shutthanandan, D.E. McCready, C.H.F. Peden, J. Mater. Res. **19**, 1315 (2004)
18. A. Aarik, A. Aidla, H. Mundar, T. Uustrate, V. Sammelselg, Thin Solid Films **408**, 97 (2002)
19. P. Goudochnikov, A.J. Bell, J. Phys.: Condens. Matter **19**, 176201 (2007)
20. V. Kopsky, Acta Cryst. A **45**, 805, 816 (1989)
21. V. Kopsky, Acta Cryst. A **56**, 370 (2000)
22. E.A. Wood, 80 Diperiodic Groups in Three Dimensions, Bell System Monograph No 4680 (1964)
23. I. Milosević, B. Nikolić, M. Damnjanović, M. Krčmar, J. Phys. A: Math. Gen. **31**, 3625 (1998)
24. P.W. Tasker, J. Phys. C: Solid State Phys. **12**, 4977 (1979)
25. F. Finocchi, F. Bottin, C. Noguera, in *Computational Materials Science*, ed. by C.R.A. Catlow, E.A. Kotomin (IOS Press, Amsterdam, 2003), p. 196
26. R.A. Evarestov, *Quantum Chemistry of Solids. LCAO Treatment of Crystals and Nanostructures*, 2nd edn. Springer Series in Solid State Sciences, vol. 153 (Springer, Berlin, 2012)
27. M. Damnjanović, M. Vujicić, Phys. Rev. B **25**, 6987 (1982)
28. V.P. Smirnov, P. Tronc, Phys. Solid State **48**, 1373 (2006)
29. R.A. Evarestov, A.I. Panin, Acta Cryst. A **68**, 582 (2012)
30. M. Damnjanović, I. Milosević, M. Vuković, R. Sredanivić, Phys. Rev. B **60**, 2728 (1999)
31. M. Damnjanović, B. Nikolić, M. Milosĕvić, Phys. Rev. B **75**, 033403 (2007)
32. S. Ijima, Nature **354**, 56 (1991)
33. E.B. Barros, A. Jorio, G.G. Samsonidze, R.B. Capaz, A.G.S. Filho, J.M. Filho, G. Dresselhaus, Phys. Rep. **431**, 261 (2006)
34. Y. Mao, S. Banerjee, S.S. Wong, Chem. Commun. **3**, 408 (2003)
35. R. Evarestov, IOP Conf. Ser.: Mater. Sci. Eng. **23**, 012012 (2011)
36. A.V. Bandura, R.A. Evarestov, Surf. Sci. **603**, L117 (2009)
37. R.A. Evarestov, A.V. Bandura, M.V. Losev, Russ. J. Gen. Chem. **80**, 1152 (2010)
38. R.A. Evarestov, Yu.F. Zhukovskii, A.V. Bandura, S. Piskunov, Cent. Eur. J. Phys. **9**, 492 (2011)
39. R. Dovesi, V.R. Saunders, C. Roetti, R. Orlando, C.M. Zicovich-Wilson, F. Pascale, B. Civalleri, K. Doll, N.M. Harrison, I.J. Bush, P. D'Arco, M. Llunell, M. Causa, Y. Noel, *CRYSTAL14 User's Manual* (University of Torino, Torino, 2014)
40. R. Dovesi, R. Orlando, A. Erba, C.M. Zicovich-Wilson, B. Civalleri, S. Casassa, L. Maschio, M. Ferrabone, M. Pierre, P. D'Arco, Y. Noel, M. Causa, M. Rerat, B. Kirtman, Int. J. Quant. Chem. **114**, 1287 (2014)
41. M. Damnjanović, I. Milosĕvić, T.V.E. Dobradzić, B. Nikolić, J. Phys. A **36**, 10349 (2003)

42. M. Damnjanović, T. Vuković, I. Milosĕvić, Acta Phys. Pol. A **120**, 224 (2011)
43. P.B. Allen, Nanoletters **7**, 6, 11, 1220 (2007)
44. C. Herring, Phys. Rev. **82**, 87 (1951)
45. D.B. Migas, V.L. Shaposhnikov, V.E. Borisenko, F.A. D'Avitaya, J. Phys. Chem. C **114**, 21013 (2010)
46. C.A. Chen, Y.M. Chen, A. Korotcov, Y.S. Huang, D.S. Tsai, K.K. Tiong, Nanotechnology **19**, 075611 (2007)
47. B. Aradi, P. Deak, H.A. Huy, A. Rosenauer, T. Frauenheim, J. Phys. Chem. C **115**, 18494 (2011)
48. A.P. Cracknell, B.L. Davies, S.C. Miller, W.F. Love, *Kronecker Product Tables, 1 General Introduction and Tables of Irreducible Representations of Space Groups* (IFI/Plenum, New York, 1979)
49. C.J. Bradley, A.P. Cracknell, *The Mathematical Theory of Symmetry in Solids* (Clarendon, Oxford, 1972)
50. http://gernot-katzers-spice-pages.com/character_tables/index.html
51. I.B. Božović, M. Vujičić, F. Herbut, J. Phys. A: Math. Gen. **11**, 2133 (1978)
52. I.B. Božović, M. Vujičić, J. Phys. A: Math. Gen. **14**, 777 (1981)
53. I. Božović, N. Božović, J. Phys. A: Math. Gen. **14**, 1825 (1981)
54. P.N. D'yachkov, D.V. Makaev, Phys. Rev. B **76**, 195411 (2007)
55. I. Noel, P. D'Arco, R. Demichelis, C.M. Zicovich-Wilson, R. Dovesi, J. Comput. Chem. **32**, 855 (2010)